Interdisciplinary study of the antidepressant effect of dexmecamylamine: a meta-analysis and computational study

Yating Yang

Faculty of Medicine and Health

The University of Sydney

A thesis submitted in fulfilment of the requirements for the degree of

Master of Philosophy

2023

Statement of originality

This is to certify that to the best of my knowledge, the content of this thesis is my own work. This thesis has not been submitted for any degree or other purposes.

I certify that the intellectual content of this thesis is the product of my own work and that all the assistance received in preparing this thesis and sources have been acknowledged.

In addition to the statements above, in cases where I am not the corresponding author of a published item, permission to include the published material has been granted by the corresponding author.

Yating Yang

Acknowledgments

Firstly, I would like to express my sincere gratitude to my supervisor Professor Thomas Balle for his continuous support of my master's study and related research, for and his patience, motivation, and immense knowledge. His guidance helped me in all the time of research and writing of this thesis. I could not have imagined having a better advisor and mentor for my Master's study. I also want to thank Ali Kusay and Yujia Luo for sharing his technical knowledge, skills and , ideas. They are super professional in their field and encouraged me a lot during I finish my Maste's project and my thesis. Besides them, I also want to express my gratitude to all the members in the lab, as they help me a lot while I cannot go back to Australia because of the COVID-19. Furthermore, I would like to thank the editor of this thesis, Min Liu, for his dedication on helping me to proofread the thesis. Last, but not least, special thanks to my parents for their unconditional support and love.

Abstract

Nicotinic acetylcholine receptors (nAChRs) are widespread ligand-gated ion channels in the human brain, playing crucial roles in various physiological processes such as hormone secretion, learning, and pain perception. These receptors have been identified as potential therapeutic targets for mental health disorders, particularly major depressive disorder (MDD). Despite extensive preclinical and clinical investigations of nAChR agonists, positive allosteric modulators, and antagonists, no antidepressant drug targeting nAChRs has been successfully marketed. Given the substantial unmet need for MDD treatment, alternative compounds with distinct mechanisms of action, such as those targeting nAChRs, warrant further exploration.

Dexmecamylamine is one such compound, and it is the dextrorotatory enantiomer of mecamylamine. Dexmecamylamine has demonstrated significant antidepressant-like effects in multiple animal studies. Nevertheless, human clinical trials have yielded conflicting results regarding its antidepressant efficacy. In this study, we employed a meta-analysis to assess the antidepressant-like effect of dexmecamylamine. After conducting an exhaustive literature search, we identified nine high-quality randomized controlled trials (RCTs) eligible for inclusion in the meta-analysis. Our analysis aimed to evaluate dexmecamylamine's efficacy as an adjunct therapy for MDD treatment. The results indicated that dexmecamylamine did not demonstrate superior efficacy compared to placebo in terms of the Hamilton Depression Scale-17 score change [mean difference = 0.70 (95% CI = -0.24 to 1.64)], the Montgomery-Asberg Depression Rating Scale score change [-0.52 (95% CI=-0.15 to -0.02)] and other secondary endpoints.

Dexmecamylamine functions as an open channel blocker. Utilizing the open-state α7 nAChR structure (PDB id: 7KOX), we illustrated dexmecamylamine's binding pose. The open-state α7 nAChR structure, ascertained through cryo-electron microscopy, was in complex with the agonist epibatidine and the positive allosteric modulator (PAM) PNU-120596. The Binding pose of PNU-120596, however, remained unresolved in the structure. Consequently, we docked PNU-120596 to the α7 nAChR open state structure (PDB id: 7KOX), executing molecular dynamics (MD) simulations in triplicate for 250 ns to substantiate PNU-120596's binding position and mode, as well as to investigate associated channel gating behavior. We then performed a molecular docking of dexmecamylamine to the open state α7 nAChR (PDB id: 7KOX), presuming the binding site on α7 nAChR is analogous to that identified through mutational studies on the $(\alpha4)_2(\beta2)_3$ nAChRs. Subsequently, MD simulations of the dexmecamylamine-α7 nAChR complex were conducted in triplicate for 250 ns to depict dexmecamylamine's binding behavior. We studied two complexes (PNU-120596-α7 nAChR and dexmecamylamine-α7 nAChR). MD simulations were performed thrice for each complex, and the RMSD value was calculated. The replica with the lowest RMSD value in each complex group was selected for further analysis.

The MD simulation with the lowest RMSD for each complex served as the representative run for additional analysis. Docking results indicated the initial binding sites of PNU-120596 and dexmecamylamine to α7 nAChR. The final docking positions for dexmecamylamine and PNU-120396 with α7 nAChR were illustrated by MD simulation results. MD simulation outcomes

revealed stable open state α7 nAChRs when bound to PNU-120596. The dexmecamylamine-α7 nAChR complex achieved a stable conformation in the MD simulation. However, dexmecamylamine moved upwards relative to the initial docking pose. In the representative structure, dexmecamylamine was situated near an α7 subunit, rather than in the central part of the channel pore as anticipated. Residue V274 is proposed as the critical residue, functioning as a hydrogen bond acceptor and interacting with the hydrogen on dexmechamylamine's positively charged nitrogen. The channel pore remained hydrophilic throughout the MD simulation. We investigated the channel pore diameter of α7 nAchR in the presence and absence of dexmecamylamine. Results demonstrated a narrower channel pore with dexmecamylamine, yet the diameter was larger than that of a calcium ion, indicating that a single dexmecamylamine molecule was insufficient to block Ca2+ influx. In conclusion, dexmecamylamine binding to open-state α7 nAChRs resulted in a narrower channel pore radius, although this constriction was insignificant. Ca2+ continued to influx through the channel pore despite dexmecamylamine binding, rendering dexmecamylamine incapable of blocking Ca2+ influx.

Table of Contents

List of Abbreviations

AD	Alzheimer's disease
CANMAT	Canadian network for mood and anxiety treatments
CHARMM	Chemistry at harvard macromolecular mechanics
CNS	Central neural system
ClinRo	Clinician-reported outcome
CGI-S	Clinical global Impression Severity Scale
DSM-5	Diagnostic and Statistical Manual of Mental Disorders (5^{th} edition)
ECD	Extracellular domain
GABAARs	γ -aminobutyric acid type A receptors
GlyRs	Glycine receptors
GROMACS	Glycine receptors
HAMD-17	The Hamilton Rating Scale for Depression-17
ICD	Intracellular domain
LGICs	Ligand-gated ion channels
mAChRs	Muscarinic acetylcholine receptors
MADRS	The Montgomery Asberg Depression Rating Scale
MAOIs	Monoamine oxidase inhibitors
MD	Molecular dynamic
MDD	Major depressive disorder
nAChRs	Nicotinic acetylcholine receptors
NPT	Constant number of particles, pressure and temperature
NVT	Constant number of particles, volume and temperature
PAM	Positive allosteric modulator
PD	Parkinson disease
PDB	Protein data bank RMSD Root mean square deviation
PME	Particle mesh Ewald, method to calculate electrostatics.
RCT	Randomized clinical trials
SAM	Silent allosteric modulators
SNRI	Serotonin-norepinephrine reuptake inhibitor
SSRI	Selective serotonin reuptake inhibitor
TCA	Tricyclic antidepressants
TIP3P	Transferable Intermolecular Potential 3-site water models
TMD	Transmembrane domain

List of amino acids and their abbreviations

Amino Acid	3-Letters	1-Letter
Alanine	Ala	A
Arginine	Arg	R
Asparagine	Asn	N
Aspartic acid	Asp	D
Cysteine	Cys	C
Glutamine	Gln	Q
Glutamine acid	Glu	E
Glycine	Gly	G
Histidine	His	H
Isoleucine	Ile	I
Leucine	Leu	L
Lysine	Lys	K
Methionine	Met	M
Phenylalanine	Phe	F
Proline	Pro	P
Serine	Ser	S
Threonine	Thr	T
Tryptophan	Trp	W
Tyrosine	Tyr	Y
Valine	Val	V

Chapter1

Background: Overview of nACh receptors, mecamylamine and depression

1.1 Major depressive disorder

1.1.1 Definition

Major depressive disorder (MDD) represents a highly prevalent mental health disorder worldwide and has emerged as a significant public health issue on a global scale (Kupfer, Frank, & Phillips, 2012). The economic impact of MDD is considerable; for instance, in the United States, the financial burden of MDD in 2000 amounted to $83.1 billion, with $26.1 billion (31%) attributed to direct medical expenses, $51.5 billion (62%) to absenteeism and reduced productivity, and $5.4 billion to suicide-related incidents (Greenberg et al., 2003). MDD is characterized by its chronic and recurrent nature (Liu et al., 2021). As per Kupfer's research (2012), 6.6% of individuals experience MDD for a minimum of 12 months (Kupfer et al., 2012). Patients with MDD typically undergo at least one distinct depressive episode lasting over two weeks, with symptoms encompassing marked shifts in mood, interests, and pleasure, as well as cognitive alterations and vegetative manifestations (Otte et al., 2016). Despite being classified as a psychotropic condition, MDD can lead to severe physical impairment and even life-threatening consequences, such as suicide (Filatova, Shadrina, & Slominsky, 2021). Although MDD is considered treatable, epidemiological investigations reveal that over 16% of MDD patients endure lifetime depressive symptoms (Kupfer et al., 2012).

The epidemiological characteristics of MDD vary across genders and ages. The gender ratio is imbalanced in patients with depression (LEE et al., 2016). Noble et al. (2005) suggested that women (21.3%) have a significantly higher lifetime prevalence of MDD than men (12.7%) (Noble, 2005). Moreover, young women around puberty have the highest risk of severe depression. At ages above 65, depression rates for both men and women begin to decline, and the prevalence between genders becomes comparable (Albert, 2015). Albert (2015) proposed that women exhibit a higher prevalence of MDD due to hormones, psychosocial stressors, and fertility (Albert, 2015).

Aside from direct effects such as mood changes and cognitive dysfunction, MDD has secondary effects. The Research demonstrates that patients with MDD often exhibit poor adherence to medical treatment and are more likely to develop chronic medical illnesses (Grenard et al., 2011) .

MDD is an inhomogeneous disorder with intricate etiologies. Its onset is insidious, making diagnosis difficult. The pathophysiology of major depressive disorder remains uncertain. The prevalent etiologies of MDD encompass psychological, biological, genetic, and social factors (Chiri ţă, Gheorman, Bondari, & Rogoveanu, 2015). Clinical manifestations of depression are diverse, including cognitive impairments, unregulated emotional depression, memory loss, motor dysfunction, and other adverse neurological symptoms. The study of depression’s etiology is complicated by the diverse array of clinical symptoms it presents (MacQueen & Memedovich, 2017).

1.1.2 Diagnosis

Diagnosing MDD accurately is challenging due to the frequent co-occurrence of symptoms with various psychiatric disorders (Filatova et al., 2021). Over-detection and under-detection can impact the precise identification of MDD (Filatova et al., 2021).

Currently, the 5th edition of the Diagnostic and Statistical Manual of Mental Disorders (DSM-V), published by the American Psychiatric Association in 2013, serves as the globally recognized manual for MDD diagnosis (First, 2013). DSM-V diagnostic criteria evaluate five depression domains (Sections A through E). The patient receives an MDD diagnosis upon meeting criteria across all sections. Section A, the critical diagnostic component, assesses depressive symptoms within the past fortnight. High MDD risk is indicated by the presence of five or more daily or near-daily symptoms outlined in Section A as summarized below (First, 2013; American Psychiatric Association, 2013):
(1) Depressive mood (e.g., sadness, emptiness, hopelessness, suicidal ideation), either subjectively reported or observed (e.g., tearfulness, irritability in children and adolescents).
(2) Diminished interest or pleasure in all or almost all activities (subjective or observed by their caregivers).
(3) Significant weight fluctuations without dietary changes (defined as over 5% change in body weight within a month) or altered food intake (note: in children, it may be shown that failure to achieve expected weight gain).
(4) Insomnia or hypersomnia.
(5) Psychomotor agitation or lethargy (observed by others, not just a subjective experience of restlessness or dullness).
(6) Fatigue or decreased energy levels.
(7) Self-denial, defined as feelings of worthlessness or guilt about oneself.
(8) Decrease in the ability to think, pay attention, and focus on a task in progress (either as a subjective experience or as observed by other caregivers).
(9) Suicidal ideation or attempts, persistent thoughts of death, or recurrent suicidal ideation without a specific plan.

1.1.3 Instruments and scales

Major depressive disorder (MDD) is a chronic condition with long recovery times for patients (Liu et al., 2021). Thus, accurate assessment of symptom severity is crucial for evaluating the effectiveness of antidepressant treatments. Although there are no approved biomarkers for diagnosing MDD (Hacimusalar & Eşel, 2018), numerous scales have been developed to quantify depression symptom severity. However, these scales are not standardized diagnostic criteria but are employed by clinicians to gauge disease severity and treatment efficacy. Commonly used scales include the Hamilton Rating Scale for Depression (HAMD) and the Montgomery Asberg Depression Rating Scale (MADRS) (Snaith, 1996; Montgomery & Asberg, 1979). Both of them are clinician-reported outcomes (ClinRO) and disease-specific scales. The Clinical Global Impression Severity Scale (CGI-S) is also frequently utilized to assess depression severity (Lin et al., 2018), although it is

not disease-specific and is less sensitive than MADRS and HAMD-17 (Lin et al., 2018). As part of our meta-analysis, these scales were also used as endpoints to measure the antidepressant efficacy of dexmecamylamine.

Developed in the late 1950s and officially published in 1960, HAMD quickly became the gold standard for evaluating the efficacy of antidepressants and other depression therapies, such as exercise or counseling(Hamilton, 1960). It is widely employed as a primary endpoint in MDD clinical trials to assess antidepressant treatments (Carrozzino, Patierno, Fava, & Guidi, 2020). The Hamilton Depression Rating Scale (HAMD-17), which is a revised version of the original scale, is widely recognised as the most commonly utilised scale among all the variations of HAMD (Leuchter et al., 2002), with total scores ranging from 0 to 52. On this scale, scores of 0-7 indicate common depression; 8-16 indicate mild depression; 17-23 indicate moderate depression; and 24-52 indicate severe depression (Davis, 2021; Goldberger, Guelfi, & Sheehan, 2011; Sun et al., 2020). Studies have been conducted to to establish the reliability and validity of HAMD-17, which have consistently supported the robustness and accuracy of this scale, indicating that HAMD-17 is a reliable and valid tool for assessing depression (Bagby, Ryder, Schuller, & Marshall, 2004). It is possible to compare the treatment effects of different therapies using this standardized criterion.

There are also limitations to HAMD-17. Firstly, it is challenging for patients to utilize clinically due to its complexity (Gerbasi et al., 2020). As opposed to the patient-self-reported outcome scale (PRO), HAMD-17 is a clinician-reported outcome scale (ClinRO) (Gerbasi et al., 2020). Consequently, patients sshould undergo a 15- to 20-minute HAMD-17 scale examination administered by two proficient and trained evaluators, with the test's duration contingent on the severity of the patient's disease condition (Ma et al., 2021). A further criticism of HAMD-17 is its limited sensitivity. Despite its widespread use as a clinical trial endpoint, the HAMD-17 does not distinguish well between depression and anxiety because both depression and anxiety will increase the HAMD-17's overall score (Ahn & Kang, 2018).

Due to the limitations of the HAMD-17 scales, the Montgomery-Asberg Depression Rating Scale (MADRS) was developed to address these shortcomings (Montgomery et al., 1979). The MADRS is another established depression assessment tool with acceptable reliability and validity (Montgomery et al., 1979). In comparison to the HAMD-17 scale, the MADRS demonstrates greater sensitivity in differentiating between depression and anxiety. Furthermore, the MADRS is more user-friendly than the HAMD-17 due to its simplicity (Bagby et al., 2004). Consequently, it has been adapted and validated in various languages, including German, Spanish, Japanese, and Persian (Heo, Murphy, & Meyers, 2007).

Both HAMD-17 and MADRS have also been employed to assess disease severity in other disorders accompanied by depressive symptoms, such as anxiety, schizophrenia, and bipolar disorder. Therefore, numerous randomized clinical trials (RCTs) utilize these scales to evaluate treatment efficacy (Keller, 2003).

The Clinical Global Impression Severity Scale (CGI-S) is a tool for clinicians to assess a patient's current illness state based on their impression of the patient. The CGI-S score ranges from 0 to 7,

with higher scores indicating increased disease severity. Unlike the MADRS and HAMD, the CGI-S is not a disease-specific scale and is applied to various disorders (Busner & Targum, 2007).

1.1.4 Treatment

MDD is regarded as a treatable disease, with numerous pharmacological interventions investigated for MDD management. Appropriate treatment should be chosen based on the severity of MDD. For mild to moderate depression, the American Psychological Association (APA) guidelines recommend monotherapy with antidepressants. In cases of severe MDD, antidepressant medications combined with psychotherapy or adjunct pharmacological therapies are advised (Health, 2010).

Two primary generations of antidepressants have been explored thus far: first- and second-generation antidepressant medications. First-generation antidepressants encompass tricyclic antidepressants (TCAs) and monoamine oxidase inhibitors (MAOIs). Second-generation antidepressants include selective serotonin reuptake inhibitors (SSRIs) and serotonin-norepinephrine reuptake inhibitors (SNRIs) (Chockalingam,R,Gott&Conway,2019). TCAs work by increasing serotonin or norepinephrine levels in the synapse (Gillman,2007). Insufficient serotonin and norepinephrine is one of the pathogenesis of depression. However, TCAs and MAOIs can cause unintended side effects by concurrently blocking histaminergic, cholinergic, and adrenergic receptors. Possible clinical side effects of these drugs include weight gain, dry mouth, drowsiness, and dizziness (Hillhouse & Porter, 2015; King & Ashraf, 2018).

Due to the side effects of first-generation antidepressant medications, second-generation antidepressants were developed. Compared to their first-generation antidepressants, second-generation antidepressants exhibit greater selectivity and target specific neurotransmitters to avoid undesired side effects. SSRIs and SNRIs have become the most frequently prescribed antidepressants in clinical settings. In addition, the therapeutic efficacy of second-generation antidepressants surpasses that of first-generation drugs (Ferguson, 2001). In the CANMAT guidelines, second-generation antidepressants are recommended as first-line therapy for patients with moderate to severe MDD (Z. Wang, Ma, & Xiao, 2019).

Although numerous treatment options for MDD are available, patients continue to face challenges such as insufficient efficacy, drug resistance, severe side effects, and relapse (Al-Harbi, 2012). Consequently, there is an urgent need to discover novel therapeutic approaches for depression. In the treatment of MDD, the primary and optimal objective is to attain complete symptom remission (Habert et al., 2016), which refers to the complete recovery of psychosocial functioning and minimal residual symptom burden (Israel, 2010). Despite rapid advancements in MDD treatment, epidemiological research reveals that only 30-40% of MDD patients achieve remission after initial treatment, and over a third remain unresponsive to multiple treatment approaches (Saragoussi et al., 2017). Consequently, second-generation antidepressants may not suffice to address existing therapeutic demands (Sforzini, 2021). Third-generation psychotropic medications (e.g., venlafaxine, mirtazapine) targeting multiple depression-related receptor sites have been introduced (Olver, Burrows, & Norman, 2001); however, most remain in the development phase.

Fortunately, residual depressive symptoms are modifiable. The CANMAT guidelines recommend increasing antidepressant dosage for patients not experiencing early remission and considering alternative antidepressants for drug-resistant patients (Voineskos, Daskalakis, & Blumberger, 2020). Nonetheless, augmenting initial antidepressant doses may result in short-term or long-term safety and tolerability issues, including gastrointestinal hemorrhage, insomnia, serotonin syndrome, weight fluctuations, as well as metabolic issues such as diabetes mellitus, dyslipidemia, and cardiac effects (Cassano & Fava, 2004). As a result, adjunct therapy appears to be the best option at present. As part of CANMAT's guidelines, adjunct therapy is recommended for patients who are resistant to antidepressant treatment (Kennedy, 2016). The term adjunct therapy refers to the administration of another treatment strategy, either pharmacological or nonpharmacological. In addition to antidepressant medications, pharmacological strategies include the addition of non-antidepressant agents such as lithium, thyroid hormones, and other antidepressant medications. Among the nonpharmacological strategies are psychology and exercise (Shelton, Osuntokun, Heinloth, & Corya, 2010; Zusky et al., 1988).

Antidepressant response typically emerges 4-6 weeks after initial administration, and the extended latency period may cause secondary damage and reduce treatment adherence, as patients may perceive the medications as ineffective (Gourion, 2008; Hansen, Gartlehner, Lohr, Gaynes, & Carey, 2005). Additionally, some patients achieving remission may still exhibit residual depressive symptoms, increasing relapse risk. Thus, it is crucial to develop alternative, effective, and safe antidepressant treatments to alleviate the MDD burden. Several pharmacological agents with diverse mechanisms, including olanzapine, mecamylamine, and aripiprazole (Berman et al., 2009; Corya et al., 2006; Marcus et al., 2008), have been identified as potential adjunct antidepressant drugs. According to a meta-analysis (Nelson, Delucchi, & Schneider, 2009), MDD patients receiving atypical antipsychotics as adjunct therapy alongside ongoing antidepressant treatment exhibited significantly improved clinical response and remission rates compared to those on antidepressant monotherapy (Nuez et al., 2022).

In this section, we have discussed the definition, diagnosis, treatment, and common scales of MDD. MDD is a highly prevalent mental illness worldwide that imposes a significant burden on individuals and society. Despite the numerous anti-depressant drugs available on the market, the treatment of depression still poses several challenges, such as poor efficacy, side effects, and drug resistance. As a result, the development of novel therapies is imperative to address these treatment gaps. Therefore, in the following section, we will introduce the nicotinic acetylcholine receptor (nAChR), which is considered a promising antidepressant drug target, and its antagonist, dexmecamylamine (Philip, Carpenter, Tyrka, & Price, 2010; Giniatullin et al., 2000).

1.2 Nicotinic acetylcholine receptors

1.2.1 Cys-loop receptors

Cys-loop receptors, a class of ligand-gated ion channels (LGICs), are prevalent throughout cell

membranes (Thompson, Lester, & Lummis, 2010), particularly in the peripheral and central nervous systems (PNS and CNS). The Cys-loop receptor superfamily comprises $GABA_A$Rs, nicotinic acetylcholine receptors (nAChRs), 5-hydroxytryptamine type 3 receptors ($5\text{-}HT_3$Rs), glycine receptors (GlyRs) (Sparling & DiMauro, 2017), as well as bacterial ion channels GLIC and ELIC, and GluCl of Caenorhabditis elegans (Alqazzaz, Thompson, Price, Breitinger, & Lummis, 2011).

Cys-loop receptors are metastable proteins in which agonists bind to pockets at subunit interfaces of the extracellular amino-terminal structural domain, controlling the distal channel structural domain to activate (Changeux & Edelstein, 1998). This long distance between binding pockets and the channel pore necessitates an interconnected metastable network between ECD and TMD to convert binding energy into gating energy (Cederholm, Schofield and Lewis, 2009). The Research on various Cys-loop receptors indicates that activation mechanisms within this family of receptors are similar (Chang, Wu, Zhang & Huang, 2009). The highly conserved 'Cys-loop' among the Cys-loop receptors, composed of 13 amino acids held in place by a disulfide bond between two cysteines on the receptor's extracellular domain (ECD) (Changeux et al., 2010), is essential for subunit assembly. The Cys-loop receptors exhibited poor assembly when the formation of the Cys-loop was blocked in the previous study by Green (Green & Halliwell, 1997). Besides the conserved Cys-loop region, the Cys-loop superfamily receptors share a similar pentameric structure. According to the typical structure among Cys-loop receptors, their properties can be derived from studying other receptors in the family (Fu, Wang, & Mu, 2016).

The Cys-loop receptors possess multiple subtypes, resulting from the combination of distinct subunits. Comprising five subunits, Cys-loop receptors are pentameric in nature, and these subunits can assemble into either homomultimeric or heterogeneous proteins (Fu et al., 2016). Arranged pseudosymmetrically, the five subunits form an ion-conducting pore (Thompson et al., 2010). Each Cys-loop receptor consists of three domains: an extensive N-terminal extracellular domain (ECD), a C-terminal transmembrane domain (TMD), and an intracellular domain (ICD) (Thompson et al., 2010).

Belonging to the ion channel family, Cys-loop receptors exhibit characteristics analogous to those of other ion channel receptors. Neurotransmitters activate Cys-loop receptors, facilitating the transportation of ions across cell membranes (Lester, Dibas, Dahan, Leite, & Dougherty, 2004). Within the human body, neurotransmitters regulate the function of Cys-loop receptors (Grothe et al.). Neurotransmitters bind to the extracellular domain of the receptors, inducing a conformational alteration that subsequently opens the ion-selective pore within the TMD (Cederholm et al., 2009). Owing to these functions, Cys-loop receptors have been implicated in numerous diseases. A plethora of drugs have been developed to target Cys-loop receptors, including anesthetics and muscle relaxants. Due to the pervasive presence of Cys-loop receptors in the human brain, various neuropharmacological agents have been developed to target these receptors (Yakel, 2010).

1.2.2 nAChRs: introduction

Acetylcholine is involved in many physiological processes. It works in both the CNS and the PNS. It

activates two different cholinergic receptors: neuronal nicotinic acetylcholine receptors and muscarinic acetylcholine receptors (Zoli, Pucci, Vilella, & Gotti, 2018).

As discussed above, the Cys-loop receptors usually have a variety of subunits. For nAChRs, there are a total of twelve neuronal subunits (α2-α10, β2-β4) (Dani, 2015). They exit as both homomeric and heteromeric nAChRs and all share the pentameric structures. All five subunits are arranged around a water-filled pore, allowing Ca2+ ions to flow (figure 1.1) (Dani, 2015). Despite sharing a similar structure, different nAChR subtypes have specific properties. α7 nAChRs and α4β2* nAChRs are the most common subtypes in the human brain. They can be found in the cerebral cortex, hippocampus and basal ganglia (Posadas, López-Hernández, & Ceña, 2013). Similar to other Cys-loop receptors, the nAChR contains a large N-terminal extracellular domain (ECD), a C-terminal transmembrane domain (TMD), and an intracellular domain (ICD) (figure 1.1) (Bondarenko, 2022).

1.2.3 nAChRs: structure

nAChRs, akin to other Cys-loop receptors, comprise an extensive extracellular N-terminal domain, a transmembrane domain, and an extracellular C-terminal domain. The transmembrane domain encompasses three hydrophobic transmembrane sections (M1-M3), a substantial intracellular loop, and a transmembrane region (M4) (Dani, 2015). The 15 amino acid sequence located within the significant N-terminal extracellular domain is connected by a disulfide bond, forming the Cys-loop, characteristic of the entire Cys-loop receptor superfamily (Unwin, 2013). In the ICD, each subunit's M2 transmembrane segment primarily lines the ionic pore, with some support from the M1 segment at the ionic pore's broadest location. The M1, M3, and M4 segments separate the hydrophobic membrane and the pore-lining area (Unwin, 2013). The nAChR's three principal domains can be identified when observed laterally (figure 1.1). The first domain is the extracellular domain (ECD), which constructs the pore's vestibule and contains the agonist-binding sites (Fasoli & Gotti, 2015). The second domain is the transmembrane domain (TMD), which forms the water-filled, hydrophilic ionic pathway through the lipid bilayer membrane when the pore is open (Fasoli et al., 2015). The third domain is the intracellular domain (ICD), the most flexible domain, featuring areas for cytoplasmic component interaction and modification (Fasoli et al., 2015).

nAChRs function as ligand-activated ion channels, with multiple agonists capable of binding and activating them (Papke & Lindstrom, 2020). The conformational transition occurs during agonist binding, resulting in various functional states that directly impact agonist and antagonist binding affinity. Consequently, understanding the structure of each functional state is crucial for structure-based drug design. Agonist binding encompasses a total of three states (Yamodo, Chiara, Cohen, & Miller, 2010; Unwin, 2013).

In the resting state, no transmitters bind to the receptors. This state maintains the ion pore in a closed position, preventing ion influx into the cell. The nAChRs' conformation shifts to the 'open state' or 'active state' upon agonist binding, opening the channel pore and permitting ion passage, thereby altering the membrane potential. Following activation, the receptor swiftly transitions to a non-conducting, desensitized state. Although the agonist remains bound to the receptor in the desensitized state, the channel pore is closed, and ions cannot traverse the channel. The receptors'

open state is transient, rapidly transitioning to the desensitized state (Unwin, 2013).

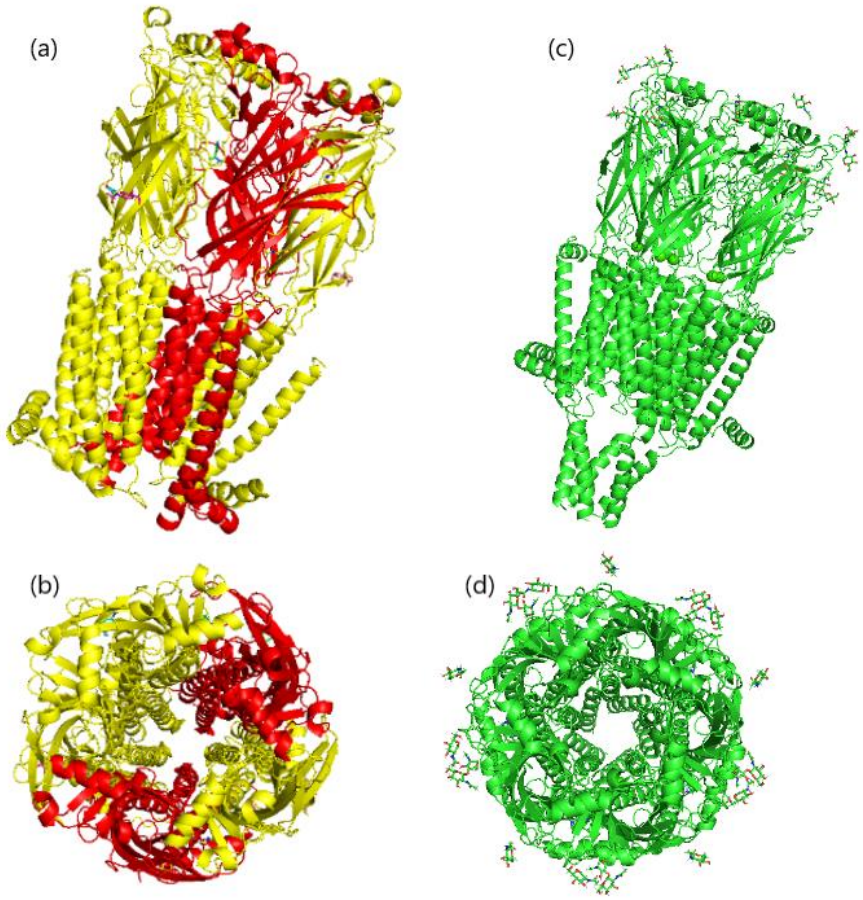

Figure 1.1 The structure of heteromeric $(\alpha4)_2(\beta2)_3$ nicotinic acetylcholine receptor (left, PDB code:5KXI) and homomeric α7 nicotinic acetylcholine receptor (right, PDB code:7KOX).
Both side view (a,c) and top view (b,d) are displayed in the figure. The α4, α7, and β2 subunits are colored in red, yellow, and green, respectively.

1.2.4 α4β2* nicotinic acetylcholine receptor

The diversity of nAChRs leads to distinct pharmacological properties. Among all subtypes, α4β2* nAChRs receive particular attention due to their predominance in the central nervous system (CNS) (Dineley, Pandya & Yakel, 2015).The α4β2* nAChRs are the most abundant and extensively expressed nAChRs in the human brain (Dineley et al., 2015). They are responsible for various crucial brain functions, such as cognition, mood, consciousness, and nociception (Sabri et al., 2018). As members of the Cys-loop receptors, α4β2* nAChRs are cation-selective ligand-gated ion channels activated by the neurotransmitter acetylcholine (Bacher, Wu, Shytle & George, 2009). Aberrant α4β2* nAChR function may contribute to several mental disorders, including Alzheimer's disease, learning disabilities, memory loss, and epilepsy (Bacher et al., 2009).

1.2.5 α7 nicotinic acetylcholine receptor

α7 nAChRs are primarily found in the hippocampus, cortex, and various limbic subcortical regions, which are associated with cognitive functions. Consequently, α7 nAChRs are considered potential targets for treating cognitive decline (Lasala, Fabiani, Corradi, Antollini, & Bouzat, 2019; Bouzat, Lasala, Nielsen, Corradi & Esandi, 2018).

α7 nAChRs play a crucial role in the human neural system and can be found in both pre- and post-synaptic locations. Zhao and colleagues have demonstrated that abnormal α7 nAChR function can result in mental illnesses, such as schizophrenia, depression, and Alzheimer's disease (Zhao et al., 2021). Additionally, Mizrachi indicated that the binding of agonists to α7 nAChRs activates the anti-inflammatory pathway, thereby reducing inflammation in the neural system (Mizrachi, Vaknin-Dembinsky, Brenner, & Treinin, 2021).

α7 nAChRs function as calcium-conducting receptors (Uteshev, 2012). The calcium influx triggered by α7 nAChR activation facilitates the release of other neurotransmitters and depolarizes the postsynaptic cell. These neurotransmitters serve as secondary messengers, mediating various neural processes. Rapid desensitization of α7 nAChRs limits calcium influx to prevent toxicity due to excessive calcium entry (Miller et al., 2020).

Similar to other nAChRs, three distinct states are observed in α7 nAChRs' gating mechanism: the closed-channel resting state, the open-channel active state, and the closed-channel desensitized state. The resting state features no ligand binding, whereas the active state involves agonist binding. In the desensitized state, the agonist remains bound to the receptor (Noviello et al., 2021).

Channel pore opening at the single-channel level is rapid, occurring within hundreds of microseconds (Noviello et al., 2021). This makes capturing a stable open-state structure of α7 nAChRs through co-crystallization difficult. Recent research by Noviello elucidated the closed, open, and desensitized state structures of α7 nAChRs using cryo-electron microscopy (cryo-EM) (Noviello et al., 2021). Antagonist α-bungarotoxin (α-BGT) maintained the channel pore in a closed resting-like state. The highly potent α7 agonist, epibatidine, was used to capture the active open state, with the positive allosteric modulator PNU-120596 also bound to the receptors to maintain the open state. In the desensitized state, only epibatidine was bound to α7 nAChRs (Noviello et al., 2021).

The development and application of synthetic positive allosteric modulators (PAMs) for α7 nAChRs have advanced significantly in recent years. PNU-120596 ((1-(5-chloro-2,4-dimethoxyphenyl)-3-(5-methylisoxazol-3-yl)urea)) is one of the PAMs of α7 nAChRs. PNU-120596 is a type II PAM of α7 nAChRs (Uwada et al., 2020). It prolongs agonist-evoked macroscopic currents' duration and enhances agonist potency and maximal efficacy. By delaying receptor transition from an active open-channel state to a desensitized state, PNU-120596 potentiates receptor activity (Young, Zwart, Walker, Sher, & Millar, 2008). Application of PNU-120596 to α7 nAChRs results in a substantial peak potentiation of the agonist-evoked response and a reduced desensitization

transition time (Williams, Wang & Papke, 2011). PNU-120596 has become a widely used PAM *in vitro* and *in vivo* for pathophysiological studies of α7 nAChRs. It is considered a potential tool and model compound for treating various mental disorders, including schizophrenia, depression, and Alzheimer's disease. Furthermore, PNU-120596 can be administered orally, intraperitoneally, subcutaneously, and intravenously in rodent models, offering advantages for future preclinical studies. *In vivo* research has shown that PU-120596 can enhance brain circuit function (Hurst et al., 2005). However, according to our search, no clinical studies of PNU-120596 have been conducted to date. The mechanisms of these allosteric modulators, particularly the binding site, remain poorly understood. Investigating the binding site of PNU-120596 to nAChRs is crucial for drug development.

Numerous investigations have been carried out, identifying vital binding residues for PNU-120596. Research demonstrates that specific amino acids in the α7 nAChR subunit's transmembrane domain significantly influence PNU-120596's ability to enhance agonist-induced responses. Recently, Noviello acquired a stable open-state α7 nAChR cryo-EM structure with a high concentration of PNU-120596, but the bound PNU-120596 could not be resolved within this structure (Noviello et al., 2021). Collins and colleagues determined that helices TM1, TM2, and TM3 are essential for regulating PNU-120596 potentiation (Collins, Young & Millar, 2011). Consequently, researchers posited that the TMD of α7 nAChRs functions as the binding site for PNU-120596. In addition to chimeric receptor studies, electrophysiological investigations were conducted by mutating critical residues within the α7 subunits, revealing several essential residues. These residues, consistent with prior research, are located in the TMD of α7 nAChRs. Mutation studies indicate that S222 and A225 in TM1, M253 in TM2, F455, and C459 in TM4 are crucial residues for PNU-120596 binding (Young et al., 2008). These residues occupy distinct helical positions within the TMD. Among these residues, A255 and M253 result in the most significant decrease in PNU-120596 potentiation (Young et al., 2008). The active site of PNU-12059 is considered to encompass both hydrophobic and hydrophilic regions, as suggested by the chemical structure of PNU-120596. Residues S222, A225, and M253 were utilized to create the grid box for molecular docking (Young et al., 2008).

1.2.6 Regional distribution of nAChRs in human brain and the relation to receptor function

Developing novel pharmaceuticals necessitates understanding the contributions of each nAChR subtype within the human brain and their corresponding therapeutic potential. Comprehending the distribution of nAChR subtypes in the human brain aids in the creation of more subtype-specific treatment drugs (Fowler, Arends, & Kenny, 2008).

The distribution of neuronal nAChRs varies among vertebrate species (Posadas et al., 2013), but is conserved in rodent and mammalian central nervous systems (CNS) (Millar & Gotti, 2009). Table 1.1 demonstrates nAChR subunit localization in rat brains, with α4, β2, and α7 subunits predominantly found in the CNS, and α3 and β4 subunits most abundant in the peripheral nervous system (PNS) (Paterson & Nordberg, 2000). The high-affinity α4β2* receptor is the most frequently

expressed nAChR subtype in the CNS (Gotti, Zoli, & Clementi, 2006).

The β2 subunit is expressed in nearly all CNS areas, often with one of the α(2-4, 6) subunits (table 1.1) (Whiteaker et al., 2006). The α4 subunit is also widely distributed, primarily co-localizing with the β2 subunit. The highest concentrations of α4 and β2 subunits are found in the thalamus, hippocampus, and cortex (Wada et al., 1989), while only the β2 subunit is observed in the locus coeruleus area (Gotti, Moretti, Gaimarri, Zanardi, Clementi, & Zoli, 2007). Additionally, the α4β2 subtype is the predominant nAChR subtype in the striatum, cortex, superior colliculus, lateral geniculate nucleus, and cerebellum of rats (Gotti et al., 2007). Furthermore, the researchers found that mice with knocked-out α4 and β2 subunits lost their high-affinity binding sites for nicotinic agonists in the CNS (Zoli, Léna, Picciotto, & Changeux et al., 1998).

The α7 subunit is extensively distributed throughout the brain, with the highest expression levels in the cortex and hippocampus, while basal ganglia and thalamic regions exhibit minimal or no α7 subunit presence (Sher et al., 2004). Other nAChR subunits demonstrate region-specific distribution (Posadas et al., 2013). The α3 and β4 subunits are predominantly expressed in the peripheral nervous system (PNS), while in the central nervous system (CNS), they are localized to the interpeduncular nucleus, locus coeruleus, and medial and dorsal habenula regions (Baddick & Marks, 2011; Gotti et al., 2006). The α2 nAChR is present in various brain areas, such as the putamen, globus pallidus, motor and somatosensory cortex, and thalamus at microscopic levels (Baddick & Marks, 2011; Posadas et al., 2013). The α5 subunit is expressed in a limited number of CNS locations, including the substantia nigra, ventral tegmental area, medial habenula, and cortical regions. The CNS exhibits scarce distribution of α6 and β3 subunits, with the combination of these subunits found in select areas such as the substantia nigra, ventral tegmental area (VTA), locus coeruleus, retina, interpeduncular nucleus, medial habenula, and to a lesser degree, the thalamic reticular nucleus (Gotti et al., 2007). Additionally, dopaminergic neurons typically located in the striatum have been shown to express the α6 subunit (Champtiaux et al., 2002).

Table 1.1 The distribution of nAChR subtypes in the rat brain

Anatomical Regions CNS	Main nAChRs subtypes
Cortex	α4β2, α4α5β2, α7
Hippocampus	α4β2, α4α5β2,α3β4, α7
Medial habenula	α3β4, α6α5β3, α4β2,α3β3
Thalamus	α4β2, α4α3β2
Corpus Striatum	α4β2, α4α5β2,α6β2,α6α4α5β2β3, α7
Hypothalamus	α4β2, α7
Amygdala	α4β2, α4α5β2, α7
Substantia nigra	α4β2,α4α5β2,α7
Ventral tegmental area	α4β2,α4α5β2,α7
Interpeduncular nucleus	α4β2, α2β2, α3β3,α7
Locus coeruleus	α3β4,α6β2β3
Cerebellum	α4β2, α3β4, α3β2, α7

1.2.7 Function of nAChRs

Numerous physiological and pathological processes are influenced by the involvement of acetylcholine receptors (Ho, Abraham, & Lewis, 2020). In the peripheral nervous system, acetylcholine receptors regulate blood pressure, heart rate, and stimulate the gastrointestinal tract. Within the central nervous system, presynaptic nicotinic acetylcholine receptors (nAChRs) govern acetylcholine release, as well as the release of virtually all other neurotransmitters (Dajas-Bailador & Wonnacott, 2004). The presence of postsynaptic nAChRs (α7, α4β2*, and α3β4*) in specific regions suggests their crucial role in modulating cellular excitability at the postsynaptic level (Sher et al., 2004). The neurotransmitter systems regulated by neuronal nAChRs serve as therapeutic targets for pain management, epilepsy, and major neurodegenerative and psychiatric disorders, including schizophrenia, anxiety, depression, Alzheimer's disease, Parkinson's disease, and Tourette's syndrome. Furthermore, nAChR ligands are vital for addressing drug addiction (Cahill, Hurley, & Fox, 2000; Ripoll, Bronnec, & Bourin, 2004; Rucktooa et al., 2012; Shytle, Penny, Silver, Goldman, & Sanberg, 2002).

1.2.8 Binding sites on nAChRs

X-ray structures of the Lymnaea stagnalis acetylcholine-binding proteins (L-AChBPs) complexed with nicotine or carbamylcholine have facilitated the understanding of binding interactions between agonists and nAChRs at the atomic level (Celie et al., 2004). Nevertheless, AChBP and nAChR share only approximately 30% identity. Consequently, a more precise structure of nAChRs with both extracellular and transmembrane domains has been recently published to illustrate the binding site of agonists (Changeux & Christopoulos, 2016).

Numerous amino acid residues contribute to acetylcholine binding sites, organized into short sequences known as loops A, B, and C (the primary component) and loops D, E, and F (the complementary component). Loops A, B, D, and F create a hydrophobic pocket, primarily composed of aromatic residues, at the center of the interface of two neighboring subunits (Taly, Corringer, Guedin, Lestage, & Changeux, 2009).

Some subunits do not directly participate in the formation of orthosteric binding sites and are referred to as accessory subunits. These accessory subunits modify the pharmacological and biophysical characteristics of nAChRs and influence their sensitivity to allosteric modulators. For maximal nAChR activation, at least two binding sites should be occupied by acetylcholine in heteromeric receptors. In homomeric nAChRs, such as native α7 receptors, acetylcholine should bind to at least three binding sites to achieve maximal activation (Kuryatov, Onksen, & Lindstrom, 2008; Moroni, Zwart, Sher, Cassels, & Bermudez, 2006).

In addition to the orthosteric binding site, binding sites for allosteric modulators on nAChRs have also been identified. These sites can be found in the ion channel, the extracellular domain, the cytoplasmic domain, and the transmembrane domain. However, the binding sites of these positive allosteric modulators (PAMs) exhibit similarities among various subtypes due to the conservation

among these subtypes (Collins et al.,2011; Gulsevin, Papke, & Horenstein, 2020).

1.2.9 Human neuronal diseases related to nAChRs

1.2.9.1 nAChRs-and Alzheimer's Disease

Alzheimer's disease (AD) accounts for approximately 70% of all dementia cases, a debilitating disorder prevalent in aging populations (Tarawneh & Holtzman, 2012). AD's primary clinical manifestation is the gradual and insidious decline of memory. Initially, patients experience mild cognitive impairment (MCI), an early stage of AD. As the disease progresses, cognitive difficulties that disrupt daily life emerge. In AD's later stages, behavioral changes and hallucinations occur, with seizures potentially arising (Lane, Hardy, & Schott, 2018).

Neuropathological hallmarks of AD include extracellular amyloid β peptide (Aβ) accumulation in plaques, intracellular tau protein deposits, neuronal loss, and substantial synaptic loss (Murphy & LeVine, 2010). Additionally, studies of AD patients' brains have revealed significant white matter loss and decreased basal forebrain cholinergic neurons. The cholinergic neurons in the central nervous system are organized into dense nuclei with extensive projections (Grothe et al., 2010).

The accumulation of Aβ protein is a major hypothesis for AD development. α7 nAChRs contribute to Aβ protein deposition. In brain samples from AD patients, researchers demonstrated α7 subunit co-localization with Aβ (H. Y. Wang et al., 2000). Immunoprecipitation and Western blot analysis confirmed the robust and specific interaction between Aβ protein and α7 subunits, revealing that Aβ protein immunoprecipitates with α7 subunits (Lombardo & Maskos, 2015; H. Y. Wang et al., 2000).

1.2.9.2 nAChRs and schizophrenia

In addition to Alzheimer's disease, nAChRs are implicated in schizophrenia. Schizophrenia, a complex psychiatric disorder, affects approximately 1% of the global population. This condition is characterized by three primary symptom clusters: positive symptoms (e.g., delusions, thought disorders, hallucinations), negative symptoms (e.g., anhedonia, blunted affect, social withdrawal), and cognitive impairments (e.g., attention and working memory deficits) (Balhara & Verma, 2012). Abnormalities in nAChR signaling have been associated with symptoms observed in schizophrenic patients (Jones, Byun, & Bubser, 2012). nAChR antagonists, such as scopolamine and mecamylamine, have shown effects on cognitive dysfunction in animals and humans.

Conversely, nAChR agonists and acetylcholinesterase inhibitors (AchEIs) have demonstrated cognitive function improvement in schizophrenia patients (Jones et al., 2012). Both mAChR and nAChR agonists were found to ameliorate some aspects of positive and negative symptoms in schizophrenic patients, as well as deficits in attention and memory (Jones et al., 2012). Altogether, these experimental and clinical findings support the notion that schizophrenia symptoms may be

related to aberrant nAChR signaling.

1.2.9.3 nAChRs and MDD

The association between nAChRs and depression is substantial (Philip et al., 2010). This concept was initially postulated in the early 1970s by Janowsky. Based on this hypothesis, MDD arises from excessive cholinergic activity and a subsequent imbalance between the cholinergic and adrenergic systems (Janowsky, David, el-Yousef, & Serkerke, 1972).

Epidemiological investigations indicate that individuals with mental disorders exhibit a higher smoking prevalence than the general populace. Patients experiencing nicotine withdrawal demonstrate elevated rates of depression and anxiety compared to the general population. Asharani et al. (2020) assert that nicotine self-administration (e.g., smoking or nicotine patch use) represents a self-medicating attempt for MDD patients (Asharani et al., 2020). Nicotine has been shown to enhance cognitive function in individuals with mental disorders (Philip et al., 2010). Nevertheless, nicotine is an inadequate therapeutic agent due to its short duration of action. Consequently, nicotine should be administered repeatedly and frequently for its antidepressant effects. Additionally, continuous nicotine consumption exacerbates cardiovascular risk. Depressive symptoms typically manifest immediately following smoking cessation (Lembke, Johnson, & DeBattista, 2007).

Varenicline, a prototypical nicotinic acetylcholine receptor agonist, has been considered as a compound with potential antidepressant effects. Rollema and colleagues investigated whether varenicline can enhance the antidepressant effects of sertraline SSRIs in mice, as well as its effect on forced swim tests (Rollema et al., 2009). The experimental group of mice received varenicline alone, sertraline alone, or both varenicline and sertraline combined. Amitriptyline was administered to the mice in the control group. Amitriptyline belongs to the TCA family, while sertraline belongs to the SSRI family. Each intervention group was evaluated and compared with the control group in order to determine whether it had an antidepressant effect. In the forced swim test, varenicline and sertraline monotherapy significantly improved antidepressant performance. Compared to the amitriptyline-controlled group, these three drugs had slightly lower antidepressant effects. However, when varenicline was used as an adjunct therapy to sertraline, experimental performance in the forced swimming test improved, surpassing the effect observed in rats treated with amitriptyline. The researchers suggested that varenicline's augmentation effect is inversely dose-dependent, as more significant augmentation-like effects were observed at lower varenicline doses (Rollema et al., 2009).

In the preceding section, we have illustrated the structure, gating mechanism, and distribution of nAChRs in the human brain, as well as their association with various mental illnesses. Of all the subtypes of nAChRs, particular attention has been given to the α4β2* and α7 subtypes, owing to their preponderance in the human brain. This emphasis is warranted given the established functional roles of these two subtypes in mediating various cognitive processes, including learning, memory, and attention, as well as their involvement in several neuropsychiatric disorders.

1.3 Mecamylamine

1.3.1 Introduction

Mecamylamine is a racemic mixture composed of (S)-(+)- and (R)-(-)-mecamylamine (figure 1.2). The (S)-(+)-mecamylamine is also known as dexmecamylamine, the dextrorotary enantiomer of mecamylamine (Papke, Sanberg, & Shytle, 2001). Figure 1.2 illustrates the structures of both dexmecamylamine and (R)-(-)-mecamylamine. Mecamylamine has a molecular weight of 167.29 and a pKa value of 11.2. Over 99% of the compound exists in a protonated state in the human body, with a pH of approximately 7.4 (Arias et al., 2010).

Initially developed for hypertension treatment in the 1950s, mecamylamine became the first oral anti-hypertensive medication. Mecamylamine demonstrated its ability to lower blood pressure and prevent seizures induced by nicotine overdose. However, due to the extensive ganglionic side effects when administered at anti-hypertensive doses (30-90 mg/day) (Shytle et al., 2002), mecamylamine was withdrawn from the hypertension market.

In subsequent investigations, mecamylamine exhibited anti-addictive and pro-cognitive properties at low pharmacological doses (2.5-5 mg b.i.d.). Mecamylamine has been demonstrated to substantially mitigate the physiological consequences of nicotine and alleviate depressive symptoms during nicotine withdrawal (Nickell, Grinevich, Siripurapu, Smith & Dwoskin, 2013). In contrast to high mecamylamine doses (30-90 mg/day), patients administered lower doses (2.5-5 mg b.i.d.) did not experience severe side effects. Mecamylamine exhibits antidepressant-like effects at lower doses, prompting increased interest in its development as a potential therapeutic target for various neurological disorders, including major depressive disorder (MDD) (Lindsley, 2010).

Mecamylamine comprises two distinct enantiomers, with differing pharmacological functions for (S)-(+)-mecamylamine and (R)-(-)-mecamylamine. In comparison to (R)-(-)-mecamylamine, (S)-(+)-mecamylamine (also referred to as dexmecamylamine) demonstrates more potent inhibitory effects on central neuronal nicotinic acetylcholine receptors (nAChRs) in studies (Papke et al., 2001; Nickell et al.,2013). The therapeutic efficacy also reflects the functional disparities between these isomers. For instance, as an antiepileptic agent, (S)-(+)-mecamylamine proved more effective than (R)-(-)-mecamylamine (Fedorov, Benson, Graef, Lippiello, & Bencherif, 2009; Papke et al., 2001). Mecamylamine exhibits high selectivity for nicotinic acetylcholine receptors over other Cys-loop receptors. Nonetheless, as a non-selective antagonist, mecamylamine inhibits all native nAChR subtypes. Presently, it is extensively employed in research to elucidate nAChR functions in central and peripheral synaptic transmission (Fedorov et al., 2009).

(a)

(b)

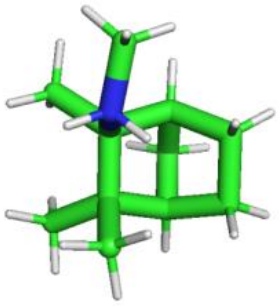

Figure 1.2 Molecular structures of (S)-(+)-mecamylamine (A) and (R)-(−)-mecamylamine (B) in the protonated state.
Nitrogen atoms are represented in blue, hydrogen in gray, and carbon in green. Ligands are depicted using stick mode, with aliphatic hydrogen atoms shown in white.

1.3.2 Binding site of mecamylamine to $(\alpha4)_2(\beta2)_3$ nAChRs

Mecamylamine's antagonistic effect on native nAChRs within autonomic ganglia constitutes a straightforward obstruction of open channels. Mecamylamine is classified as an open channel inhibitor (Bacher et al., 2009). Various investigations offer a novel characterization of the potent nAChRs blockade in chromaffin cells elicited by mecamylamine. Mecamylamine's impact can be rapidly diminished through its combination with nicotine (Giniatullin et al., 2000). Mecamylamine is thought to be confined and ensnared within nAChRs, later being released upon channel reopening. These findings collectively suggest that mecamylamine functions as an nAChRs channel blocker (Giniatullin et al., 2000). As a crucial non-selective nAChRs channel inhibitor, the binding site of mecamylamine ((R)-mecamylamine and (S)-(+)-mecamylamine) to nAChRs has been identified in numerous studies (Bondarenko Targowska-Duda, Jozwiak, Tang, & Arias, 2014; Papke et al., 2001;Giniatullin et al., 2000).

Bondarenko's research discovered that mecamylamine's enantiomers possess a luminal binding site at the base of the TMD. As a simple channel inhibitor, it is logical to anticipate the existence of a lower luminal binding site (Bondarenko et al., 2014). Bondarenko depicted the binding sites of both mecamylamine enantiomers to the $(\alpha4)_3(\beta2)_2$ and $(\alpha4)_2(\beta2)_3$ nAChRs. They utilized purified TMD of human-origin α4 and β2 subunits to attain this goal. Critical residues impacted by mecamylamine binding were investigated using a high-resolution nuclear magnetic resonance (NMR) test. Additionally, supplementary [^{3}H] imipramine competition experiments were conducted to examine whether the mecamylamine isomer binds to the [^{3}H] imipramine binding site (Bondarenko et al., 2014).

The focus is on (S)-(+)-mecamylamine, as prior research indicates that it is the enantiomer with higher efficacy in preventing nicotine-induced seizures and reducing depressive symptoms compared to the (R)-(-)-enantiomer (Newman, Manresa, Sanberg & Shytle, 2001; Bondarenko et

al., 2014). The NMR experiment outcomes identified several specific residues in the ACh TMD involved in (S)-(+)-mecamylamine binding. All these residues exhibited a substantial chemical shift change upon (S)-(+)-mecamylamine binding. The residue chemical changes illustrate the specific residues that directly or indirectly affect (S)-(+)-mecamylamine binding. The results indicate that α4-L235, α4-L239, and β2-V230 at TM1, β2-G238 and β2-K260 at TM2, β2-L287 at TM3, and β2-T449 at TM4 are involved in binding procedures. Further molecular docking should be performed at this binding site to determine the (S)-(+)-mecamylamine binding position (Bondarenko et al., 2014).

In the [^{3}H] imipramine competition experiments, the findings indicate that neither enantiomer of mecamylamine binds to the specific [^{3}H] imipramine binding site in $(\alpha4)_3(\beta2)_2$ and $(\alpha4)_2(\beta2)_3$ nAChRs in the resting or desensitized states. Furthermore, the NH values are significantly lower than unity (~0.5), suggesting a negative cooperative interaction between imipramine and mecamylamine enantiomers. Consequently, the mecamylamine binding site does not overlap with the imipramine binding sites in the $(\alpha4)_3(\beta2)_2$ and $(\alpha4)_2(\beta2)_3$ (Bondarenko et al., 2014). Table 1.2 presents the critical residues identified by chemical shift or peak intensity in high-resolution NMR after renumbering.

Table 1.2: Essential residues for binding of dexmecamylamine to $(\alpha4)_2(\beta2)_3$ nAChRs (PDB:5KXI) detected by chemical shift or peak intensity in high-resolution NMR after renumbering.

Approaches	Receptor	Crucial Residues
High resolution NMR: Chimical shift or peak intensity	$(\alpha4)_2(\beta2)_3$ nAChRs PDB:5KXI	α4-TMD： TM1：L237，V238，L241 TM2：**T250，G246** β2-TMD： TM1：V230 TM2：**G238，K260** TM3：I287 TM4：T449

1.3.3 Binding site of mecamylamine to α7 nAChRs

The α7 nAChR, a homopentameric ligand-gated ion channel within the Cys-loop receptor superfamily, is found in the human brain, central nervous system, and other tissues. The α7 nAChRs exhibit a low probability of opening (C. R. Yu & Role, 1998), high calcium permeability (Séguéla, Wadiche, Dineley-Miller, Dani, & Patrick, 1993), and rapid desensitization (Couturier et al., 1990). This receptor has been targeted for the treatment of schizophrenia (Martin & Freedman, 2007), Alzheimer's disease (Wallace, Ballard, Pouzet, Riedel, & Wettstein, 2011), and major depressive disorder (Mineur, Mose, Blakeman, & Picciotto, 2018). Additionally, the α7 receptor is involved in the cholinergic anti-inflammatory pathway, with α7 receptor ligands demonstrating anti-inflammatory activity *in vitro* and *in vivo* (Gulsevin et al., 2020).

Crucially, α7 nAChRs have been implicated in major depressive disorder (Zhang et al., 2016). Prior research has examined the binding affinity of mecamylamine for α7 nAChRs. The findings reveal that pre- and co-application of 10 μM mecamylamine effectively inhibits the activation of α7 receptors in oocytes, reducing peak currents by 95% during mecamylamine application. This outcome suggests that mecamylamine interacts with α7 nAChRs and serves as an antagonist for these receptors (Miller et al., 2020).

In the present section, the configuration of dexmecamylamine and its corresponding binding site on $(\alpha4)_2(\beta2)_3$ nAChRs and α7 nAChRs, in its capacity as a channel blocker, were expounded. The aforementioned details are poised to serve as a valuable foundation for upcoming molecular modeling inquiries.

1.4 Aim and objectives

nAChRs are considered a potential target for antidepressant drugs. Both preclinical and clinical findings suggest that α7 nAChR antagonists exhibit considerable potential in depression treatment. Numerous studies have confirmed the antidepressant effects of mecamylamine, an agonist and antagonist targeting nAChRs. Lippiello et al. (2008) assessed the antidepressant properties of a mecamylamine enantiomer, (S)-(+)-mecamylamine (dexmecamylamine), in rodent models, finding that dexmecamylamine can enhance performance in forced swimming and behavioral despair tests, thereby exhibiting potential antidepressant effects (Lippiello et al., 2008). Although animal models demonstrate significant antidepressant effects, the impact of dexmecamylamine on humans remains contentious. Our literature search revealed no meta-analyses investigating the antidepressant effect of dexmecamylamine on depression. In addition, existing meta-analyses on nAChRs and depression do not mention dexmecamylamine. Consequently, we conducted the first meta-analysis to elucidate the antidepressant effect of dexmecamylamine.

Furthermore, nAChRs are composed of various subunits and exist in multiple subtypes. These receptors undergo three states during the gating process (open state, closed state, and desensitized state), which result in a broad range of functional profiles. The nAChR ion channel is a potential pharmacological target for drugs. Techniques such as electrophysiology, mutagenesis, and photoaffinity labeling have identified the ion channel as a site for receptor channel blockers. A group of compounds binds within the channel pore when the receptor is in the open state. The channel blocker binding site is the target of numerous pharmacologically and clinically significant drugs. Thus, examining the selectivity and affinity of a drug molecule is critical. Our research indicates that blocking nAChRs, particularly α7 nAChRs, may produce antidepressant effects. We selected dexmecamylamine, a well-known nAChR channel blocker with potential antidepressant properties, for study. Dexmecamylamine has demonstrated promising results in various animal models of anxiety and depression. However, prior clinical research on mecamylamine's antidepressant effect has produced inconsistent findings. Consequently, our project's primary objective is to evaluate mecamylamine's efficacy in treating depression through meta-analysis. Investigating mecamylamine's antidepressant efficacy and structure will enable us to explore how nAChR ligands address depression.

Several dexmecamylamine binding site locations on $(\alpha4)_2(\beta2)_3$ nAChRs have been identified in previous research (Bondarenko et al., 2014). However, the binding site of dexmecamylamine to α7 nAChRs remains uncertain. Moreover, as previously discussed, α7 nAChRs represent vital treatment targets for major depressive disorder (MDD). Our project's second aim is to employ computational studies to investigate the binding position of dexmecamylamine to α7 nAChRs. Understanding dexmecamylamine's binding behavior to α7 nAChRs will facilitate further optimization of its structure and the development of innovative antidepressant medications. In this project, we utilized molecular docking and molecular dynamics simulation to study dexmecamylamine binding to α7 nAChR.

In conclusion, there remains a significant gap in the treatment of MDD, with patients often experiencing drug resistance, poor efficacy, and adverse effects. Several studies suggest that adjunct therapy shows promise as a means of avoiding drug resistance. As such, dexmecamylamine was introduced, and its efficacy in the human body was evaluated through several clinical trials. However, the results of these studies were inconclusive regarding the antidepressant effect of dexmecamylamine. To address this, we conducted a meta-analysis in our study. Additionally, we illustrated the binding site of dexmecamylamine and PNU-120596 to the open state α7 nAChRs in further research, with the detailed method outlined below.

Chapter 2

Theory and methods

2.1 Theory

2.1.1 Meta-analysis

Medical professionals encounter the demanding task of staying current with the vast number of medical studies published annually. Furthermore, biases may emerge if they depend solely on individual study findings, which might not be reproducible (Murad, 2014). Clinical trial outcomes can be affected by various factors, such as sample size, demographic features, treatment duration, and administration route (Yanagawa, Tam, Mazine, & Tricco, 2018). Hence, performing a systematic review of multiple randomized controlled trials or epidemiological studies is deemed essential for overcoming these constraints and offering evidence across diverse medical disciplines (Lau, Schmid, & Chalmers, 1995).

A crucial aspect of systematic reviews is the meta-analysis, which entails the quantitative synthesis of results from numerous clinical studies employing comparable methodological approaches and addressing identical research questions (Ahn & Kang, 2018). Statistically, a meta-analysis is considered more dependable than individual studies for detecting effects. In evidence-based medicine, it is recognized as the highest-quality evidence since it generates the least bias and the most accurate estimate of a clinical issue (Murad, 2014). Consequently, a meta-analysis represents an objective and quantitative synthesis of study outcomes, augmenting the statistical robustness and precision of estimated effects by consolidating and examining the conclusions of prior investigations.

Moreover, meta-analysis plays a critical role in counteracting the limitations of small sample sizes and insufficient statistical power (Egger, Smith, & Phillips, 1997). It enables the evaluation of source heterogeneity and the identification of factor-associated subgroups (Gøtzsche, 2000), with additional subgroup analyses performed in cases where the heterogeneity is significant. By integrating data from multiple studies, meta-analysis allows for a more accurate estimation of effect size and provides compelling evidence concerning the intervention's influence on the disease. As such, meta-analysis serves as an essential instrument in addressing the issues that arise due to small sample sizes.

Nevertheless, meta-analysis has certain drawbacks that should be taken into account. One major limitation is the potential inclusion of various study types such as randomized controlled trials, single-arm studies, and open-label studies, which can result in discrepancies in the effect size owing to heterogeneity among the studies (Stevens & Wu, 2007). To tackle this issue, heterogeneity among the chosen studies are required to be measured, and if it is high, a subgroup or sensitivity analysis should be conducted to explain the heterogeneity (Bailar, 1997).

Another significant challenge in performing a meta-analysis is the inclusion of low-quality papers, which can lead to biased and inaccurate results (Sharpe, 1997). Therefore, it is vital to establish specific inclusion and exclusion criteria for the meta-analysis and implement a comprehensive quality assessment process to ensure the validity and reliability of the findings.

2.1.2 Glide docking

Drugs show their effects by binding to their corresponding targets and inducing physiological activity (Berger & Iyengar, 2011). The drug-receptor complex is formed through a variety of interactions, including van der Waals forces and hydrogen bonds, between the drug and residues of the receptor. Although many compounds are considered potential drugs, identifying them using traditional pharmacological experimental methods can be a time-consuming process. Therefore, computational technologies have been introduced into modern drug development (Meng, Zhang, Mezei & Cui, 2011).

Protein-ligand interactions are essential for numerous physiological processes in the human body (Berger et al., 2011). Molecular docking, a virtual computational method, has become an indispensable tool for studying the interactions between small molecules (ligands) and receptors. By predicting binding modes and estimating affinity, molecular docking enables further investigations into pharmacological activities and aids in the design of novel drugs. Computer-aided drug design (CADD) involves the use of computational simulations, calculations, and predictions for drug design and optimization, and has recently become one of the most prevalent methods for drug design and improvement (Guedes, de Magalhães, & Dardenne, 2014; W. Yu & MacKerell, 2017). Molecular docking is a crucial component of CADD, utilizing computer technology to dock molecules into receptor binding sites and calculating physical and chemical parameters of binding force to predict the interactions (such as ionic interactions, hydrogen bonds, and van der Waals interactions) between the ligand and receptor (G. Chen, Seukep, & Guo, 2020).

Molecular docking was first developed based on the Lock-Key model principle, which Fisher hypothesized in 1894 (Salmaso & Moro, 2018). The lock-key model was applied to understand the relationship between receptors and ligands. In this model, both the ligand and receptor are regarded as rigid bodies, and the structures do not undergo any conformational changes during docking. In the rigid docking calculation, the conformation of the ligands and receptors are regarded as rigid and does not change during the docking process. The advantage of rigid docking calculation is that it is fast. This model explains the binding procedures precisely if there are small conformational changes during docking. However, if there are significant conformational changes during the binding process, it is hard to investigate and explain using the Lock-Key model (Salmaso et al., 2018).

Because of these limitations, the induced fit theory was introduced by Koshland in 1958 (Koshland, 1958). In this theory, the spatial conformation of the active site in the receptor changes after interacting with the ligand. Both ligands and proteins are considered flexible during molecular docking. The result would be more precise if the induced fit theory were used in the drug molecule-receptor interaction investigation. However, there are some disadvantages to flexible docking. It takes a long time to calculate and requires the high performance of the computer because of the large number of atoms in the system. A third docking method, semi-flexible docking, was subsequently developed. Here, the receptor is considered rigid, whereas the ligand is allowed to change within a given range. Semi-flexible docking is the most common calculation method and

has been widely used in molecular docking, especially for binding of small molecules to proteins.

Molecular docking, which is based on the Lock-Key model principle proposed by Fisher in 1894, has been used to understand the relationship between receptors and ligands. In this model, both the receptor and the ligand are considered rigid bodies, and the structures remain unchanged during the docking process. The advantage of this method, known as rigid docking, is its computational speed. However, rigid docking has limitations in explaining binding processes that involve significant conformational changes (Salmaso et al., 2018).

To overcome these limitations, the induced fit theory was introduced by Koshland in 1958 (Koshland, 1958). According to this theory, the spatial conformation of the receptor's active site changes after interacting with the ligand. Both ligands and proteins are considered flexible during molecular docking in the induced fit model. The use of this theory can result in more precise investigations of drug molecule-receptor interactions (Silva, Bowman, Sosa-Peinado & Huang, 2011). However, flexible docking requires longer computational time and high-performance computing due to the large number of atoms in the system.

A third method, semi-flexible docking, was subsequently developed, in which the receptor is considered rigid, while the ligand is allowed to change within a specified range. Semi-flexible docking is the most common calculation method and has been widely used in molecular docking studies, especially for the binding of small molecules to proteins (Zhang, Li, Yu & Jin, 2022).

Molecular docking is the most commonly used tool for computer-aided drug design (CADD). However, the docking result and procedures involve many approximations. Moreover, the docking result provides information only on the ligand-protein interaction at a specific moment in time. In contrast, molecular dynamics (MD) is a computational method that can study the interaction between the ligand and protein over a range of time (Hollingsworth, 2018). Therefore, MD should be used as a follow-up study to the complex obtained from molecular docking. By examining parameters such as RMSD and FEL, the stability and structural constancy of the system can be evaluated in MD, providing additional information about the complex.

Although molecular docking has limitations, it remains a valuable tool for CADD. MD can be used to complement the results of docking studies, and the combination of these techniques can provide a more complete understanding of the ligand-protein interaction.

2.1.3 Molecular dynamics simulations

Molecular dynamics (MD) simulation is an approach used to monitor the movement of individual atoms within a protein system over time (Hollingsworth & Dror, 2018). Alder and Wainwright conducted the first MD simulation (Alder & Wainwright, 1957), utilizing instantaneous collisions to examine the solid-fluid transition in a system of hard spheres (Alder et al., 1957). Since then, MD simulation has undergone extensive development and become a valuable tool in numerous scientific fields. Martin Karplus, Michael Levitt, and Arieh Warshel were awarded the Nobel Prize in 2013 for their contributions to developing multiscale models for complex chemical systems. The

MD approach can simulate various biochemical processes, ranging from ligand binding to protein folding, and assists in investigating atomic positions with femtosecond temporal resolution (Karplus & McCammon, 2002). MD simulation can help predict how molecules will react to alterations in the system, such as ligand binding, ligand removal, mutation, and protonation. MD simulation should be performed on experimental structural data obtained through biological techniques, including X-ray crystallography, cryo-EM, and NMR spectroscopy (Hollingsworth et al., 2018).

Molecular docking is now frequently employed to circumvent the trial-and-error nature of drug discovery and significantly enhance drug discovery efficiency (Meng et al., 2011). Molecular docking does not account for the dynamic changes within the system. Consequently, the MD simulations method has been developed to assess the efficacy of potential drugs with flexible targets and consider target flexibility over a specific time range. Protein structure was once believed to be the primary determinant of protein function. However, mounting evidence suggests that proteins are entirely or partially intrinsically disordered (Charlier et al., 2017). As a result, focus should be placed not only on the static structure but also on protein motion. MD simulation enables protein movement, allowing for the visualization of conformational changes over time (Koshland, 1958). MD simulations have become an essential method for selecting the most potent compound in drug discovery. Furthermore, MD simulations may aid in understanding compound-target interactions and effectively optimizing lead compounds.

The fundamental principle of molecular dynamics (MD) simulations involves assigning initial positions to all atoms within the protein system and computing their positions after a specific time range (Hollingsworth et al., 2018). Newton's laws of motion are employed to predict the spatial positions of atoms over time. This calculation step is performed iteratively, using force to update position and velocity in each calculation. After the calculation process, a trajectory file is obtained, which is a three-dimensional coordinate file describing the position of each atom at every point during the simulation time range (Hollingsworth et al., 2018). MD simulations serve as powerful tools for protein systems since capturing the position and motion of each atom at every moment in a time duration by experimental techniques is not feasible. Moreover, the impact of molecular perturbations, such as mutations and modifications, can be identified by comparing simulation performance under different perturbations. MD simulation can also aid in recognizing the default binding pocket of an agonist and antagonist by comparing simulation performance with and without ligand binding to the pocket (Hollingsworth et al., 2018).

A force field characterizes the chemical and resultant interactions within the system, including interaction of the bond, bond angles, and torsional angles, and non-bond interactions, such as van der Waals and Coulombic. Several force fields are commonly used for the biomacromolecule MD simulation, such as CHARMM, AMBER, and OPLS (Lin & MacKerell, 2019). Force field selection depends on the protein system features, such as solvent and ions. Except for the protein system, solvents are calculated in the entire system for MD simulations, and each force field is designed to fit a specific solvent system, making correct force field selection in MD simulation essential (Zapletal et al., 2020).

The fundamental theory of MD simulation is as follows: considering a system of n molecules or atoms, the total energy at this time comprises internal molecular potential and kinetic energy. We regard the total potential energy of the positions of molecules or atoms as V. This includes the intermolecular interaction of van der Waals force V_{vdW} and molecular potential energy inside.

Therefore, $V=V_{vdW}+V_{int}$. (1)

Van der Waals forces for molecular interactions can be expressed by the superposition of van der Waals forces between each pair of atoms that constitute the molecule:

$V_{vdw}=V_{12}+V_{13}+...V_{1n}+V_{23}+V_{24}+.....=\sum_{i=1}^{n=1}\sum_{j=i+1}^{n} v_{ij}(r_{ij})$ (2)

r_{ij} is the distance between atoms I and j; The total internal potential energy of Vint was represented as summation of various types of internal coordinates between atoms (such as bond extension and dihedral Angle torsion).

According to classical mechanics, the force on atom i in the simulated system is the potential energy gradient.

$\overrightarrow{Fi}=-\Delta_i V=-(\overrightarrow{i}\frac{\partial}{\partial xi}+\overrightarrow{j}\frac{\partial}{\partial yi}+\overrightarrow{k}\frac{\partial}{\partial i})$(3)

Accordingly, the acceleration of atom i can be obtained by Newton's equation of motion as follows:

$\overrightarrow{a_i}=\frac{\overrightarrow{Fi}}{m_i}$ (4)

The following equations can predict the velocity and the corresponding position after the time (t).

$\frac{d^2}{dt^2}\vec{r_i}=\frac{d}{dt}\vec{v_i}=\vec{a_i}$ (5)

$\vec{v_i}=\vec{v_i^0}+a_i t$ (6)

$\vec{r_i}=\vec{r_i^0}+v_i^0+\frac{1}{2}\vec{a_i}t^2$ (7)

It can be seen from the above formula that the basic MD theory relies on Newton's laws of motion. First, the total potential energy, V, is calculated based on each atom's position. Equations (3) and (4) determine the van der Waals force and acceleration on each atom, respectively. Assuming t is a very short time interval, equation (7) calculates the velocity and position of each atom after each time scale. Repeated iterations obtain the position, velocity, and acceleration of each molecule or constituent atom at different times, known as a trajectory. Trajectory files facilitate further calculations of root mean square deviation (RMSD) and extraction of representative structures. Interactions in the protein system are complex, and the motion of molecules cannot be calculated using general analytical methods. Common algorithms include Gear and Verlet algorithms, with the latter often used in MD simulations (Verlet, 1967). Verlet algorithm modifications, such as the

Leap-Frog Method and Velocity-Verlet Method, improve efficiency. Our program employed the leap-frog method for MD simulations.

In the previous discussion, the integration of Newton's equations of motion enabled the examination of a system's constant-energy surface. However, maintaining constant temperature and pressure during molecular simulations is essential for emulating experimental conditions. This can be accomplished by generating and employing various statistical ensembles, depending on the fixed state variables (e.g., energy E, volume V, temperature T, pressure P, and number of particles N). The most frequently utilized ensembles comprise the constant-temperature, constant-volume (NVT) ensemble, the constant-temperature, constant-pressure (NPT) ensemble, and the constant-energy (NVE) ensemble (Allen & Tildesley, 1987; Bosko, Todd & Sadus, 2005). Although employing the NVE ensemble during MD simulations conserves energy, it is not advised for equilibration as the system necessitates energy flow to attain the desired temperature. The NPT ensemble, which adjusts the volume to control both temperature and pressure, is a prevalent choice for equilibration. In contrast, the NVT ensemble regulates temperature using a temperature-bath coupling rate and is optimal for heating a system in a heat bath that is sufficiently large to encompass the entire system (Andersen, 1980). In this research, we employed an NPT simulation followed by an NVT simulation to manage both the pressure (volume) and temperature of the system, achieving the desired ideal conditions ((Hopkins, Le Grand, Walker, & Roitberg, 2015).

2.2 Methods

2.2.1 Meta-analysis

2.2.1.1 Search ctrategy

Pertinent information was obtained from three databases: MEDLINE, the Cochrane Library, and Embase. MEDLINE was accessed via PubMed (https://pubmed.ncbi.nlm.nih.gov/), while the Cochrane Library (www.CochraneLibrary.com) was used to search the Cochrane database. The reference lists were also manually examined for any relevant supplementary data. Additionally, unpublished clinical trials on the clinical trial registration platform (www.clinicaltrials.gov) were screened. A search query incorporating [mecamylamine*, TC-5214, or dexmecamylamine] and [depression*, depressive disorder*, or depressed] was devised for exploration. An asterisk indicates the utilization of MeSH terms. Complete search terms can be found in table 2.1.

Upon completing the database search, all initial results were imported into EndNote X9. Duplicates were removed using EndNote. Subsequently, two reviewers (YTY and YJL) assessed the titles and abstracts of the gathered papers. Papers meeting the inclusion and exclusion criteria were retained. In cases of disagreement between the two reviewers, a third party was consulted. Articles irrelevant to the subject matter were discarded, as were systematic reviews, editorials, and case studies. Following the preliminary screening, the full texts were meticulously reviewed by the two

reviewers (YTY and YJL), and any articles not adhering to the inclusion and exclusion criteria were excluded.

Table 2.1: The search string of meta-analysis

Data base	Item	Searching terms
MEDLINE	1	Mecamylamine[Mesh]
	2	((mecamylamine[Title/Abstract]) OR (dexmecamylamine[Title/Abstract]))) OR (TC-5214 [Title/Abstract])
	3	Depression [Mesh] OR Depressive Disorder [Mesh]
	4	Depression[Title/Abstract] OR depressive disorder[Title/Abstract] or depressed[Title/Abstract]
	5	#3 OR #4
	6	#1 OR #2
	7	#5 AND #6
Embase	1	'depression' exp
	2	'depression' ab.ti OR 'depressive' ab.ti OR 'depressed' ab.ti
	3	'mecamylamine' exp
	4	'mecamylamine' ab.ti OR 'dexmecamylamine' ab.ti OR 'tc-5214' ab.ti
	5	#1 OR #2
	6	#3 OR #4
	7	#6 AND #7
Cochrane	1	MeSH descriptor:[Depressive disorder]
	2	MeSH descriptor:[Depression]
	3	(depression):ti.ab.kw OR (depressed): ti.ab.kw OR (depressive dsorder) ti.abkw
	4	MeSH descriptor: [Mecamylamine]
	5	(mecamylamine) ti.ab.kw OR (dexmecamylamine) ti.ab.kw OR (TC-5214) ti,ab.kw
	6	#1 OR #2 OR #3
	7	#4 OR #5
	8	#6 AND #7

2.2.1.2 Inclusion criteria

The following criteria were met by the included studies:

1. Studies should be conducted on humans;
2. Interventions in the studies should encompass mecamylamine or dexmecamylamine (administered as either monotherapy or adjunct therapy);
3. Studies should be acute-phase;
4. Participants in the studies should be diagnosed with Major Depressive Disorder (MDD) or depression.

2.2.1.3 Exclusion criteria

Studies were excluded if they exhibited the following characteristics:

1. The population of the studies also included animal models or cadavers;
2. Studies were published as case studies, systematic or narrative reviews, editorials, commentaries, or opinion-based articles;
3. Study participants were diagnosed with other psychological disorders such as anxiety, schizophrenia, or bipolar disorder. The combination may impact the evaluation of therapeutic effects.

2.2.1.4 Assessment of methodological quality and risk of bias

Systematic reviews employ methodologies that minimize bias across all collected studies that meet predetermined eligibility criteria. Evaluating the quality of included studies is crucial, with "quality" often dependent on a study's design, conduct, and analysis. Numerous resources exist for appraising the quality of randomized trials, such as metrics and checklists. In 2005, the Cochrane Collaboration's methodology groups introduced the Cochrane Collaboration's Tool for Assessing Risk, a novel approach to evaluating the quality of randomized trials, which quickly gained popularity (Higgins et al., 2011). Two reviewers (YTY and YJL) assessed the risk of bias in the included studies. Two scales were employed to evaluate the risk of bias in these studies, with the Cochrane Collaboration's Tool for Assessing Risk of Bias test form being utilized first to gauge each study's quality (Higgins et al., 2011). Each assessment item was evaluated based on the study's content, categorizing studies into 'high-risk bias,' 'unclear,' and 'low-risk bias' based on descriptions in each item. The results were visualized using a risk of bias graph and a risk of bias summary created with RevMan 5.3 software.

In addition to the Cochrane Collaboration's Tool for Assessing Risk, the PEDro assessment scale was applied to evaluate the quality of the included studies. The PEDro scale is a widely used rating system to assess the methodological quality of clinical trials (Maher et al., 2003). Originally designed to assess the validity and quality of clinical trials focusing on physiotherapies, the PEDro scale has been increasingly employed in systematic reviews and meta-analyses across various fields of medical research to provide validity assessments (Elkins, Moseley, Sherrington, Herbert, & Maher, 2013). The PEDro scale comprises ten aspects (11 items), including randomization, allocation concealment, baseline similarity, blinding of subjects, blinding of therapists, blinding of the assessor, patient adherence to the primary outcome, intention-to-treat analysis, intergroup data statistics for at least one key outcome, and variability assessment for at least one key outcome. Item one is an external validity item assessing eligibility criteria and source, and is not included in the final score. A clinical study's quality is described by its total PEDro scale score, with one point given for each affirmative answer, and zero for a negative response. The PEDro scale's maximum score is 10 (summing items 2 to 11), with higher scores indicating superior quality.

Two independent reviewers assessed the studies' quality using the PEDro scale. The third reviewer will be induced if conflict happens. Scores below four are considered 'poor,' four to five as 'fair,' six

to eight as 'good,' and nine to ten as 'excellent.' Each study was evaluated using these criteria.

2.2.1.5 Data extraction

Data from the included studies were independently extracted by two reviewers (YYT and YJL). In cases of disagreement, a third reviewer was consulted. Two types of data were extracted: study characteristics and study outcomes.

Regarding study characteristics, information on the lead author, publication year, study design (country, study period, study type, intervention duration, intervention dosage), and study population (sample size, gender ratio, mean age, clinical diagnosis) was obtained and tabulated. Each study was labeled using the 'author and year' for identification. If multiple studies shared the same author and year, a unique identifier ("A" and "B") was assigned to distinguish them.

For the experimental data group, all necessary data for meta-analysis were extracted. Outcome data were classified into nine categories based on the endpoints. If an endpoint was measured in the study, the respective result was recorded in the table. Data on HAMD-17 score change, MADRS score change, and CGI-S score change are continuous; hence, the mean value, standard error value, and sample size for both experimental and control groups were extracted for these endpoints. For response rate, remission rate, sustained response rate, sustained remission rate, and CGI-I response rate, the event number and sample size for both experimental and control groups were extracted, as they represent binary data.

2.2.1.6 Quantitative data analysis

Meta-analysis computes the collective effect size of all studies by determining the weight of the data based on the varying amounts of information from each individual study. Weights are calculated according to the sample size or variance of the included studies. To perform the meta-analysis, it is necessary to select the appropriate effect model for calculation. The fixed-effect model and the random-effects model are the two most prevalent models for meta-analysis in the literature. The Q statistic and the I^2 statistic are commonly used as criteria for selecting the most suitable model for each group. In our project, the heterogeneity I^2 is low for each group, so we employed the fixed-effect model for calculation. The fixed-effects model is crucial for meta-analysis, particularly when only a few studies are included in the group. STATA software (Version 12.0; Stata Corporation) was utilized to evaluate the pooled effect size and heterogeneity. The sample size and standard deviations are required for calculations within the fixed-effects model (Wan, Wang, Liu & Tong, 2014). If the standard deviations could not be obtained directly from the original paper, the equation would be as follows:

$SE=SD/\sqrt{n}$

Standard deviations were calculated using a provided standard error and sample size. The 95% confidence intervals of the individual study's effect size and overall effect size were computed. If the p-value is less than 0.05, the effect is considered significant, whereas $p > 0.05$ is deemed to have no significant effect.

2.2.1.7 Heterogeneity analysis

Meta-analyses are conducted to synthesize the quantitative results of multiple studies with internal consistency (Gopalakrishnan & Ganeshkumar, 2013). These quantitative results are usually expressed as effect sizes, such as Hedges'g or correlation coefficients. However, the epidemiological characteristics, study design, and project implementation differences among the studies may impact the effect size or direction. Consequently, heterogeneity analysis is performed to illustrate and explain the variance of different trials. If heterogeneity exists, a random-effect model should be employed. In the absence of heterogeneity, we selected the fixed-effect model. The random-effect model has a broader range of confidence intervals (CIs) compared to the fixed-effect model. We computed heterogeneity using Cochrane's Q and I^2 statistics. I^2 values greater than 50% indicate a high degree of heterogeneity, while I^2 values less than 50% are considered low heterogeneity.

We used STATA software to calculate each group's heterogeneity. Statistical heterogeneity is represented in our study by Cochrane's Chi-Squared test (Cochran's Q) and Hedges' I^2 statistics (Guyatt et al., 2011). Hedges' I^2 is the percentage of the variation between sample estimates due to heterogeneity rather than sampling error (indicating the percentage of total variation from study to study beyond chance) (Ioannidis, Patsopoulos, & Evangelou, 2007). I^2 statistics and Cochran's Q were conducted to estimate the heterogeneity of inter-group studies. I^2 values range from 0% to 100%, and the values of I^2 indicate the proportion of inter-study variability due to heterogeneity. Studies with I^2 higher than 50% are considered to exhibit high heterogeneity, whereas those with I^2 lower than 50% are considered to have low heterogeneity. We selected the fixed-effect model when heterogeneity was high and the random-effect model when heterogeneity was low.

2.2.1.8 Publication bias

Despite the benefits of meta-analysis, several limitations persist. The distinct features of each incorporated study might result in a combined assessment and an extended inferential analysis of individual investigations. To resolve this issue, the pertinent data of all included studies should be gathered, ensuring that the aggregated effect sizes are valid. Publication biases, particularly those stemming from meta-analyses exclusively based on published scientific literature, are notably problematic. Various empirical estimates uphold the general assumption that the likelihood of research being published in scientific journals is unequal. Statistically significant results are crucial determinants of whether findings will be published. Researchers may refrain from submitting inconsequential findings, and editors might not publish them either. Consequently, articles with significant statistical outcomes are more likely to be accepted and published, leading to publication bias. It is essential to identify publication bias as it can induce errors in meta-analyses. To further examine the publication bias of the included studies, we employed STATA software to conduct two tests: the Egger test and the funnel plot test (Egger, Davey, Schneider & Minder, 1997).

2.2.1.9 Trim and fill method

The trim and fill method was devised to mitigate and elucidate publication bias (Duval & Tweedie,2000). This approach relies on formalizing a qualitative technique using a funnel chart, subsequently assessing the number of studies in the asymmetric portion. It removes the asymmetrical outer segment of the funnel and recalculates the publication bias of the remaining studies. The method then employs the symmetric remnant to estimate the funnel's true center and replaces the trimmed studies with their absent counterparts around the center. The final estimate of the true mean is subsequently displayed. STATA software was used to implement the trim and fill method.

2.2.2 Molecular modeling

2.2.2.1 Structure preparation for ligand and protein

Ligand and protein structure preparation and molecular docking procedures were conducted in accordance with Schrödinger's user manuals (Sastry, Adzhigirey, Day, Annabhimoju, & Sherman, 2013). Molecular docking was executed utilizing Glide software within the Schrödinger-Maestro v13.0 platform. PNU-120596 was docked to the open-state α7 nAChR (7KOX), followed by dexmecamylamine docking to the PNU-120596-α7 nAChR complex. Subsequent to initial docking, MD simulations were performed for the PNU-120596-α7 nAChRs complex and dexmecamylamine-PNU-120596-α7 nAChRs complex.

Prior to Glide docking, protein and ligands were prepared utilizing the protein preparation wizard and Ligprep in Schrödinger-Maestro (Schrodinger, LLC, NY, USA). PNU-120596's PDB structure was procured from the NCBI PubChem database (https://www.ncbi.nlm.nih.gov/pccompound) in two-dimensional (SDF) format. The structure of PNU-120596, uncharged at pH=7, is depicted in figure 2.1.

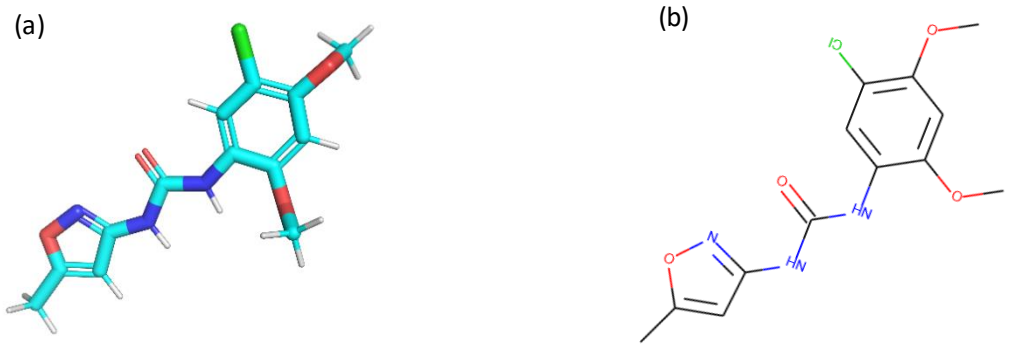

Figure 2.1 displays PNU-120596's molecular structures in both 3D (a) and 2D (b) formats. (a), the 3D structure of PNU-120596 is represented as a stick model with nitrogen atoms colored blue, hydrogen atoms gray, carbon atoms cyan, oxygen atoms red and chloride atom green. (b) exhibits the 2D structure of PNU-120596, with nitrogen and oxygen atoms, as well as chloride, distinctly labeled.

The structure of dexmecamylamine was obtained from the NCBI PubChem database. Mecamylamine comprises a racemic mixture of (S)-(+)-mecamylamine and (R)-(-)-mecamylamine enantiomers. Figure 1.2 presents the three-dimensional structures of these enantiomers. As previously mentioned, the (S)-(+)-mecamylamine enantiomer exhibits greater efficacy as an antidepressant. Consequently, our study focused on (S)-(+)-mecamylamine. At physiological pH, dexmecamylamine was assumed to be fully protonated. The Epik module was employed to simulate protonation at pH 7.0.

The open state α7 nAChRs (PDB ID: 7KOX) structure was prepared for molecular docking as follows: the three-dimensional structure of the open state α7 nAChRs (PDB ID: 7KOX) complexed with co-crystallized ligands NAG, EPJ, and $CA2^{+}$ was acquired from the Protein Data Bank (https://www.rcsb.org/). The Protein Preparation Wizard facilitated protein preparation. During the preprocessing stage, missing hydrogen atoms were added, non-bonded interactions were optimized, and protonation states at pH 7.0 were assigned. Subsequently, protein water orientations were optimized, and all-atom positions were refined using the OPLS3e force field. The RMSD was restricted to below 0.3Å to prevent atom clashes, and bonds and angles with abnormally high energy were optimized. Molecular docking was then performed on the prepared protein.

2.2.2.2 Molecular docking

Upon preparing the protein and ligand, the grid generation tool was employed for molecular docking. Research predicting the binding sites of PNU-120596 and dexmecamylamine to nAChRs informed the docking process. In sections 1.3.1 and 1.3.2, key binding residues on $(\alpha4)_2(\beta2)_3$ nAChRs (PDB ID:5KXI) for dexmecamylamine binding were demonstrated. We hypothesized that dexmecamylamine, as a channel blocker, exhibits similar binding properties to $(\alpha4)_2(\beta2)_3$ nAChRs.

We aligned α7 nAChRs to $(\alpha4)_2(\beta2)_3$ nAChRs and examined the essential binding residues for dexmecamylamine to α7 nAChRs. Box size limitations were set at 15 Å for PNU-120596 docking and 10 Å for dexmecamylamine docking. An initial docking procedure predicted dexmecamylamine binding poses to α7 nAChRs, followed by an MD simulation procedure to observe binding positions and movement of dexmecamylamine to α7 nAChRs.

The molecular docking was performed using Glide as implemented in Maestro with the previously prepared ligand and protein. Several parameters were set up for the PNU-120596 and dexmecamylamine docking. Ligand sampling's energy window was set at 2.5 kcal/mol. van der Waals radii scaling was set as a scaling factor of 0.50 and a partial charge cutoff of 0.15 to soften the potential for nonpolar parts of the ligand. We set to refine the protein residues within 5 Å of the ligand. Glide XP (extra precision) was used for the ligand sampling and scoring. Epik state penalties were added to the docking score to mimic the natural docking environment. Ten poses for dexmecamylamine docking was selected and the most proper binding pose based on the docking score and glide energy was used for further analysis.

2.2.2.3 Molecular dynamic simulation system setup

MD simulation procedures adhered to the GROMACS protocol, accessible at www.manual.gromacs.org (Arasteh & Bagheri, 2017) (Jo, Kim & W, 2007). I also referred to the contents of Nair's (2022) and Jefferies (2021) literature, including how to set the volume of the bilayer-protein system, set the corresponding resolution, choose the force field of different components in the system, and run the simulation (Nair & Gorfe, 2021). Details of this method are stated below. The protein was inserted into a lipid bilayer and solvated with water prior to MD simulation. CHARMM-GUI (https://www.charmm-gui.org/) was employed to generate the solvated lipid bilayer system for the protein (Jo et al., 2008). The CHARMM-GIU is a graphical interface that supports several dynamic simulations including CHARMM, NAMD, GROMACS, and AMBER. CHARMM-GUI is used to generate a protein-lipid bilayer in a solvent using the following steps.

The PDB structure obtained from the Protein Data Bank does not include information about the position of the lipid membrane. Consequently, the OPM (Orientations of Proteins in Membranes) database was employed to acquire orientation data for the protein within a membrane. The OPM database (http://opm.phar.umich.edu) contains a collection of transmembrane, monotopic, and peripheral proteins sourced from the Protein Data Bank (Lomize, Lomize, Pogozheva, & Mosberg, 2006). The protein in the OPM database displays the spatial positions of peptides in the membrane, as well as their three-dimensional structures within the lipid bilayer. The orientations and arrangements of the protein in the lipid bilayer were calculated and compared to experimental data.

Following protein alignment within the membrane using the OPM database, the structure was uploaded to CHARMM-GUI. The membrane builder module generated the protein bilayer, aligning the PDB file with the OPM database. Ligands and ions (PNU-120596, epibatidine, dexmecamylamine, and $Ca2^+$) were uploaded as mol2 files. CHARMM-GUI added missing disulfide

bonds, generating a heterogeneous bilayer system for the protein. A hexagonal box was selected for its suitability for the circular α7 open state nAChRs shape. Water thickness was set to 15 Å, with upper and lower leaflet ratios set as 4:1 for cholesterol (CHOL) and phosphatidylcholine (POPC). A membrane containing approximately 200-250 lipids per leaflet was constructed, approximating real-life conditions. The X and Y dimensions were adjusted to modify the lipid quantity. Subsequently, Na+ and Cl- at a 0.15M concentration were utilized to neutralize ions. CHARMM36 was employed as a force field, and GROMACS was used for input generation, with the final package downloaded for further MD simulation.

2.2.2.4 Molecular dynamic simulations

Compare to the united atom model, the all atom (AA) models, provide outcomes that more closely resemble experimental evidence (Wu & Mukherji, 2022). Thus, a protein–membrane-water system was constructed as described above and involved in the all atom model MD simulation (Nair et al., 2021). The α7 open-state nAChRs' stability with PNU-120596 and the dexmecamylamine binding position were ascertained through MD simulations utilizing GROMACS 2021.5 (http://www.gromacs.org/Downloads). The PNU-120596-α7 nAChR complex with bilayer's PDB file was generated by CHARMM-GUI. As the PDB file structure only contains atomic coordinates, a topology file was created, providing atom type, charge, and bond formation information. The Charmm36, lipid14, TIP3P, and GAFF2 force fields were used for protein backbone, lipid, water, and ligand molecules, respectively.

GROMACS 2021.5 software package was employed to simulate protein and ligand interactions. The MD simulation workflow comprised four steps: energy minimization, NVT equilibrium, NPT equilibrium, and production dynamics simulation. Prior to production runs, the system underwent equilibration through NVT (constant volume) simulation, followed by NPT (constant pressure) simulation. The specific methodology and parameter set are detailed below.

The steepest descent method, with 50,000 steps in the energy minimization step, was applied to constrain H-bonds and water molecules. Post energy minimization, the algorithm file was modified to extend the system's equilibration time to 10 ns, allowing for complete channel hydration. During the NVT simulation, the system was heated to 300K for laboratory conditions using the Berendsen-thermostat method with a temperature bath. Positional restraints were imposed on the protein and ligands, with periodic boundary conditions applied. The simulation maintained a temperature of 300K and a pressure of 1 bar. Particle Mesh Ewald (PME) summation determined electrostatic interactions, while direct computation calculated nonbonded interactions between atoms within 10Å (cut-off distance) of each other. Positional restraints of 1000 KJ/mol/nm2 limited protein atom movement, excluding hydrogen.

Upon equilibration completion, position restraints were removed, and a 250-ns production molecular dynamics (MD) simulation ensued at 300K using the V-rescale thermostat method and 1 bar pressure. Periodic boundary conditions were applied, and leap-frog algorithm motion equations employed a 2 fs time step. During production simulation, the system was unrestrained.

Utilizing the NPT ensemble, hydrogen-involved bonds were constrained. Data was saved every 5,000 steps. Six MD simulations were conducted, with three replicates for both PNU-120596-α7 nAChR and dexmecamylamine-α7 nAChR complexes. A velocity seed was included in the MDP file for each run.

A 250-ns molecular dynamics simulation was performed in triplicate for each complex. Frames were extracted at 0.1 ns intervals, yielding 2,500 stable production stage frames. Protein backbone atoms were aligned to the first frame's structure. The most stable conformation within the free energy landscape (FEL) cluster, exhibiting minimized energy, was selected as the representative structure for each simulation.

2.2.3 Trajectory analysis

2.2.3.1 RMSD calculation

Root mean square deviation (RMSD) for specific atoms in a molecule relative to a reference structure was computed using the 'gmx rms' command in GROMACS. RMSD values for total protein, backbone, and ligands were calculated using MD analysis to quantify average distances between pertinent atoms (Michaud-Agrawal et al., 2011).

2.2.3.2 PCA analysis and free energy landscape calculation

A principal component analysis (PCA), a multivariate statistical method, was conducted to distinguish overall motion from background fluctuations (Taidi, Maurady & Britel, 2022). The 'gmx anaeig' and 'gmx covar' commands in GROMACS generated the PCA map. PCA efficiently reduces dimensions needed to characterize protein dynamics (Makarewicz & Kaźmierkiewicz, 2016). We used the PCA method to recognize the most prominent displacements in both PNU-120596-α7 nAChRs and the dexmecamylamine-α7 nAChRs complex forms during the MD simulations. The first two eigenvectors, which can explain most variances of the system, were projected to a 2D space than contains Carbon-alpha residues to analyze the conformational changes of the complexes during MD.

The two components (PC1 and PC2) accounting for the majority of variance were illustrated as principal components and employed for FEL calculation. The 'gmx sham' command calculated the free energy landscape (FEL). By reducing the data dimensionality of generated trajectories, FEL methodology facilitates analysis of representative protein motions (Balsera et al., 1996).

2.2.3.3 Ligand binding pose analysis

The visual molecular dynamics (VMD) tool was employed to produce trajectory animations based on the trajectory file and the simulation interaction diagram generated in Maestro 13.1, for the

purpose of analyzing ligand-protein interactions. Hydrophobic interactions were assessed and annotated by determining the distance between the aromatic binding site residues of the protein and the centroids of the ligand's phenyl rings. The pore diameter was measured using GROMACS. The water molecule movement in the representative α7 nAChRs structure, both with and without dexmecamylamine, was depicted by VMD. The channel pore diameter was computed utilizing the HOLE program in GROMACS (https://github.com/rjdkmr/gmx_hole). The HOLE program was integrated into GROMACS and employed to calculate the channel radius as a function of time. The HOLE program was installed in GROMACS by command "gmx_hole" and it can bu used to calculate radius of protein channel for GROMACS MD trajectory (Smart & Wallace, 1993).

In this section, we have discussed the theoretical framework and research methods that we will use to answer our research question. Our chosen methods, meta-analysis, molecular docking and molecular dynamic simulation, help to investigate the antidepressant effect of dexmecamylamine and to explore the binding position of dexmecamylamine to α7 nAChRs, which aligns with the objective of our research. We have chosen a qualitative research method that will allow us to gain a deep understanding of dexmecamylamine's effect on antidepression and it's binding behaviour. In the next chapter, result of meta-analysis, molecular docking and MD simulation will be presented and discussed.

Chapter 3

Result of Meta-analysis

3.1 Identification of included studies

The PRISMA flowchart illustrating the study selection process is depicted in figure 3.1. We identified 577 articles across three databases (Medline, Embase, and Cochrane Library). Additionally, two more articles were discovered through manual searches on the clinical trial registration platform (www5.clinicaltrial.gov). After importing all search results into the information management software (EndNote), 109 duplicate articles were removed. Two independent reviewers (YTY and YJL) conducted an initial screening of titles and abstracts. Consequently, 429 articles were excluded due to not fulfilling the inclusion and exclusion criteria, leaving 41 articles for further assessment. In the second step, both reviewers thoroughly assessed the remaining papers, and those not meeting the inclusion criteria or meeting the exclusion criteria were excluded. Ultimately, nine articles met the criteria for meta-analysis. All nine included studies were written in English, and no translation service was required.

Table A1 In the appendix presents essential study characteristics, including country, study period, study type, intervention duration, intervention dosage, and sample characteristics (sample size, gender ratio, average age, and clinical diagnosis). According to the results, all included studies were published between 2008 and 2015. The nine studies comprised a total of 2,480 participants, with all participants being randomly allocated to the experimental group (1,142) and control group (1,038), and diagnosed with major depressive disorder (MDD) or depression. All nine included studies were randomized controlled trials, conducted worldwide, including the U.S., Canada, India, and Europe. The ethnicity of subjects, socio-environmental information, and baseline conditions for each study are detailed below.

Study 1 incorporated 21 patients aged between 18 and 65 years, diagnosed with MDD according to the Diagnostic and Statistical Manual of Mental Disorders, Fourth Edition (DSM-IV), by licensed clinicians. These patients should have received at least three months of SSRI antidepressant treatment and displayed no response or only a partial antidepressant response to the treatment. Moreover, patients should possess a score of 12 or higher on the HAMD-17, indicating that they were initially diagnosed with major depressive disorder. All included patients were assigned to the study group and the control group in a 1:1 ratio. Throughout the study, all patients were permitted to maintain their background treatment and their prior SSRI antidepressant medication dose. The study dose of mecamylamine hydrochloride began at 5 mg daily, orally, and increased to 10 mg daily thereafter. The total trial lasted for eight weeks.

Study 2 was a double-blind, randomized, parallel assignment study that included patients meeting the DSM-IV criteria and diagnosed with MDD. In this study, patients' MADRS scores should be higher than 27, and the CGI-S score should be higher than 4. Initially, all patients received eight weeks of open-label treatment with the SSRI citalopram hydrobromide. Patients with an inadequate response to the treatment were randomized at a 1:1 ratio between the study group and the control group. These patients received eight weeks of double-blind treatment with add-on dexmecamylamine or placebo before continuing the SSRI. The dosage of dexmecamylamine ranged from 1 mg BID to 4 mg BID, as determined by the investigator.

Study 3 was a 52-week, double-blind, placebo-controlled investigation examining the impact of 2mg, 4mg, and 8 mg of dexmecamylamine. This study necessitated that participants undergo concurrent treatment with an antidepressant (SSRI or SNRI) for MDD. Participants should have exhibited an inadequate response to SSRI or SNRI therapy. Results from week 8 will be gathered for meta-analysis. Patients with MDD will be assigned to the dexmecamylamine adjunct to the SSRI/SNRI group and the placebo adjunct to the SSRI/SNRI group at a 3:1 ratio. Eligible patients should have a Hamilton Depression Rating Scale (17-item) total score of 10 or higher during initial treatment.

Studies 4 and 5, conducted in various regions, were designed similarly (excluding drug dosage). Study 4 took place in the USA and India, while Study 5 occurred in Europe, South America, and Africa. Both were multi-center, 8-week clinical trials. Eligible patients should be diagnosed with MDD according to the DSM-IV and have HAMD-17 scores below 20 at baseline. All patients underwent an 8-week open-label standard antidepressant treatment, except those who responded inadequately to standard treatment (defined as a 50% reduction in the 17-item HAM-D at treatment completion). Selected patients were randomly assigned to control and experimental groups at a 1:1:1:1 ratio for the subsequent 8-week double-blind active treatment phase. In Study 4, experimental group doses were 0.1, 1, or 4mg BID dexmecamylamine, while in Study 5, they were 0.5, 2, or 4mg BID dexmecamylamine, both as adjuncts to standard treatment. Week 8 results will be collected for meta-analysis.

Studies 6 and 7, akin to Studies 4 and 5, were identical phase III studies conducted in different regions and timeframes. Patients diagnosed with MDD by DSM-IV and with a HAMD-17 score of 20 met inclusion criteria. All patients received 8-week open-label antidepressant treatment at doses at the upper end of the approved range. Similar to Studies 4 and 5, patients who responded inadequately to SSRI or SNRI standard treatment were randomized to dexmecamylamine 1mg BID or placebo at a 1:1 ratio. Dexmecamylamine was administered as an adjunct treatment.

Study 8 was a randomized, double-blind investigation. Patients with a clinical diagnosis of MDD and an inadequate response to no more than one antidepressant were selected. Patients were not required to have a HAMD-17 or MADRS score. Patients received dexmecamylamine (4mg BID) and a placebo at a 1:1 ratio.

Study 9 was a randomized, double-blind investigation. Patients should be diagnosed with MDD by DSM-IV and alcohol dependence by SCID. Included patients should also have been on a stable SSRI dose for 2 weeks. A total of 21 patients were assigned to the experimental and control groups at a 1:1 ratio. Experimental group patients received mecamylamine 10mg for 12 weeks.

For the experimental data, we identified nine outcome measures, encompassing HAMD-17 score alterations, MADRS score variations, response rates, remission rates, sustained response rates, sustained remission rates, CGI-I response rates, and CGI-S score modifications. The data obtained for each group are presented in tables A2 to A9 in the supplementary material. The treatment duration for all included clinical trials was eight weeks, with the exception of Study 3. Study 3 was

a long-term investigation with a 52-week intervention period; consequently, we extracted data from week 8 in Study 3 to minimize bias. Dexmecamylamine was administered orally in all studies, except for Studies 1 and 9. In Study 1, participants received mecamylamine hydrochloride (MEC), a racemic mixture of mecamylamine and dexmecamylamine, instead of dexmecamylamine. In Study 9, mecamylamine was administered. Dexmecamylamine dosages ranged from 2 to 8 mg/day, and MEC dosage was 10 mg/day. All included participants demonstrated resistance to first-line MDD therapies (SSRI/SNRI). Notably, in Study 9, patients were required to be diagnosed with both MDD and alcohol dependence. Interventions (dexmecamylamine or MEC) were administered as adjunct therapies to first-line antidepressant treatments. In all studies except Studies 8 and 9, patients received dexmecamylamine/mecamylamine as monotherapy.

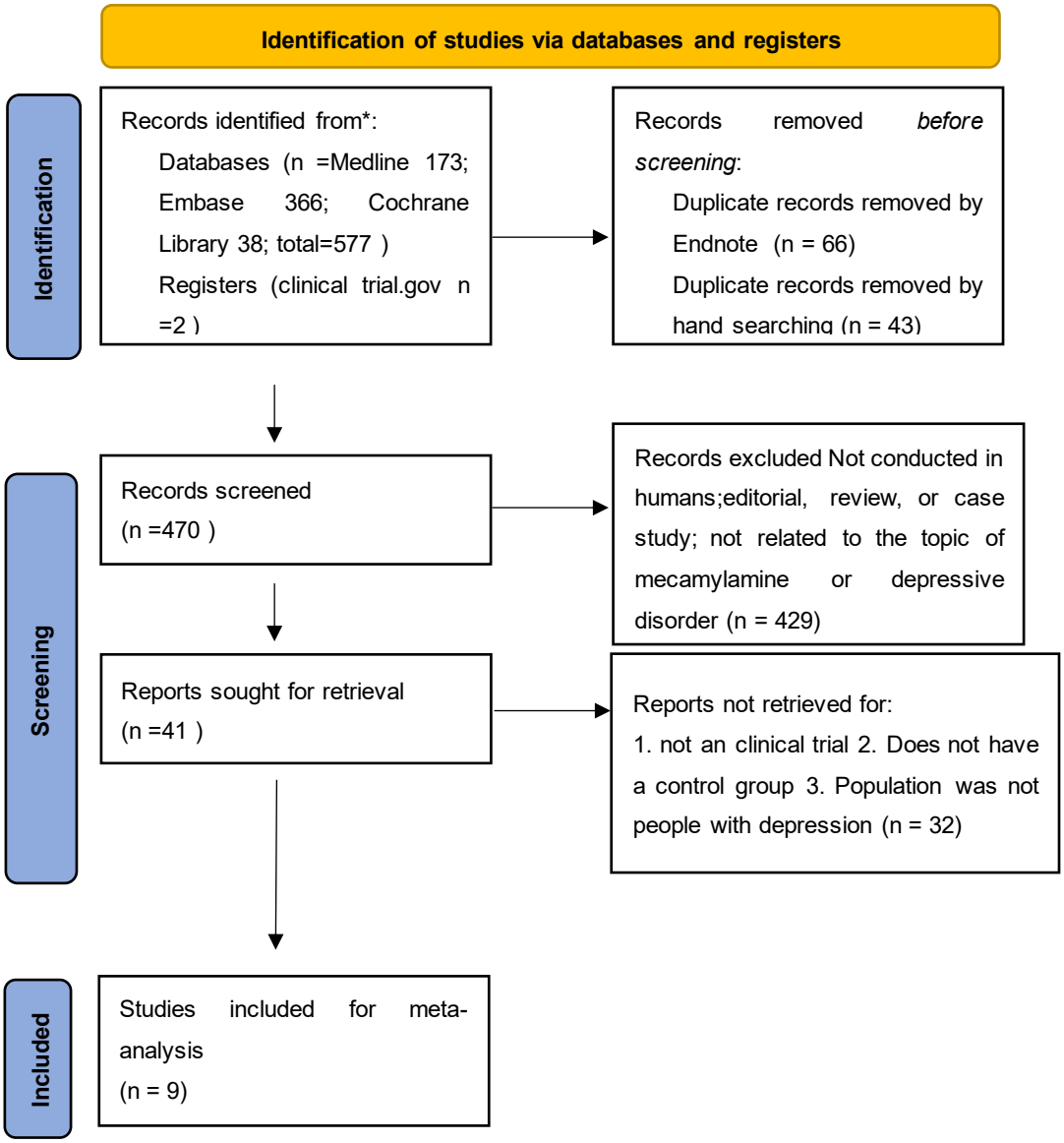

Figure 3.1 PRISMA flowchart for the meta-analysis investigating the effect of the mecamylamine to the patients with MDD.

A total of 577 articles and 2 clinical trials were identified in our meta-analysis. Sixty-six duplicates were removed using EndNote, and 43 duplicate records were eliminated through manual searching.

Of the remaining 470 articles, 429 were excluded due to their status as editorials, reviews, or case studies, or because they were unrelated to the topic of mecamylamine or MDD or were not conducted in humans. From the 41 articles, 32 were removed for not meeting the inclusion and exclusion criteria, resulting in the retrieval of nine clinical trials.

3.2 Quality of included studies and risk of bias assessment

The Cochrane Risk of Bias assessment tool was employed to evaluate the risk of bias in each included study. The detailed assessment scores for each item in every included study were documented in table A2 in the appendix. We utilized RevMan software (version 5.3) to generate summaries of risk of bias and risk of bias graphs, which are displayed in figures 3.2 and 3.3. In figure 3.2, we displayed the summary of risk of bias for our meta-analysis and in figure 3.3, we displayed the risk of Bias graph for the meta-analysis.

According to figures 3.2 and 3.3, we suggested that among all included studies, Studies 4 and 5 had the lowest risk of bias, while Study 2 had the highest risk. The overall risk of bias in our meta-analysis was deemed insignificant and thus acceptable. Selective bias was identified as the most systematic bias among all biases measured by the Cochrane Risk of Bias assessment tool, as some selected studies did not report results for all outcome measures.

Figure 3.2. The summary of risk of bias for the meta-analysis investigating the effect of the mecamylamine to the patients with MDD.

The assessment result of each study on each item was illustrated. The green circle represent to low risk, the red circle represent to high risk and the yellow circle represent to unclear risk. According to the summary of risk of bias, study 2 has the highest risk of bias. On the other hand, study 4 and study 5 have the most acceptable risk of bias.

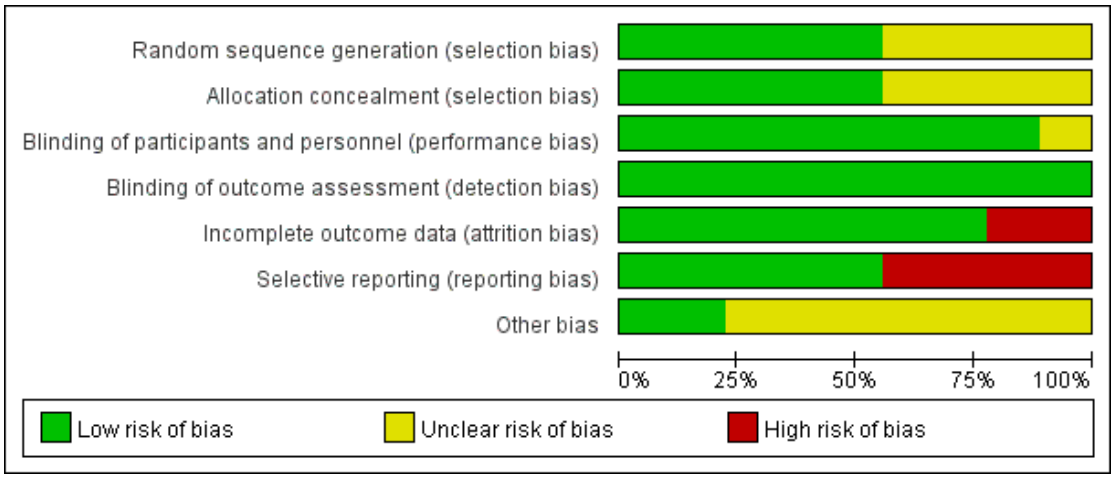

Figure 3.3 Risk of Bias graph for the meta-analysis investigating the effect of the mecamylamine to the patients with MDD.

The risk of bias of each item was illustrated in the figure. Green, yellow and red represent to low risk of bias, unclear risk of bias and high risk of bias, respectively.

3.3 Meta-analysis stratified

We established nine distinct groups based on outcome measures, including HAMD-17 score changes, MADRS score changes, CGI-S score changes, response rates, remission rates, early and sustained response rates, sustained response rates, sustained remission rates, and CGI-I response rates. All extracted data are provided in tables A2 to A9 in the supplementary material. A meta-analysis was performed within each group.

3.4 Pooled effect size and heterogeneity

3.4.1 HAMD-17 score change

In the HAMD-17 score change group, we incorporated four studies that utilized HAMD-17 score change as an endpoint. Extracted data for this group are provided in table A2 in the appendix. Figure 3.4 exhibits the overall pooled effect size and individual study pooled effect sizes. As indicated in the Forest plot, the overall pooled effect size for the experimental intervention (n=608) versus the placebo group (n=619) was 0.70 (95% CI: -0.24 to 1.64; p=0.212). The p-value of 0.212, exceeding 0.05, suggests that the antidepressant effect of the experimental intervention (dexmecamylamine or MEC) group was not superior to the placebo group. With an I2 of 33.4% and below 50%, the heterogeneity among the four included studies is considered low and acceptable.

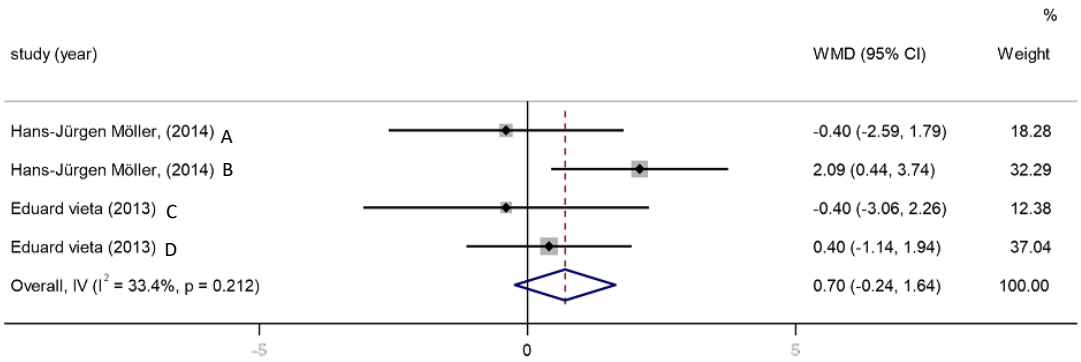

Figure 3.4. Forest figure of HAMD-17 score change group.A refers to study ID 4, B refers to study ID 5, C refers to study ID 6, D refers to study ID 7; Weight%, effective size, confidential interval for each study and overall are displayed

3.4.2 MADRS score change

Regarding MADRS score changes, six studies were retrieved. Necessary data were extracted and presented in table A3 in the appendix. Figure 3.5 depicts the pooled effect size of the experimental group versus the placebo group, with an overall pooled effect size of -0.18 (95% CI=-1.08 to 0.72; p=0.782) for all six included studies. The p-value of 0.782, greater than 0.05, indicates that the antidepressant effect of the intervention group (MEC or dexmecamylamine) was comparable to that of the placebo group in MADRS score change. Dexmecamylamine failed to demonstrate an antidepressant effect. Heterogeneity among the six included studies is low (I^2=0.00%).

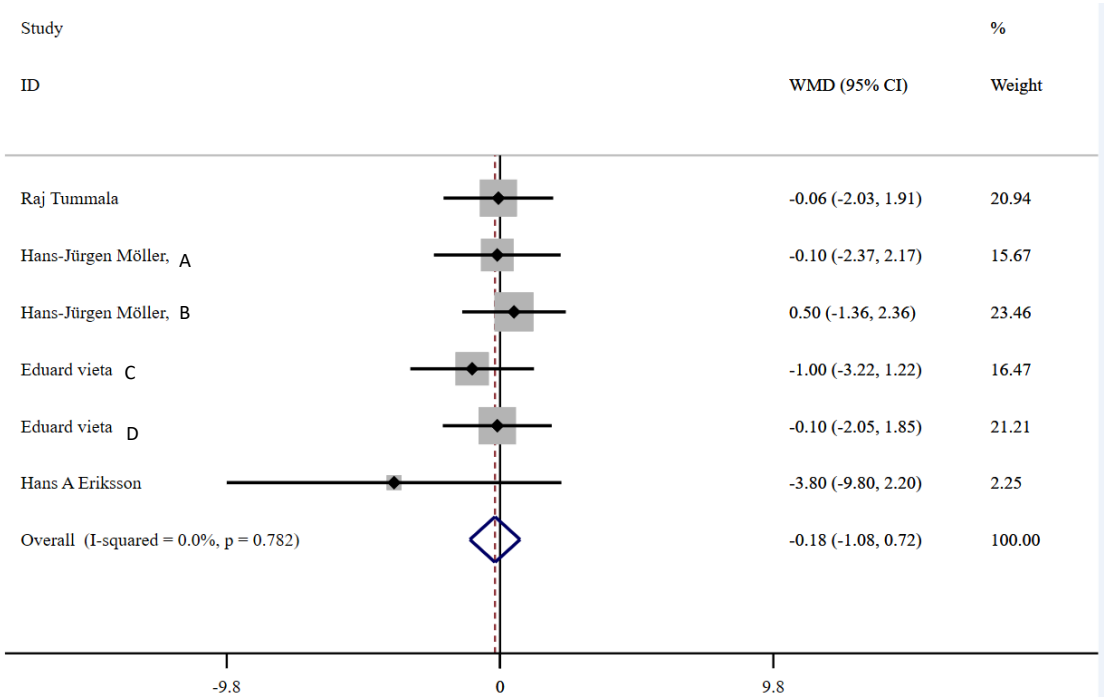

Figure 3.5. Forest figure of MADRS score change.A refers to study ID 4, B refers to study ID 5, C refers to study ID 6, D refers to study ID 7; Weight%, effective size, confidential interval for each study and overall are displayed

3.4.3 Response rate

The response rate signifies a reduction exceeding 50% from randomization in MADRS total score upon treatment completion. This data is binary in nature. For this category, the event count (number of individuals achieving the endpoint) and total participant count for both experimental and control groups were extracted. All extracted data can be found in Appendix table A4. The Forest plot (figure 3.6) depicts the pooled effect result, with an overall pooled effect size of 0.88 (95% CI=0.71 to 1.08, p=0.838). Given that the p-value surpasses 0.05, the results indicate no significant difference between the experimental and control groups. The heterogeneity analysis of the included studies in this group accounts for approximately 0% heterogeneity (I^2=0.00%), which positively correlates with effect size.

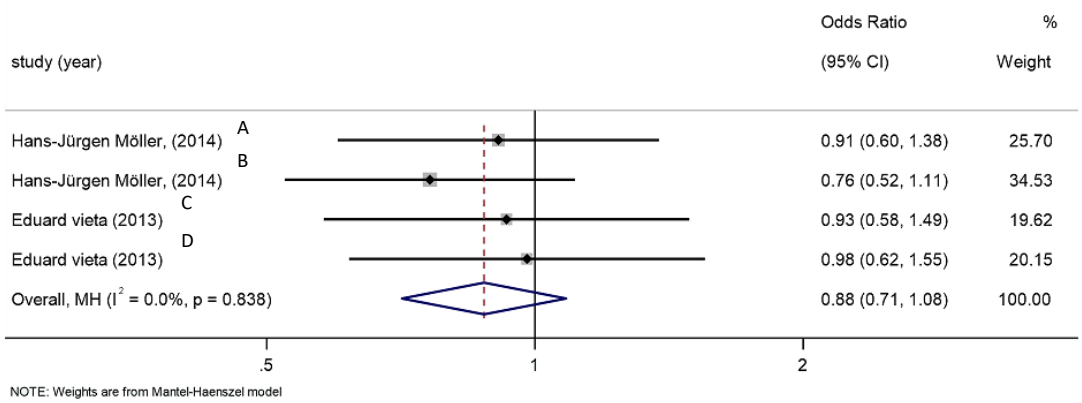

Figure 3.6. Forest plot of respond rate group: A refers to study ID 4, B refers to study ID 5, C refers to study ID 6, D refers to study ID 7; Weight%, effective size, confidential interval for each study and overall are displayed

3.4.4 Remission rate

'Remission' denotes the alleviation of MDD depressive symptoms. The remission rate is determined by the proportion of patients with a MADRS total score equal to or less than 8. In this category, the endpoint achievement count and total participant count for both experimental and control groups were collected, with relevant data depicted in Appendix table A5. The pooled effect size for the remission rate is 0.97 (95% CI=0.76 to 1.24, P=0.331). The p-value of 0.331 exceeds 0.05. The Forest plot (figure 3.7) illustrates that the pooled effect size reveals no significant difference between experimental and control groups. Concerning heterogeneity, the I^2 value equals 12.3%, less than 50%, signifying acceptable heterogeneity.

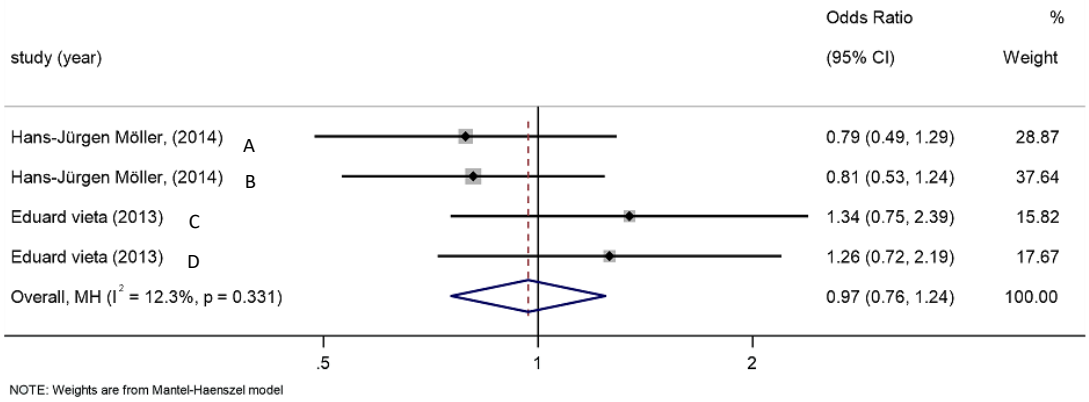

Figure 3.7. Forest plot of remission rate group: A refers to study ID 4, B refers to study ID 5, C refers to study ID 6, D refers to study ID 7; Weight%, effective size, confidential interval for each study and overall are displayed

3.4.5 Sustained response rate

A persistent response is characterized by a reduction greater than 50% from randomization in the MADRS total score, with a MADRS total score below 12 at Week 12, Week 14, and the conclusion of treatment (Week 16). We exclusively concentrate on the study outcome at treatment completion (week 16), spanning an eight-week treatment duration. Five studies were included in this group, with all extracted data presented in table A6 in the appendix. We procured information regarding the event number and total event number for both the experimental and control groups. Basic information (study ID, study year, researchers, study region) was also collected. The pooled effect size was calculated, with the result depicted in the forest plot (figure 3.8). The pooled effect of the persistent response rate group is 0.70 (95% CI 0.44 to 1.11), with a p-value of 0.052, exceeding 0.03. Consequently, the antidepressant effect of dexmecamylamine on patients with MDD is not significant. Heterogeneity among the five included studies is 57.4%, surpassing 50%.

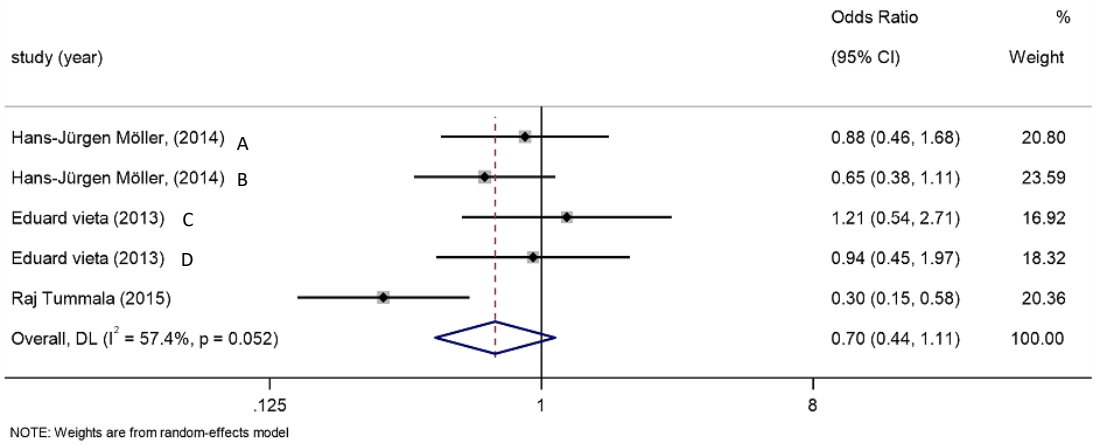

Figure 3.8. Forest plot of sustained response group: A refers to study ID 4, B refers to study ID 5, C refers to study ID 6, D refers to study ID 7; Weight%, effective size, confidential interval for each study and overall are displayed

3.4.6 Sustained remission rate

The persistent remission rate is defined as the proportion of patients with a MADRS total score below eight at treatment completion. Extracted data for this group is provided in table A7 in the appendix, with the Forest plot displayed in figure 3.9. The following data was extracted for analysis: the number of participants who achieved the final goal and the total number of participants in the experimental and control groups. The pooled effect size result indicates a total effect size of 0.86 (95% CI=0.57-1.31, P=0.635) for the four included studies. The p-value exceeds 0.05, suggesting no significant effect difference between the experimental and control groups. Heterogeneity among the included studies is low, as represented by I^2 equating to 0.0%.

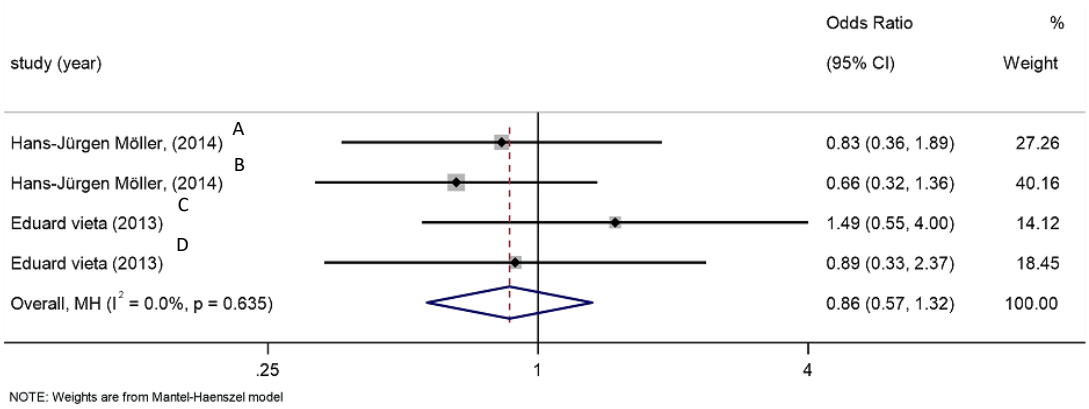

Figure 3.9. Forest plot of sustained remission group: A refers to study ID 4, B refers to study ID 5, C refers to study ID 6, D refers to study ID 7; Weight%, effective size, confidential interval for each study and overall are displayed

3.4.7 CGI-I response rate

Response in the Clinical Global Impression-Improvement (CGI-I) is defined as a CGI-I Rating of "Very Much Improved" or "Much Improved" at the end of treatment. During data extraction, three studies that tested the CGI-I response rate were retrieved. Among these three studies, the event number of patients who reached the endpoint and the total number of patients in the experimental and control groups were extracted. The extracted data is displayed in table A8 in the appendix. The pooled effect size in this group was 0.90 (95% CI=0.72 to 1.13, P=0.451), with the Forest plot shown in figure 3.10. The result indicates that the statistical significance of the observed difference is higher than 0.05 (P=0.451), suggesting that the effect of dexmecamylamine on improving patients' clinical performance is not significant. The heterogeneity among the included studies, represented by I^2, is low based on I^2=0.0%.

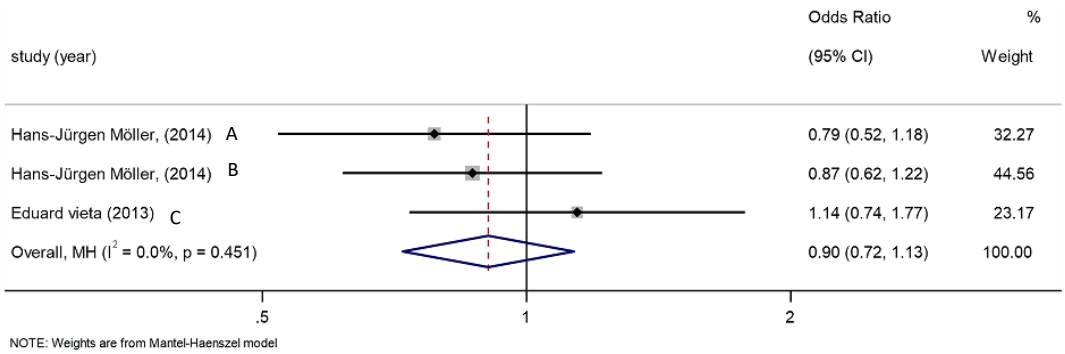

Figure 3.10. Forest plot of CGI-I response group: A refers to study ID 4, B refers to study ID 5, C refers to study ID 6; Weight%, effective size, confidential interval for each study and overall are displayed

3.4.8 CGI-S score change

The alteration in CGI-S scores is characterized by the change in CGI-S scores from randomization to the conclusion of an eight-week treatment period. Data from the five included studies, such as mean, standard deviation, and sample size for experimental and control groups, were extracted. Detailed information is provided in table A9 in the appendix. As shown in the figure 3.11, the combined effect size for CGI-S score changes across the five studies was -0.05 (95% CI: -0.18 to 0.08, P=0.868). Heterogeneity was assessed using the I^2 statistic, which was 0.0% for this group, suggesting acceptable heterogeneity levels within the study.

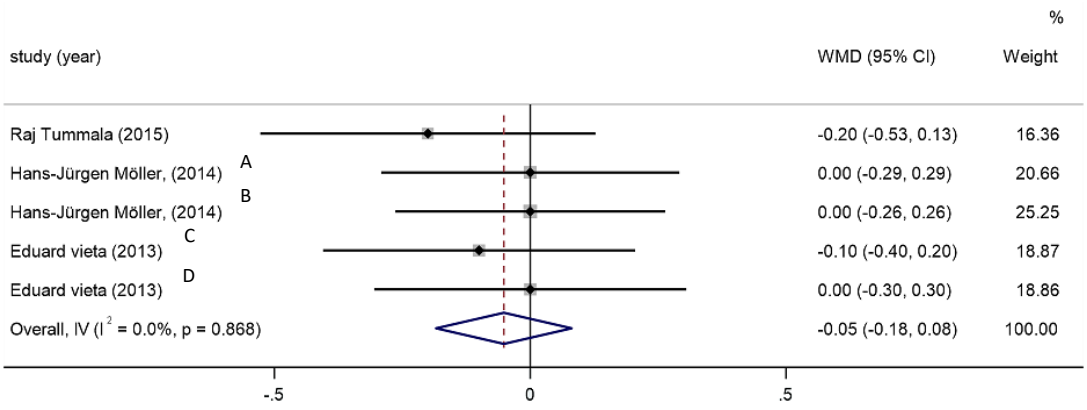

Figure 3.11. Forest plot of CGI-S score change group;A refers to study ID 4, B refers to study ID 5, C refers to study ID 6, D refers to study ID 7; Weight%, effective size, confidential interval for each study and overall are displayed

3.5 Publication bias

Funnel plot results for 'MADRS score change,' 'HAMD-17 score change,' 'response rate,' 'remission rate,' 'sustained response rate,' 'sustained remission rate,' and 'CGI-S score change' are depicted in figures 3.12 to 3.18. As only three studies were included in the CGI-I response rate group, a funnel plot evaluation was not conducted due to the insufficient number of studies. Publication bias was

assessed for each group by examining the symmetry of the funnel plots. As per to these figures, the symmetries were shown in figures 3.13, 3.14, 3.15, 3.16, 3.17 and 3.18. However, due to the small number of studies included, the symmetries were not obvious. In figure 3.12, which referred to the MADRS score change group, the plots of all included studies were asymmetrically distributed. In addition to funnel plots, Egger's regression test was performed to evaluate publication bias. Apart from the MADRS score change group, Egger's test results for other groups indicated minimal publication bias. The MADRS score change group had a p-value of less than 0.05 in Egger's test (P-value=0.003), suggesting publication bias within this group.

The funnel plot asymmetry and Egger's test results indicate publication bias in the 'MADRS score change' group. Egger's regression test result also reveals a highly significant publication bias for this group, with a p-value of 0.003. Furthermore, the 'score change of MADRS' group's funnel plot asymmetry suggests the existence of publication bias. No publication bias was detected in the other groups across the nine studies. Therefore, additional research should be conducted to elucidate the publication bias.

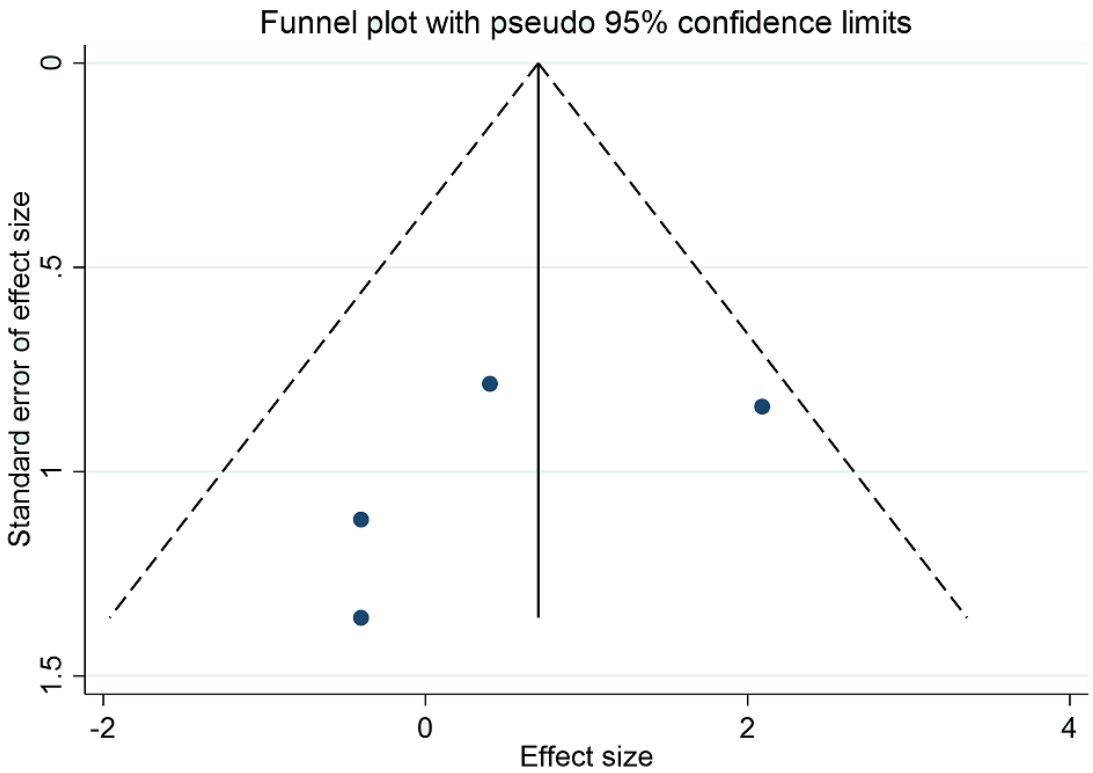

Figure 3.12. The funnel plot of HAMD-17 score change group.

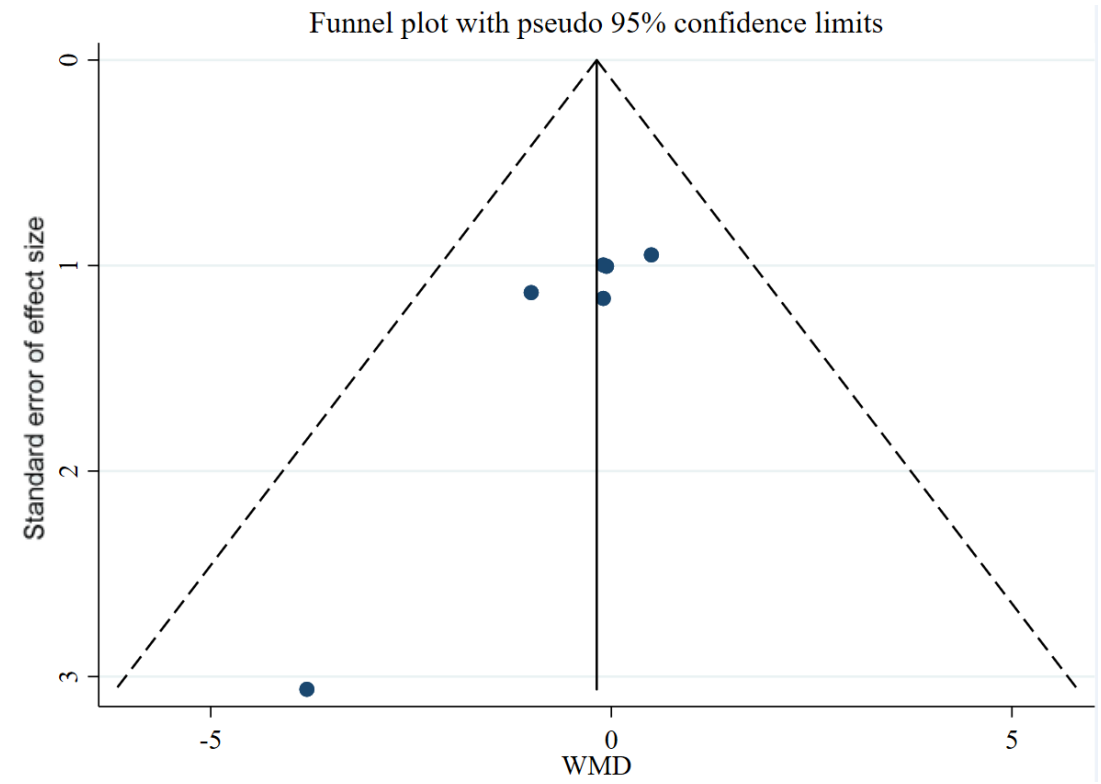

Figure 3.13. The funnel plot of MADRS score change group.

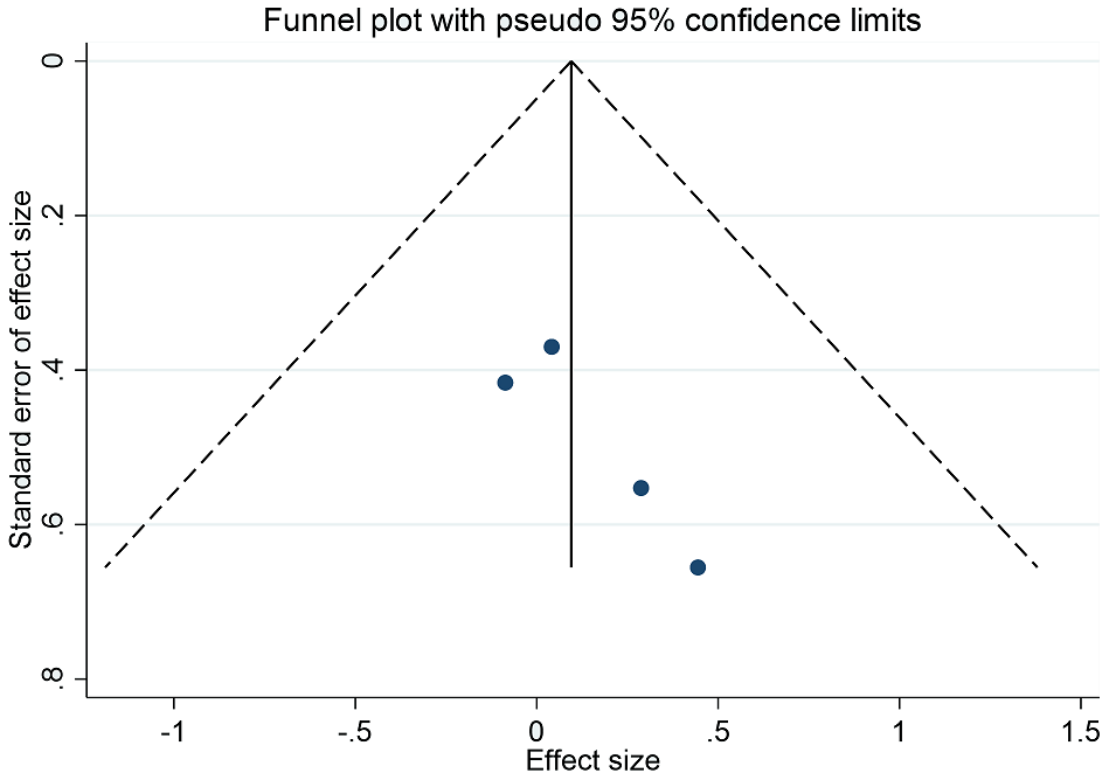

Figure 3.14. The funnel plot of early and sustained response rate group.

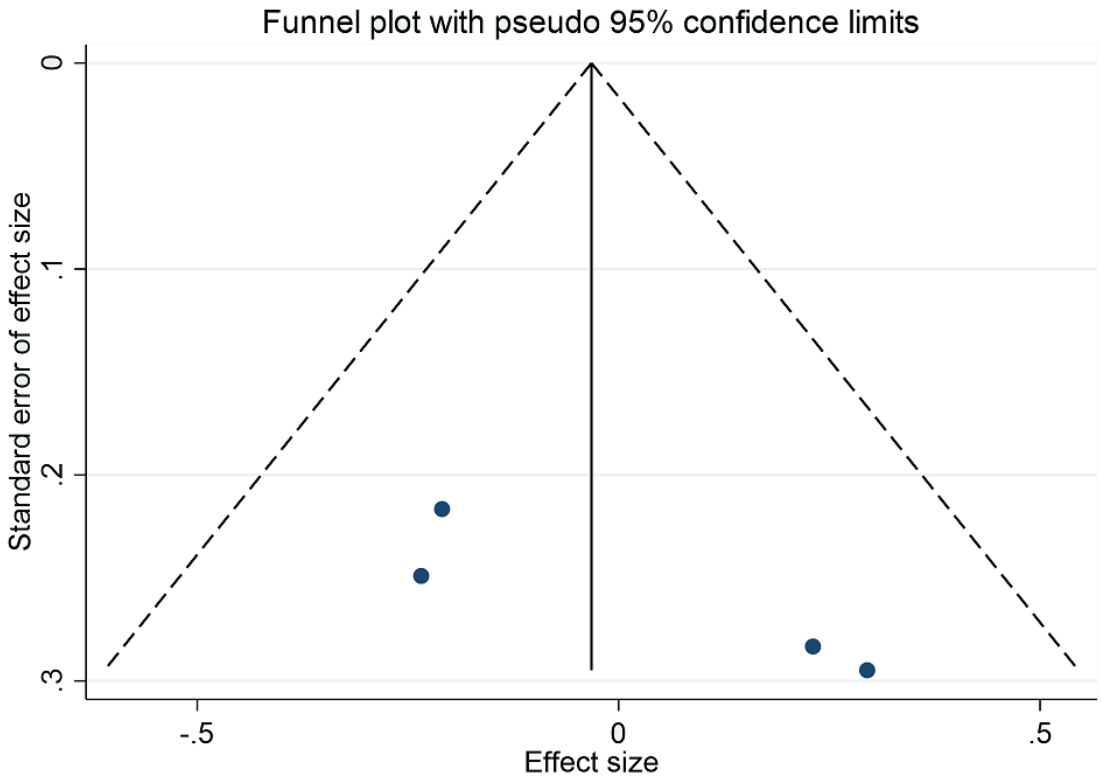

Figure 3.15 The funnel plot measures of remission rate group.

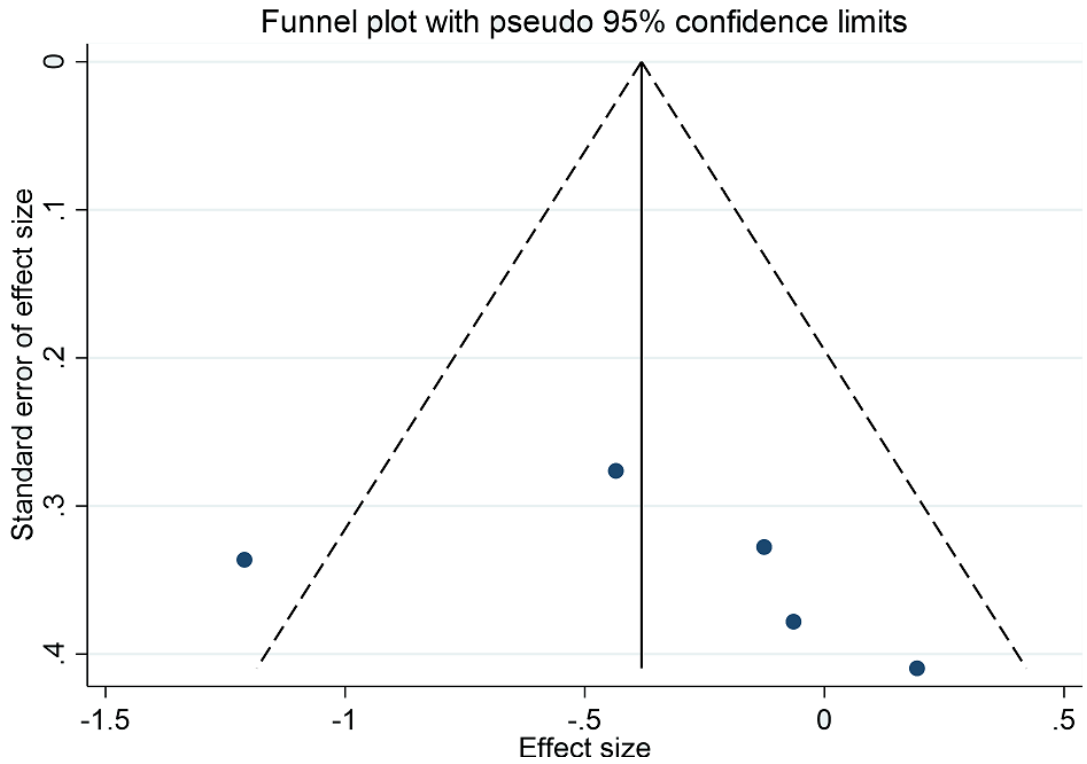

Figure 3.16 The funnel plot of sustained response rate group.

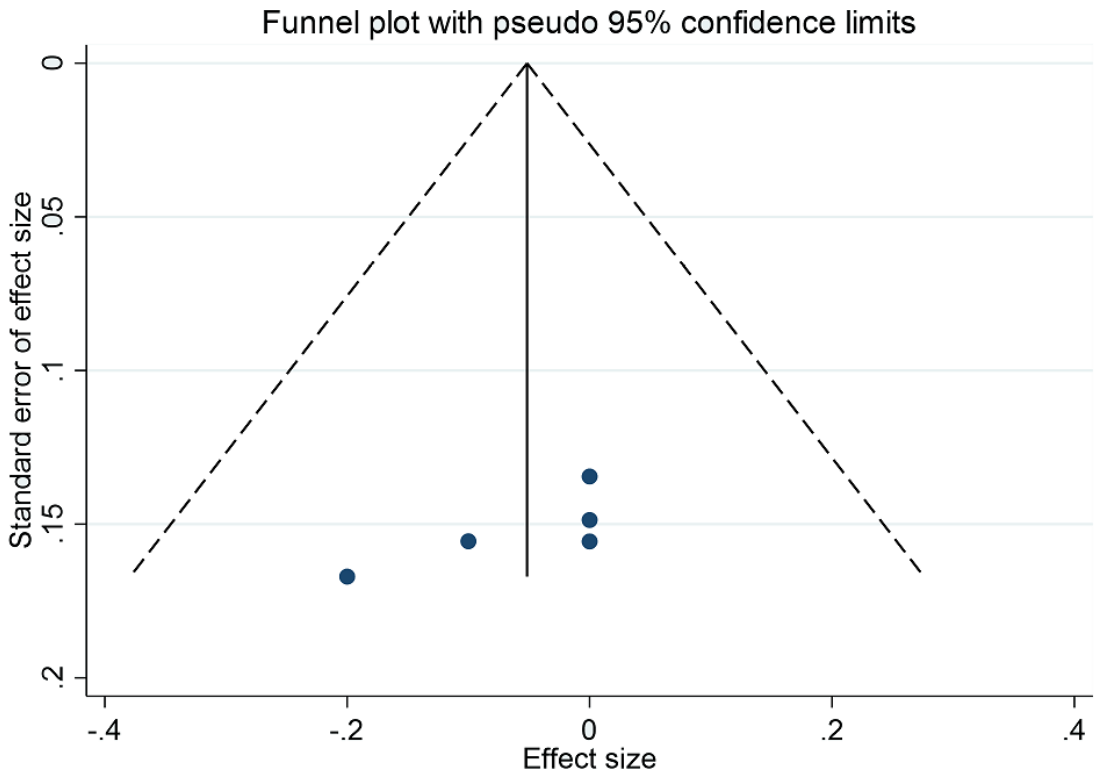

Figure 3.17 The funnel plot of sustained remission rate group.

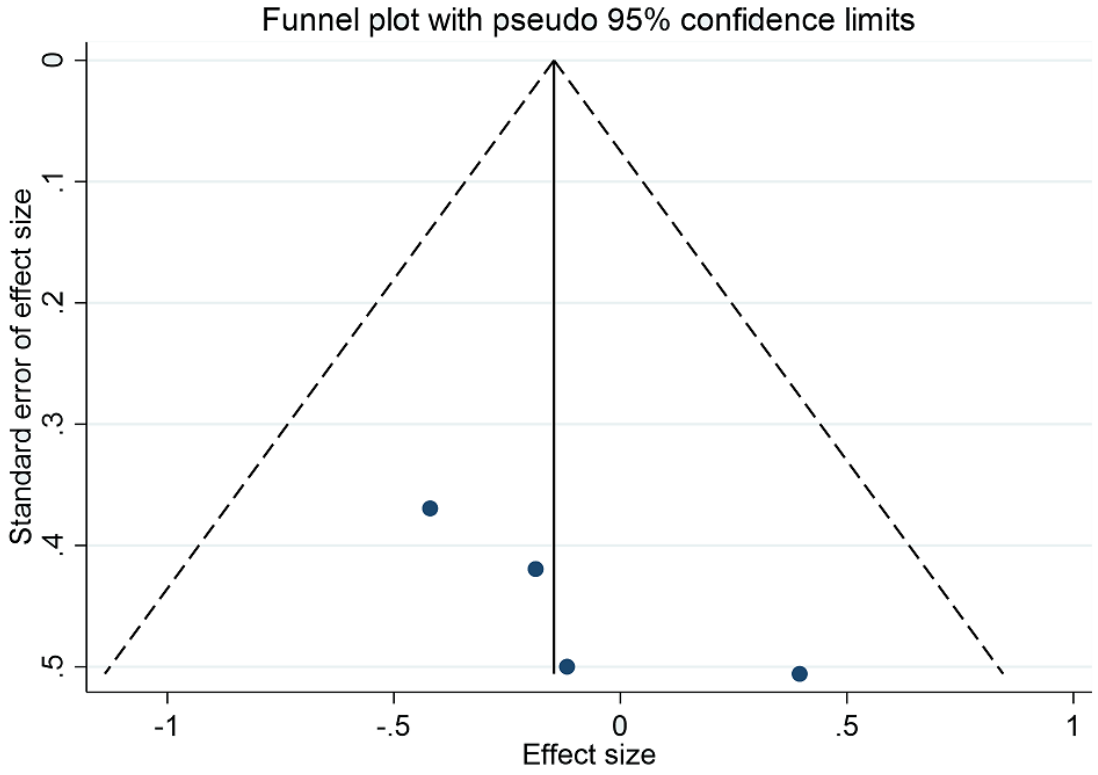

Figure 3.18 The funnel plot of CGI-S total score change of group.

3.6 Trim and fill methods

To mitigate publication bias, we employed the trim and fill approach to address the publication bias within the MADRS score change group. Based on the findings, two iterations were executed during the trim and fill procedure. However, no studies were either filled or trimmed. The results indicated an absence of discernible publication bias within this group. The discrepancy between the trim and fill outcome and publication bias outcome may be attributed to the insufficient number of studies incorporated into this group.

3.7 Overall results of meta-analysis

We procured nine studies for the meta-analysis. The risk of bias among all included studies is deemed acceptable. In accordance with the meta-analysis outcome, mecamylamine does not demonstrate an antidepressant effect on MDD patients, as evidenced by the decreased scores of HAMD-17 and MADRS. Heterogeneity results reveal that, aside from the sustained response rate group, the heterogeneity among the included studies for each group is acceptable. In the sustained response rate group, the I^2 value exceeds 50%. However, performing subgroup analysis to assess heterogeneity in this group proves challenging due to the inclusion of merely five studies. Publication bias is acceptable across the eight groups, except for the 'MADRS score change' group. The trim and fill analysis was conducted to elucidate the publications. Following two iterations, no studies were filled or trimmed, suggesting an absence of discernible publication bias within this group.

Dexmecamylamine is recognized as a channel blocker, and nAChRs serve a vital role in MDD pathology. The reasons underlying dexmecamylamine's failure to exhibit an antidepressant effect in our meta-analysis are multifaceted and varied. Despite dexmecamylamine's unsatisfactory antidepressant efficacy, nAChRs remain a promising drug target for MDD. Consequently, we further expound on dexmecamylamine's binding position to nAChRs. Dexmecamylamine's binding position can offer a potential binding site for a channel blocker drug and information on the optimization of dexmecamylamine and its derivatives.

Chapter 4

Result of molecular modeling studies

4.1 Aims

Numerous objectives were established for the molecular modeling studies, including:
(1) Identifying the binding pose of PNU-120596 to the open-state α7 nAChRs;
(2) Depicting the binding position of PNU-120596 to the α7 nAChRs through MD simulation;
(3) Examining the binding pose of dexmecamylamine to the open-state α7 nAChRs via structural alignment;
(4) Elucidating the binding position of dexmecamylamine through MD simulation to guide further drug optimization.4.2 Initial molecular docking

4.2.1 Binding of PNU-120596 to α7 nAChRs

Preliminary molecular docking was performed using GLIDE within Schrödinger-Maestro 13.0. The results revealed no hydrogen bonds formed between PNU-120596 and the surrounding residues. The interactions between the ligand and residues were hydrophobic, involving M276, A298, Q295, L235, and A294 (figure 4.1). No hydrogen bonds were identified between PNU-120596 and α7 nAChRs. However, due to the presence of a benzene ring in PNU-120596, non-covalent π-interactions occurred between residues and PNU-120596. Further molecular dynamics simulations should be conducted to determine the binding pose of PNU-120596 to α7 nAChRs.

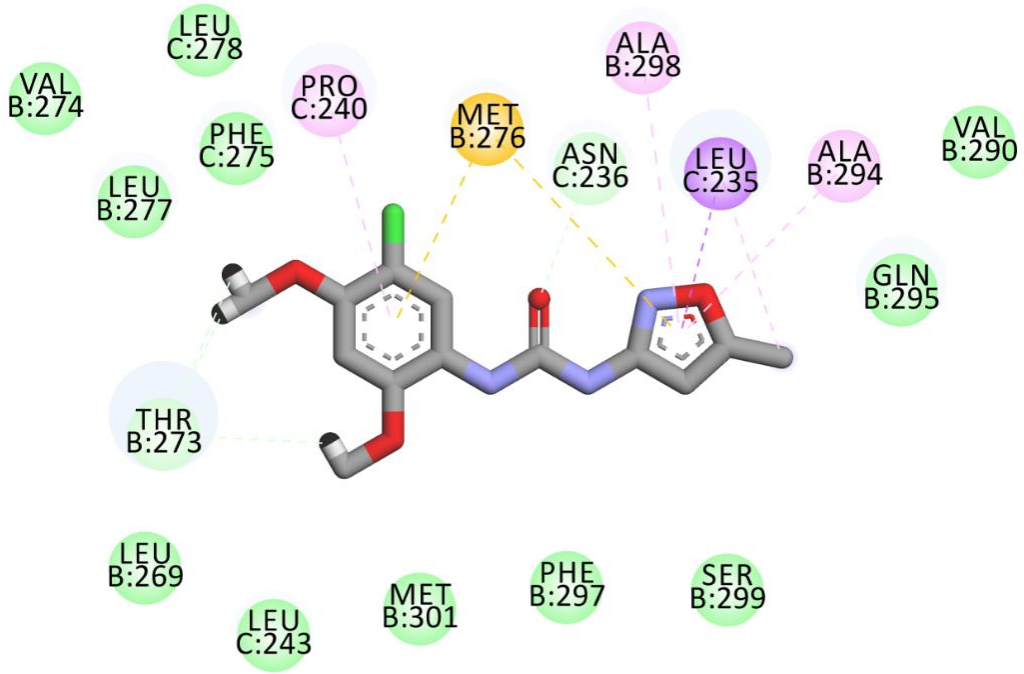

Figure 4.1 The 2D interaction map between PNU-120596 and the surrounded residues.
The yellow dashed lines represent to the pi-sulfur reaction. Purple dashed line represents to the pi-sigma reaction. Pink dashed lines refers to the pi-alkyl reaction. The carbon atom, oxygen atom, nitrogen atom, and hydrogen atom of PNU-120596 are coloured gray, red, blue, and black, respectively. Hydrogen atoms that have no interactions with surrounding residues are not

displayed in the figure.

4.2.2 Alignment of α7 nAChRs and $(\alpha4)_2(\beta2)_3$ nAChRs

In table 1.2 (Section 1.3.2), key binding residues of dexmecamylamine to the $(\alpha4)_2(\beta2)_3$ nAChRs were identified through NMR studies (e.g., G238 on the β2 subunit). However, the binding position and critical binding residues of dexmecamylamine to α7 nAChRs remain unclear. Therefore, we aligned α7 nAChR subunit with β2 nAChR subunit, using PYMOL to identify potential binding residues for dexmecamylamine on the α7 subunit. According to the sequence, residues 231-244 on the β2 subunit are 'FYLPSDCGEKM', while residues 229-239 on the α7 subunit are 'FLLPADSGEKI'. Based on this alignment, we inferred that Gly236 on the α7 subunit is a critical binding residue corresponding to G238 in β2. The structural alignment of β2 and α7 subunits is illustrated in Figure 4.2. The dashed line circles the binding pocket of dexmecamylamine to the $(\alpha4)_2(\beta2)_3$ nAChRs. As seen in figure 4.2 and sequence analysis, the dexmecamylamine binding pocket area is conserved between β2 and α7 subunits.

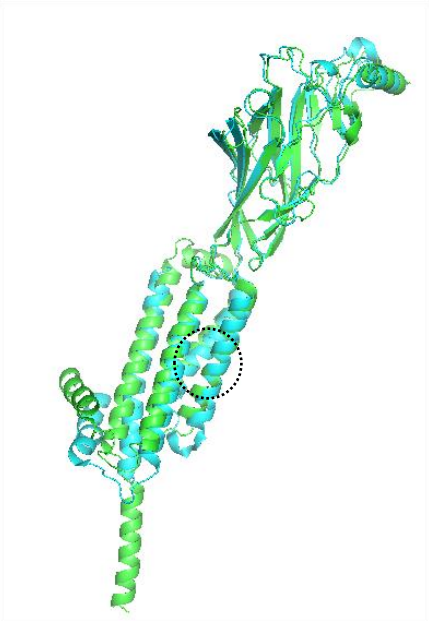

Figure 4.2 The structure alignment of β2 and α7 subunits.
The β2 subunit is coloured in cyan, while the α7 subunit is coloured in green. The position of Gly238 on β2/Gly236 on α7 is circled by dash lines.

4.2.3 Binding of dexmecamylamine to α7 nAChRs

To investigate the binding mode of dexmecamylamine to the identified binding site in the open state of α7 nAChRs by MD simulation, we first docked dexmecamylamine to the open state α7 nAChR, using G236 as the grid box center. We generated ten binding poses and determined the most appropriate binding pose based on Glide score, Glide energy, and visual inspection. Binding energy and Glide score were extracted and listed in table 4.1. Each generated pose was assigned a

unique Pose ID. According to the table 4.1, the glide energy of dexmecamylamine binding arranged from -21.655 kcal/mol to -16.573 kcal/mol, and the glide score arranged from -5.68 kcal/mol to -4.73 kcal/mol. Binding pose one was identified as the representative pose, exhibiting a glide energy of -21.655 kcal/mol and a glide score of -5.68 kcal/mol (table 4.1).

Table 4.1 The docking result (glide score and docking score) and glide energy of dexmecamylamine on the open state α7 nAChRs

Title (ID)	Glide energy (kcal/mol)	Glide score (kcal/mol)
Dexmecamylamine(1)	-21.655	-5.68
Dexmecamylamine(2)	-19.156	-5.34
Dexmecamylamine(3)	-17.164	-5.193
Dexmecamylamine(4)	-18.98	-5.14
Dexmecamylamine(5)	-17.567	-5.07
Dexmecamylamine(6)	-16.573	-5.065
Dexmecamylamine(7)	-17.778	-4.998
Dexmecamylamine(8)	-17.429	-4.835
Dexmecamylamine(9)	-17.367	-4.825
Dexmecamylamine(10)	-17.18	-4.732

In a prior study (Bondarenko et al., 2014), dexmecamylamine was situated within the central pore of $(\alpha4)_2(\beta2)_3$ nAChRs. However, our docking results revealed dexmecamylamine to be positioned nearer to the interface of two α7 subunits, rather than remaining at the channel pore's center. The hydrogen of the ammonium on dexmecamylamine interacts with residues S263 and T267 (figure 4.3).

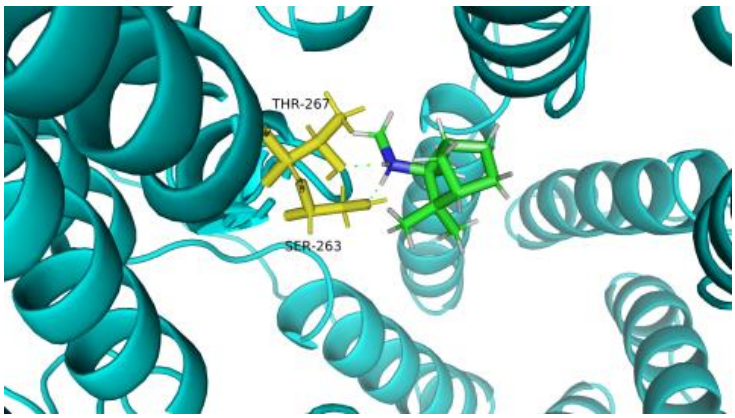

Figure 4.3 Binding mode of dexmecamylamine to the open state α7 nAChR.
Figure 4.3 is the depiction of dexmecamylamine binding position within the open-state α7 nAChRs (PDB code: 7KOX). It illustrated the dexmecamylamine binding sphere and surrounding residues. α7 subunits are colored cyan, dexmecamylamine in green, and residues in yellow. Residue numbering follows the sequence numbering in the captured structure. Green dashed lines represent hydrogen bonds between dexmecamylamine and residues T267 and S263.

4.3 Molecular Dynamics Simulation

4.3.1 Binding of PNU-120596 to α7 nAChRs

4.3.1.1 System set up and MD simulation

To investigate PNU-120596 binding poses to the open-state α7 nAChRs structure and examine channel pore movement, a 250 ns molecular dynamics simulation was performed in triplicate at 300K to simulate laboratory conditions. The CHARMM-GUI was utilized to generate the bilayer-protein complex, embedding the protein's transmembrane domain within a POPC lipid bilayer, while the extracellular and intracellular domains were inserted into water molecules and Na+ or Cl− ions. Figure 4.4 depicted the complete system that generated using CHARMM-GUI from both side view (figure 4.4 (a)) and top view (figure 4.4 (b)). As shown in the figure, the red sphere refers to the water molecules, while the other purple and green spheres refer to sodium ions and chloride ions. The box was hexagonal and the protein was located in the central of the box. This complex were used in the further MD simulations.

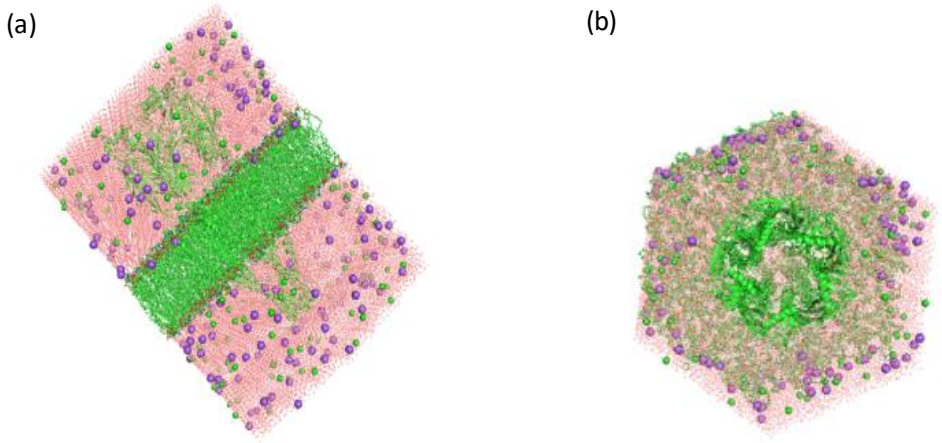

Figure 4.4 Solvent box for the α7 nAChRs by CHARMM-GUI.
Complete system generated using CHARMM-GUI. Side view (a) and top view (b). The protein-ligand complex is embedded within the bilayer system. Purple, red, and green spheres represent sodium ions, water molecules, and chloride ions, respectively. The protein-ligand complex is located centrally within the system.

The MD simulation workflow comprised four steps: energy minimization, NVT equilibrium, NPT equilibrium, and production dynamics simulation. The initial step minimized the system's energy by constraining heavy atoms in the protein backbone and PNU-120596 while minimizing water molecules' energy. The energy minimization step involved 5,000,000 steps using the steepest descent method with a 2 fs time step (for details, see Section 2.2.3.5). The maximum force endpoint was set at 10.0 kJ/mol. Following energy minimization, a NVT simulation (constant volume) and a NPT simulation (constant pressure) were performed to calibrate the system. During the NVT simulation, heavy atom constraints from the first step were maintained, and a 50,000-step NVT ensemble simulation was conducted for the entire system with a 2 fs time step, totaling 0.1 ns. Subsequently, an NPT ensemble simulation was performed at 300K to stabilize pressure and density with a friction coefficient of 1. After equilibration, a 250 ns production run was conducted with a 2 fs time step. Relevant parameters were analyzed using the GROMACS software package module.

4.3.1.2 RMSD calculation

To evaluate the stability of the molecular dynamics (MD) systems, we employed the root-mean-square deviation (RMSD) calculation through the "gmx rms" command. We determined the RMSD values for the protein complex, backbone, and PNU-120596 individually by measuring the average distance between corresponding atoms using MD simulation analysis. For scientific rigor, we ran the MD simulations in triplicate, ensuring that each atom's initial velocity was different across the three runs through the use of a velocity seed. As a homologous pentamer, α7 nAChRs are capable of binding five PNU-1205996. The RMSD value of each PNU-120596 compound was calculated

separately to investigate the movement of each PNU-120596 during the MD. The RMSD value was calculated for each PNU-120596, the protein backbone, and the complex and presented in figures 4.5, 4.6, and 4.7. The results revealed that the RMSD values of the protein-ligand complex were significantly similar and converged at approximately 0.4 nm in all three MD simulations. We selected the MD simulation with the lowest RMSD value for further analysis, as shown in figure 4.5. The RMSD value of the protein backbone stabilized at around 0.4 nm (4Å) for each component, while the RMSD value of the PNU-120596 ligands stabilized at approximately 0.1 nm (1Å). Throughout the simulation, all five PNU-120596 ligands maintained stable positions when bound to the default pocket. However, the significant fluctuation of the PNU-120596 RMSD curve at around 50 ns (as illustrated in figure 4.6(c)) suggests that the initial binding pose for one of the PNU-120596 compounds was not stable at the α7 subunit interface site. Nonetheless, the PNU-120596 achieved a stable pose after the MD simulation, as indicated by the RMSD value.

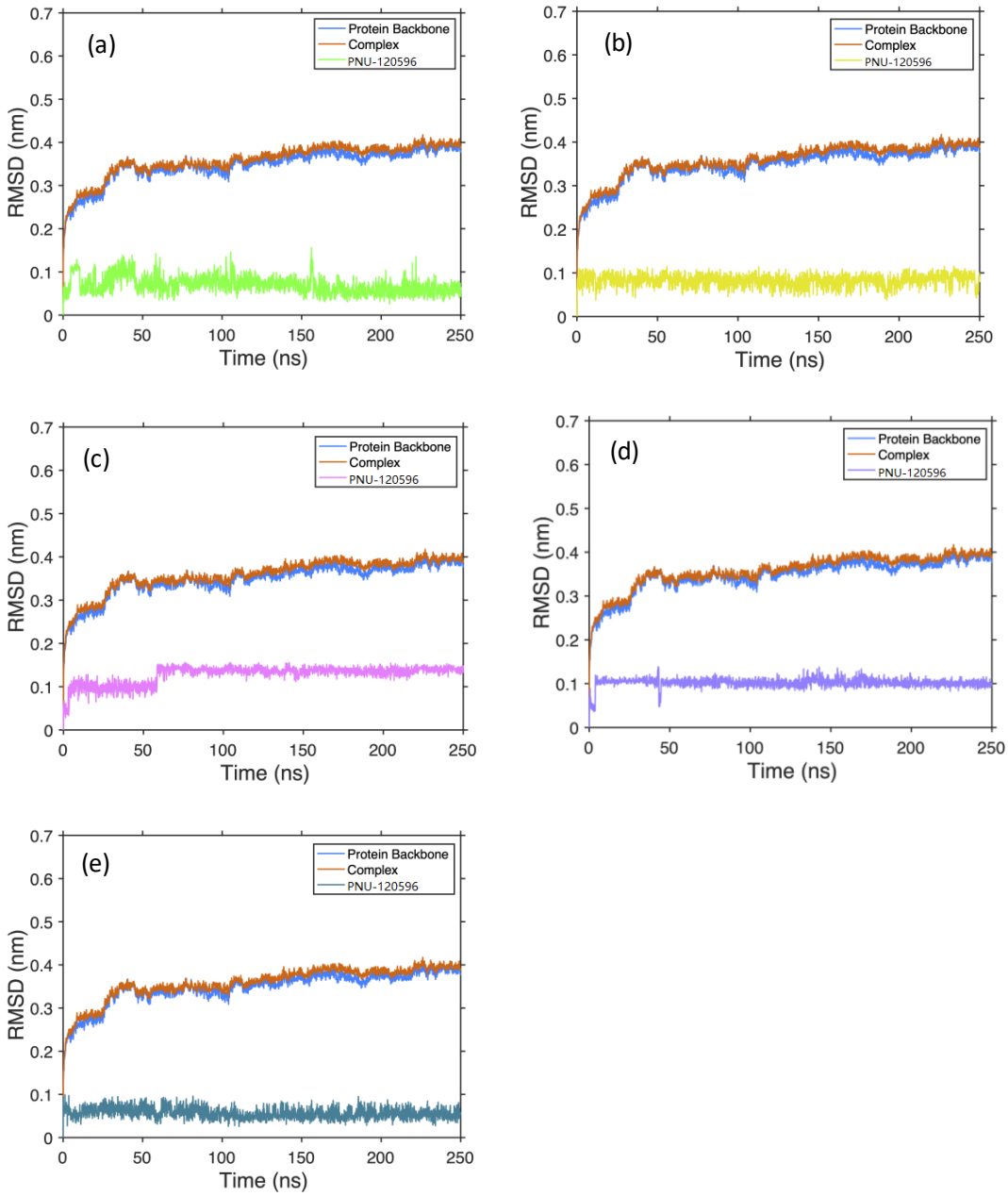

Figure 4.5 RMSD value for the complexes of PNU-120596-α7 nAChRs complex in the sumulations (first replica).

Figure 4.5 displays the RMSD values from the first 250 ns MD simulation of PNU-120596 binding to the active state α7 nAChRs. Each panel represents different elements' RMSD values, with the blue and red curves indicating protein backbone and ligand-protein complex, respectively. The green, yellow, pink, purple, and mazarine curves represent the RMSD values measured over each PNU-120596 (figure 4.5 (a-e)).

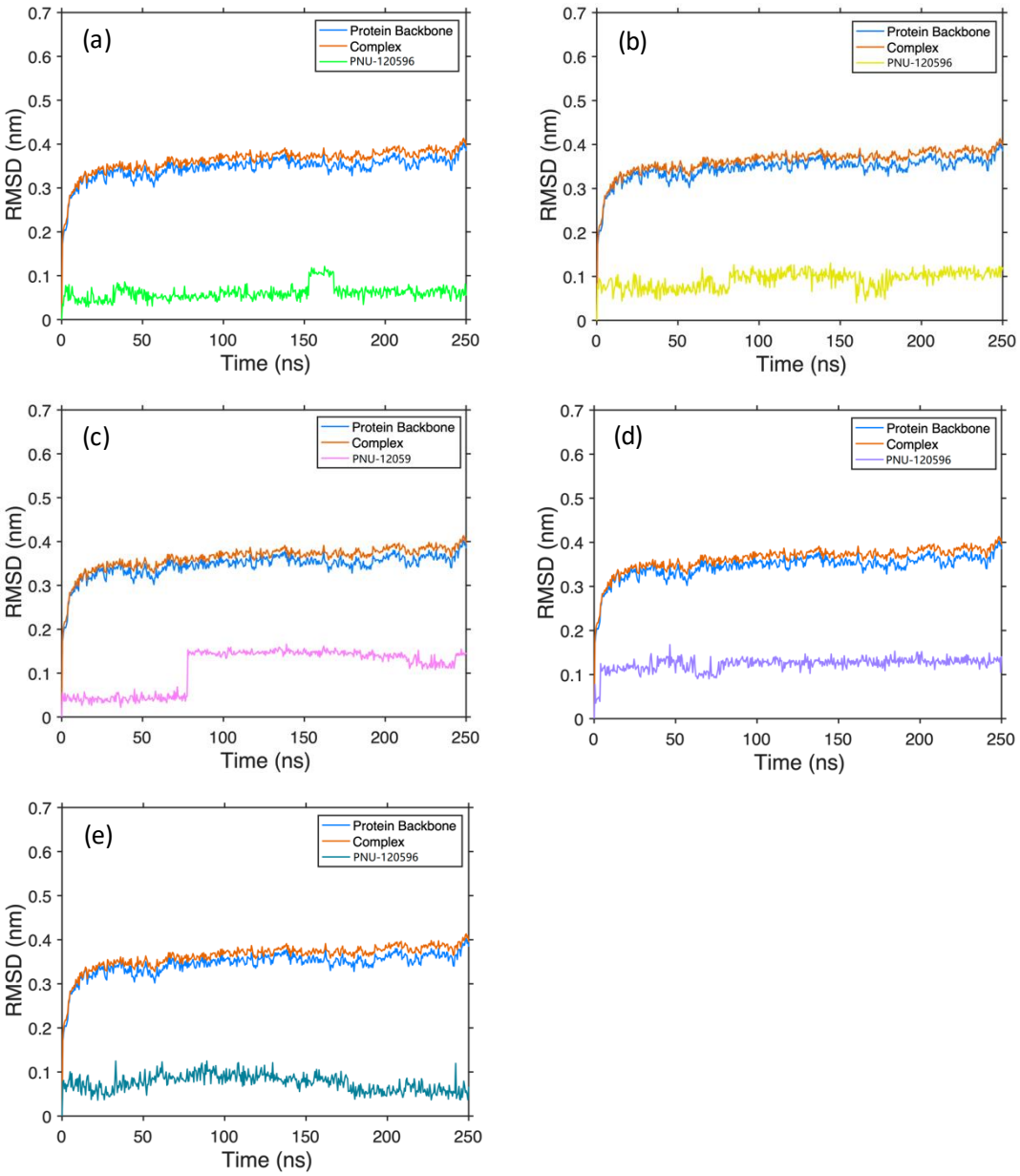

Figure 4.6 RMSD value for the complexes of PNU-120596-α7 nAChRs complex in the sumulations (second replica).

Figure 4.6 presents the RMSD values from the second 250 ns MD simulation of PNU-120596 binding to the active state α7 nAChRs. As in Figure 4.5, each panel represents different elements' RMSD values, with the blue and red curves indicating protein backbone and ligand-protein complex, respectively. The green, yellow, pink, purple, and mazarine curves represent the RMSD values measured over each PNU-120596 (figure 4.6 (a-e)).

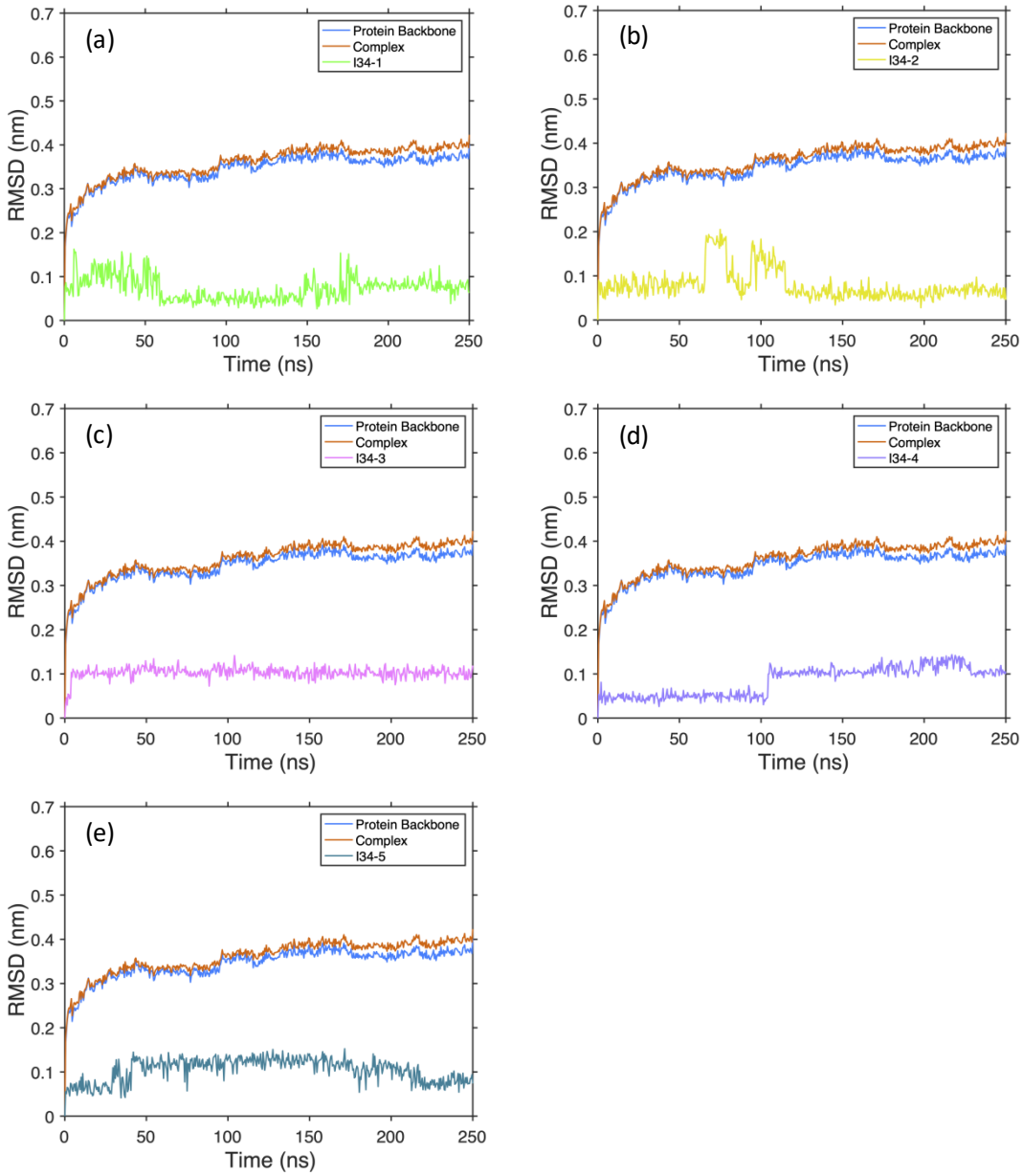

Figure 4.7 RMSD value for the complexes of PNU-120596-α7 nAChRs complex in the sumulations (third replica).

Figure 4.7 illustrates the RMSD values from the third 250 ns MD simulation of PNU-120596 binding to the active state α7 nAChRs. Each panel represents different elements' RMSD values, with the blue and red curves indicating protein backbone and ligand-protein complex, respectively. The green, yellow, pink, purple, and mazarine curves represent the RMSD values measured over each PNU-120596 (figure 4.7 (a-e)).

4.3.1.3 PCA analysis and free energy landscape calculation

Among the three replicas, the second replica exhibited the lowest RMSD value (figure 4.5) and was selected for further principal components analysis (PCA) and free energy landscape (FEL)

calculations. A PCA was conducted on the complex structure to identify the principal components of the system. The cumulative proportion was utilized to determine the variance explained by the principal components. The principal components accounting for an acceptable level of variance were retained for subsequent free energy analysis. Components explaining more than 90% of the variance were considered principal components. Figure 4.8 displays the scree plot of PCA. The scree plot arranges eigenvalues from largest to smallest, presenting a steep curve followed by a bend and a straight line. The steep curve components were used before the first point initiated the line trend. According to figure 4.8, the first and second components (PC1 and PC2) accounted for the majority of the system's variance. Consequently, PC1 and PC2 were utilized as the principal components of the system for further free energy analysis.

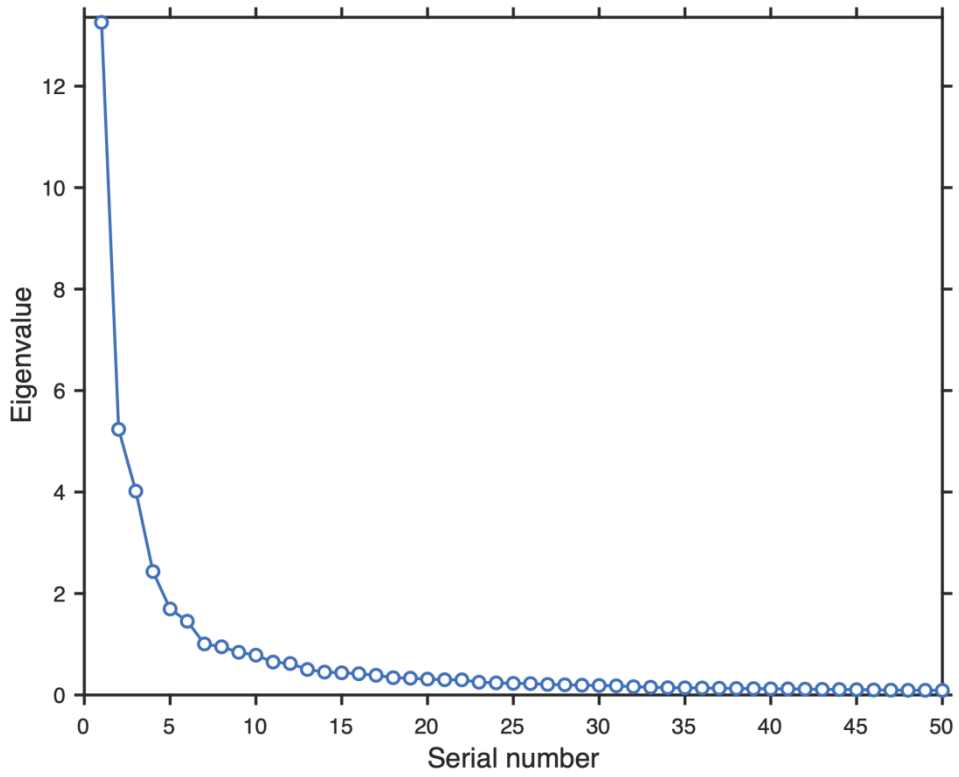

Figure 4.8 Scree Plot of Eigenvalue analysis of PNU-120596-α7 nAChRs complex.
In the figure presented, each dot symbolizes a component. The initial five principal components possess eigenvalues exceeding 1. As illustrated by the scree plot, the eigenvalues begin to follow a linear pattern after the fifth principal component. The majority of the variance is predominantly accounted for by the first two components, namely PC1 and PC2.

Figure 4.9 depicts the bidimensional free energy landscape (FEL) contour maps for the PNU-120596-α7 nAChRs complex. Based on the FEL, two minimal energy clusters and extensive structural distributions are evident during the molecular dynamics (figure 4.9a). The minimal energy clusters suggest that PNU-120596 achieves stable and robust interactions with α7 nAChRs throughout the MD simulations, corroborating our structural stability analysis. We further extracted the most representative structure possessing the lowest energy from the minimal energy regions. As per the FEL, the PNU-120596-α7 nAChRs complex attains its lowest energy conformer

at 230 ns snapshots. We extracted the snapshot from the free energy minimum cluster, dominating most portions of the FEL. The stable conformation with the lowest energy at 230 ns was acquired based on the FEL.

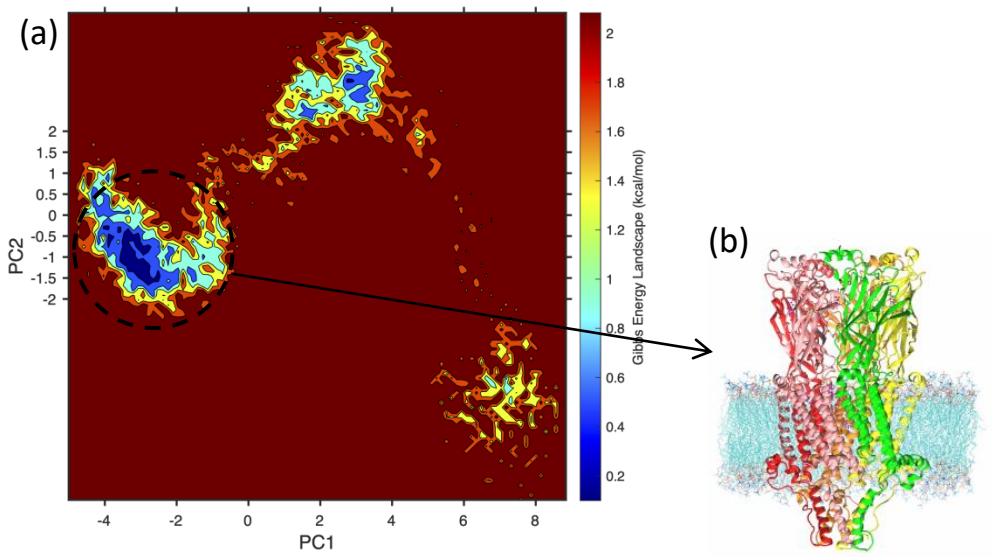

Figure 4.9 Free energy landscape (FEL) and representative structure of α7 nAChRs with PNU-120596 binding.

Bidimensional free energy landscape (2D-FEL) of dexmecamylamine (a) and the representative conformation (b) of dexmecamylamine and α7 nAChRs are displayed as a function of two principal components, with cosine contents below 0.2. The representative cluster of structures of dexmecamylamine binding forms (b) with minimal energy are magnified to reveal residues critical for ligand binding. The minimal energy clusters are emphasized using black dotted circles.

4.3.1.4 Ligand-binding behaviour and protein behaviour in the MD simulations

We performed a 250 ns molecular dynamics simulation three times and selected the simulation exhibiting the lowest RMSD value. Each extracted frame has a 0.1 ns time interval, resulting in 2500 frames with a stable production stage. During the MD simulation, water influx was observed in the PNU-120596-α7 nAChRs complex. The cross profile of the channel pore with water molecules in the extracted representative structure is displayed in figure 4.11. The figure reveals molecular water influx through the channel pore from the extracellular domain to the intracellular domain, indicating stable channel pore opening throughout the MD simulation.

We generated the trajectory animation within the VMD software. The binding pose of PNU-120596 during the final 50 ns of the simulation was clustered based on the RMSD measured over its non-hydrogen atoms while superimposing binding site residues. The representative pose of each PNU-120596 to the α7 nAChRs is illustrated in figure 4.10. Figure 4.10 (a)(b) represents two binding poses of five PNU-120596 compounds to the open state α7 nAChRs, extracted at 230 ns.

Figure 4.10 (a) and (b) display two distinct binding positions for five instances of PNU-120596. We provide an overhead perspective of the overall ligand-protein complex and the interaction between PNU-120596 and surrounding residues from top and side viewpoints. Based on visual inspection during the simulation, PNU-120596 stabilizes at the binding site between two α7 nAChRs subunits. Nevertheless, the binding positions of the five ligands differ. Four of the five PNU-120596 instances share the same binding position (figure 4.10(a)), while one has a unique binding position. Figure 4.10(a) portrays the overhead perspective of the overall ligand-protein complex. As per visual inspection during the simulation, PNU-120596 establishes a stable position at the binding site between two α7 nAChRs subunits. The four PNU-120596 insertions occur between two M2 helices. A hydrogen bond forms between PUN-120596 and residue P274 of α7 nAChRs, represented by the blue dashed line in figure 4.10(a) with a distance of 0.28 nm. In figure 4.10(b), we exhibit the binding position of a PNU-120596 to the α7 nAChRs from the overhead view, along with the interaction between PNU-120596 and adjacent residues. The PNU-120596 inserts horizontally into the two M2 helices between the α7 nAChRs subunits at this binding site. PNU-120596 achieves a stable position at the binding site. A hydrogen bond forms between PNU-120596 and A279 with a distance of 0.25 nm.

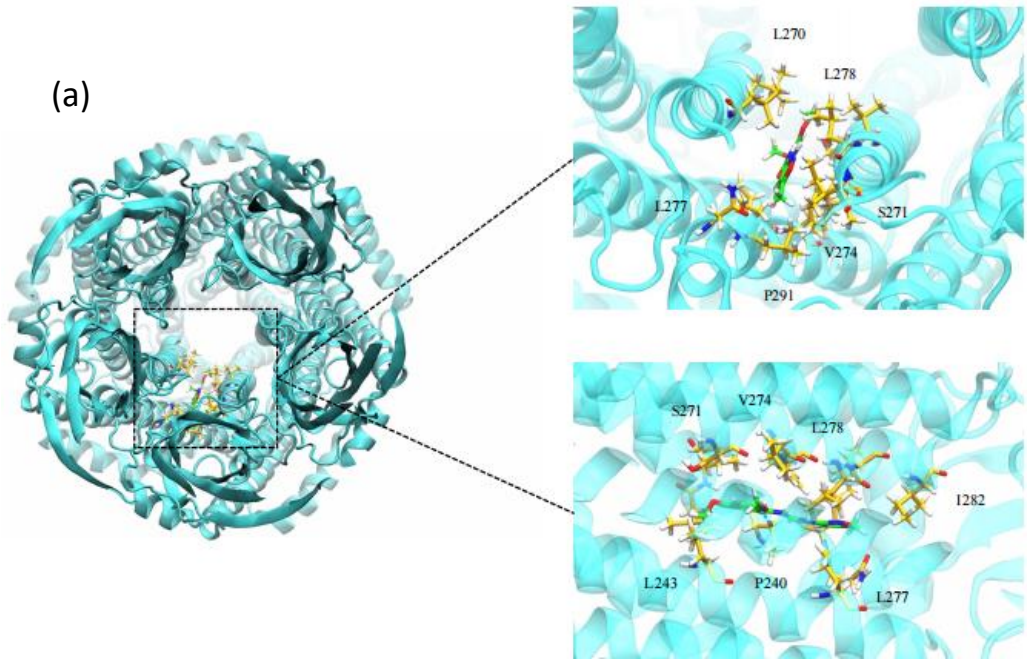

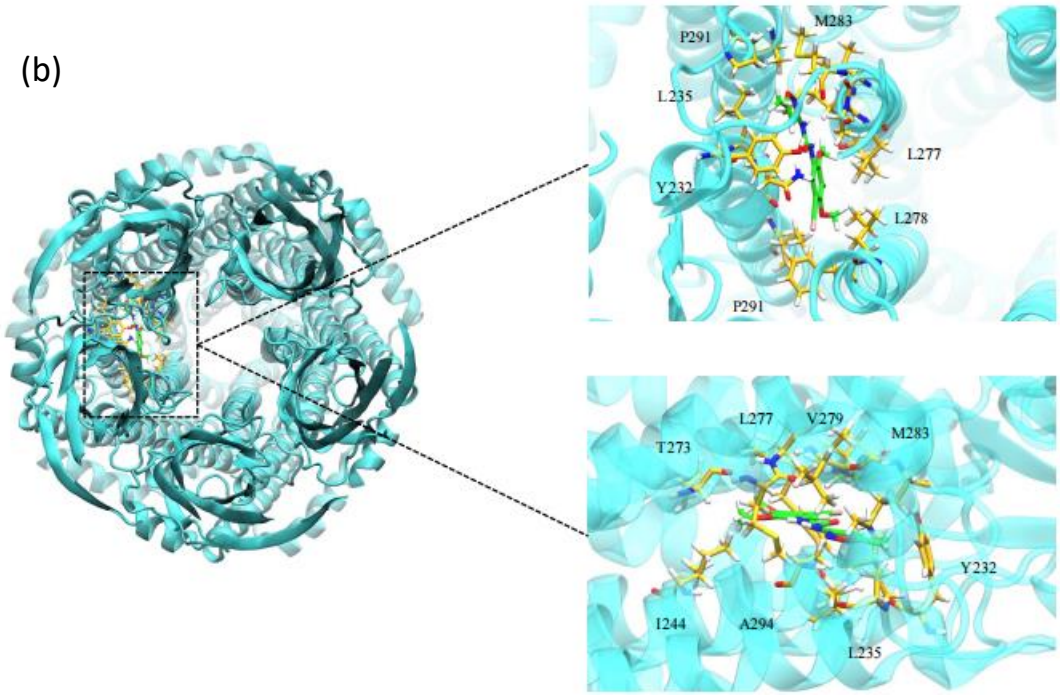

Figure 4.10 Representative binding pose of PNU-120596 at the α7 nAChRs binding site.
The top view of the overall representative binding pose of PNU-120596 docked at the α7 nAChRs ion channel binding site is presented, with relevant bold residues. The figure 4.10 (a) and figure 4.10 (b) represent two different binding positions of PNU-120596. The α7 subunits are depicted in cyan. Carbon atoms in PNU-120596 are colored green, and bold residues surrounding PNU-120596 are shown and colored yellow.

We generated a water flow trajectory during the MD simulation. Figure 4.11 reveals the water flow of the representative structure. Water molecules pass smoothly through the channel pore during the MD simulation. According to the results, α7 nAChRs maintain an open state throughout the entire MD simulation process. No channel pore collapse occurs during the MD simulation, and the channel pore remains hydrophilic.

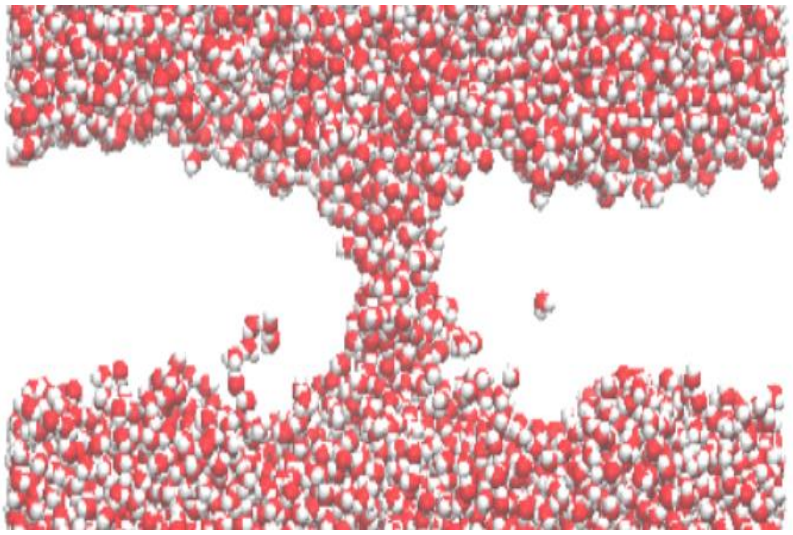

Figure 4.11 A snapshot depicting the solvation of the final frame in PNU-12059 binding to α7 nAChRs.
Oxygen and hydrogen atoms of water molecules are represented by red and white, respectively. As per the solvation visualization, the channel pore remained open throughout the molecular dynamics simulation process.

4.3.2 Binding of dexmecamylamine to α7 nAChRs

4.3.2.1 RMSD calculation

Prior molecular dynamics simulations of PNU-120596 binding to α7 nAChRs suggested that PNU-120596 facilitated the maintenance of a stable open state in α7 nAChRs. Consequently, we further docked dexmecamylamine to the PNU-120596-α7 nAChRs system to investigate the channel-blocking effect of dexmecamylamine. We executed molecular dynamics simulations of dexmecamylamine-α7 nAChRs thrice (figure 4.12 (a--c)), selecting the iteration with the lowest RMSD value for subsequent analysis. According to figure 4.12, the overall trend of RMSD values across the three simulation rounds is comparable. RMSD values for the three simulations stabilized at 0.35, 0.4, and 0.4, respectively. Thus, we employed the first-round simulation for further investigation. We examined dexmecamylamine's binding behavior to the open-state α7 nAChRs and channel pore movement based on molecular dynamics simulation results. Each simulation was performed for 250 ns. To conform to laboratory conditions and environment, we set the temperature to 300 K. The CHARMM-GUI was utilized to generate the bilayer-protein complex module.

A total of four steps in the MD procedure were conducted. The first step is energy minimization. The energy of heavy atoms in the protein backbone, the ligands, and water molecules was constrained to 50.0 kJ/mol. After the minimization, the equilibration procedure, including an NVT (constant volume) simulation followed by an NPT (constant pressure) simulation, was conducted to equilibrate the whole system. In the equilibration step, we conducted 5,000,000 steps by the

steepest descent method, and the time step was set as 2 fs (for details, refer to Section 2.2.3.5). In the final step, the MD simulation was conducted for 250 ns with a time step of 2 fs. We analyzed the MD simulation result in the GROMACS software package.

A total of four steps were executed in the molecular dynamics procedure. The initial step involved energy minimization, wherein the energy of heavy atoms in the protein backbone, ligands, and water molecules was constrained to 50.0 kJ/mol. Following minimization, the equilibration process, including an NVT (constant volume) simulation succeeded by an NPT (constant pressure) simulation, was conducted to equilibrate the entire system. During the equilibration step, we executed 5,000,000 steps using the steepest descent method, setting the time step to 2 fs (refer to Section 2.2.3.5 for details). In the final step, the molecular dynamics simulation was conducted for 250 ns with a time step of 2 fs. We analyzed the simulation results using the GROMACS software package. Figure 4.12 displays the RMSD of dexmecamylamine, protein backbone, and ligand-protein complex. RMSD values over the protein backbone and dexmecamylamine converged to approximately 0.3 nm and 0.05 nm, respectively. All measured elements, including the protein backbone and dexmecamylamine, attained stable conformations during the molecular dynamics simulation process. Dexmecamylamine reached a stable conformation after 50 ns, and the entire system achieved stability after 100 ns.

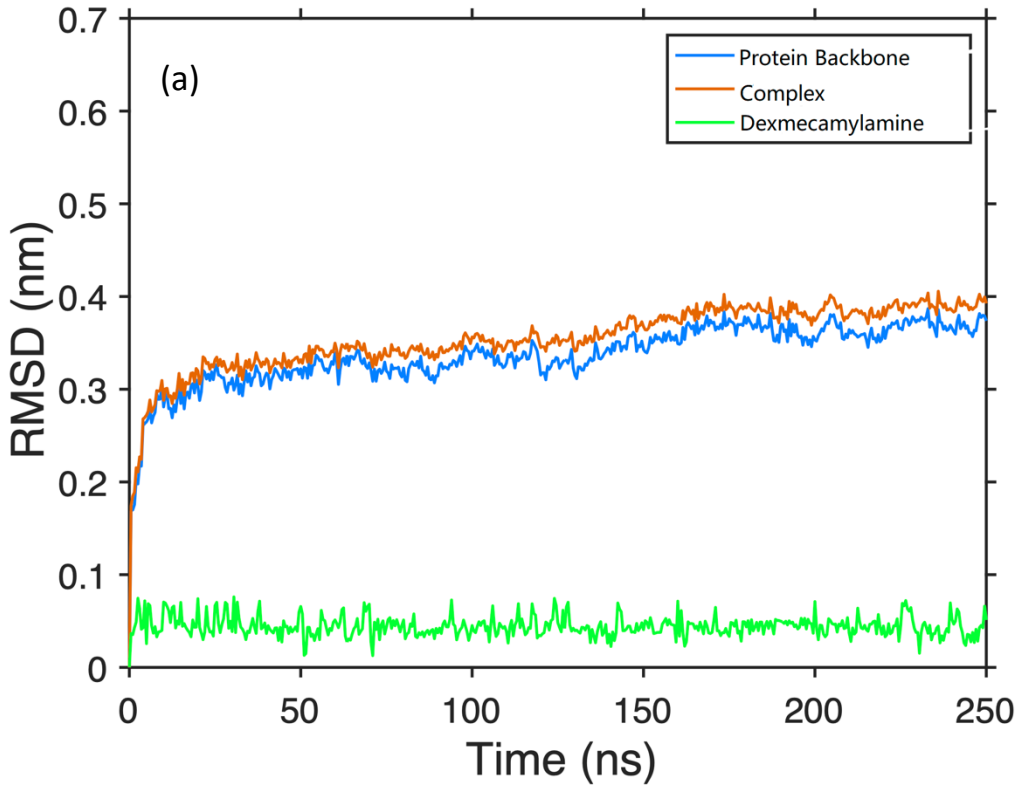

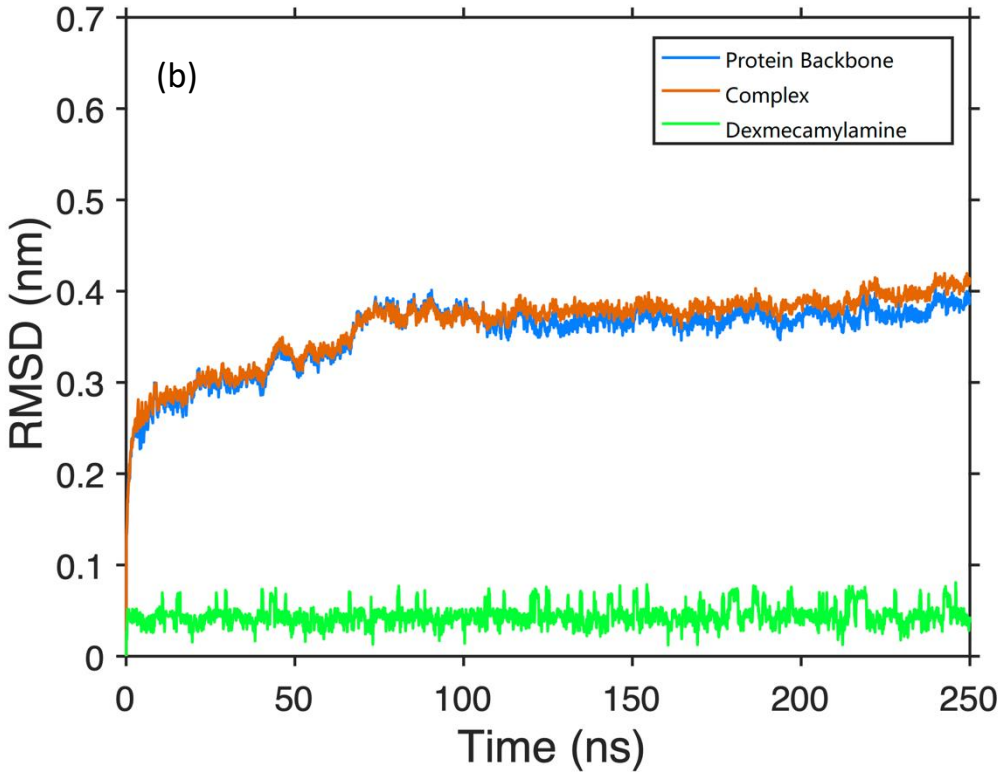

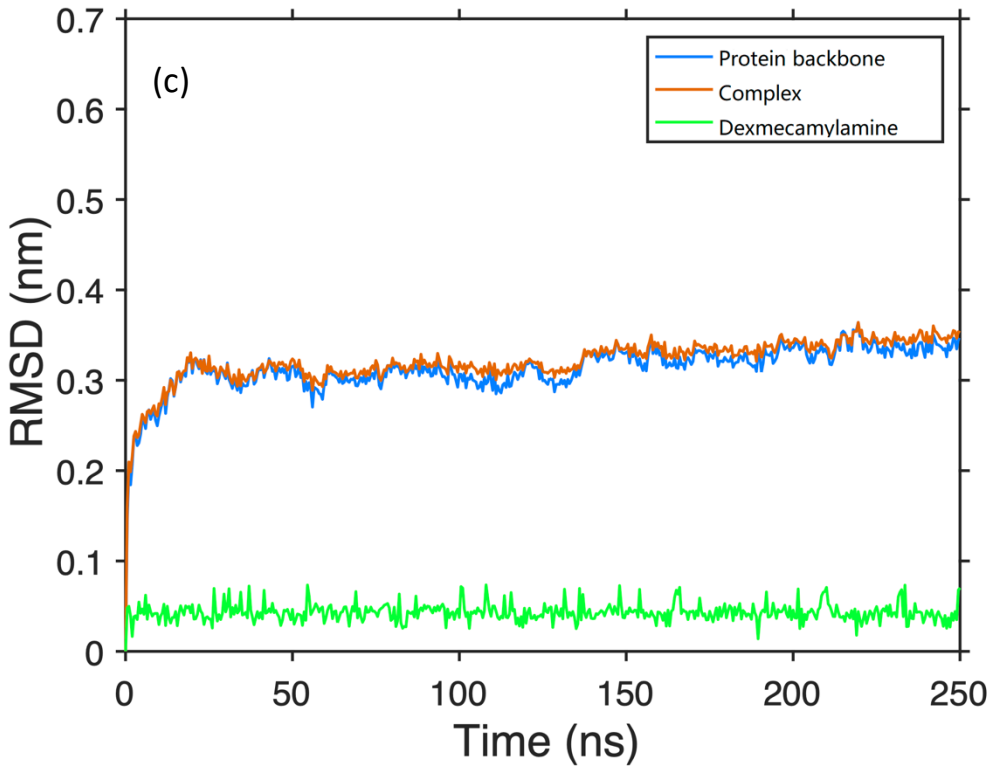

Figure 4.12 RMSD plots for the complexes of dexmecamylamine-α7 nAChRs complex in the sumulations.

Three molecular dynamics (MD) simulations were conducted for the dexmecamylamine-α7 nAChR complex. RMSD values for the three MD simulation runs are depicted in figure 4.12 (a-c),

representing the first, second, and third replicas, respectively. The simulation exhibiting the lowest RMSD value was selected for analysis. The panel illustrates RMSD plots for various elements measured during dexmecamylamine binding to the active state α7 nAChRs within a 250 ns simulation. Blue and red curves represent the protein backbone and ligand-protein complex, respectively, while the green curve displays RMSD values for dexmecamylamine.

4.3.2.2 PCA analysis and free energy landscape calculation

A principal component analysis (PCA) was performed to identify the system's principal component, with results illustrated as scree plots in figure 4.13. The principal component accounts for the cumulative proportion of determined variance. Components explaining the majority of the variance are considered principal components. In figure 4.13, scree plot eigenvalues are ordered from largest to smallest, displaying a steep curve followed by a bend and a straight line. Components within the steep curve preceding the initial point initiating the line trend are utilized for further FEL analysis. Based on figure 4.13, the first and second components, PC1 and PC2, explain over 90% of the system's variance; thus, they were employed as principal components for FEL analysis.

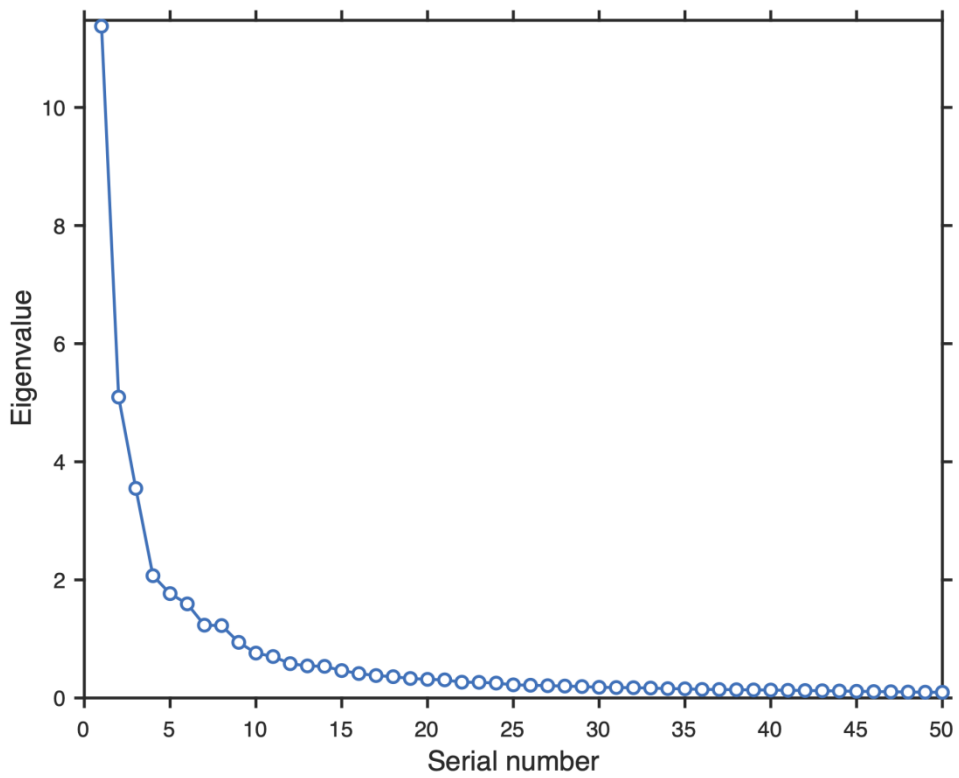

Figure 4.13 Scree plot of eigenvalue analysis of dexmecamylamine-α7 nAChRs complex
The first four principal components possess eigenvalues greater than 1 and explain over 90% of data variation. Consequently, the first two components (PC1 and PC2) were employed as principal components for free energy landscape (FEL) construction. The scree plot reveals that eigenvalues begin to form a straight line after the fifth principal component.

Figure 4.14 presents the two-dimensional FEL contour maps for the dexmecamylamine-α7 nAChR complex. Within the FEL, a large minimal energy cluster exists during molecular dynamics. The FEL indicates substantial structural distributions throughout molecular dynamics (figure 4.14(a)). Minimal energy clusters suggest that dexmecamylamine achieves stable and robust interactions with α7 nAChRs, where Gibbs energy is lower than 0.4. The representative structure at the lowest energy snapshot was extracted.

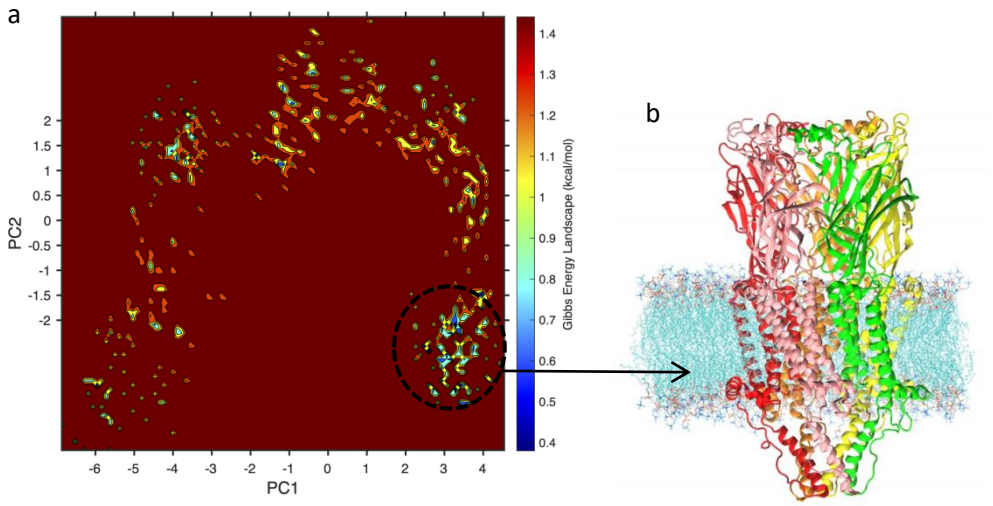

Figure 4.14 Free energy landscape (FEL) and representative α7 nAChRs structure with dexmecamylamine binding.

The two-dimensional free energy landscape (2D-FEL) of dexmecamylamine (A) and the representative conformation (B) of dexmecamylamine and α7 nAChRs are displayed as functions of two principal components with cosine contents less than 0.4. Representative structures of dexmecamylamine binding forms (B) with minimal energy are magnified to exhibit critical residues for ligand binding. Minimal energy clusters are highlighted using black dotted circles.

4.3.2.3 Ligand-binding behaviour and protein behaviour in the molecular dynamics simulation

As previously mentioned, molecular dynamics simulations were performed in triplicate to assess ligand-binding characteristics and protein dynamics. The second iteration, which exhibited the lowest RMSD value, was chosen for analysis. Each frame had a time interval of 0.1 ns, resulting in a total of 2500 frames with a stable production stage.

The interval between each frame was 0.1 ns, allowing for the extraction of 2500 frames with a stable production stage. Water influx into the PNU-120596-α7 nAChRs complex during the molecular dynamics simulation was observed. The cross-sectional profile of the channel pore with water molecules is depicted in figure 4.16. As shown in the figure, water flows from the extracellular domain to the intracellular domain through the channel pore, indicating stable pore

opening during the simulation. Trajectory animations were generated using Visual Molecular Dynamics (VMD) software. Dexmecamylamine binding poses during the final 50 ns were clustered based on RMSD values measured over non-hydrogen atoms, with binding site residues superimposed. The representative pose of dexmecamylamine binding to α7 nAChRs is shown in figure 4.15. According to the figure, dexmecamylamine forms two hydrogen bonds with the V274 amino acid residue at a distance of 0.28 nm. In comparison to the initial docking result, dexmecamylamine shifted upwards during the molecular dynamics simulation and stabilized near the extracellular mouth of the TMD. It is situated not at the center of the channel pore but near the interface of two α7 nAChR helices.

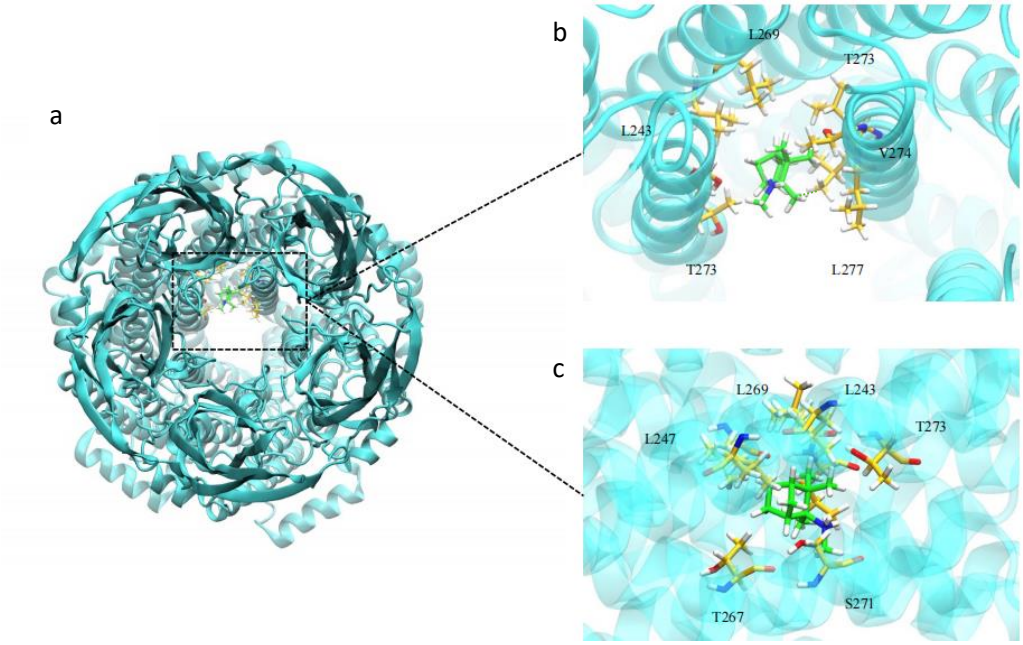

Figure 4.15 Representative binding pose of dexmecamylamine at the α7 nAChRs binding site.
The top-view of the representative binding pose of dexmecamylamine docked at the α7 nAChRs ion channel binding site is shown in panel (a). The binding position of dexmecamylamine is displayed from the top view (b) and side view (c), respectively. The homologous α7 nAChRs are colored blue. Dexmecamylamine atoms are green, while surrounding bold residues are yellow. Dexmecamylamine forms two hydrogen bonds with the V274 amino acid residue at a distance of 0.28 nm, indicated by the green dashed line.

The positions of water molecules in the representative structure are further illustrated in figure 4.16. As shown in the figure, the binding of dexmecamylamine allows water to fill the channel pore and flow through it. The channel pore remains hydrophilic during the molecular dynamics simulation.

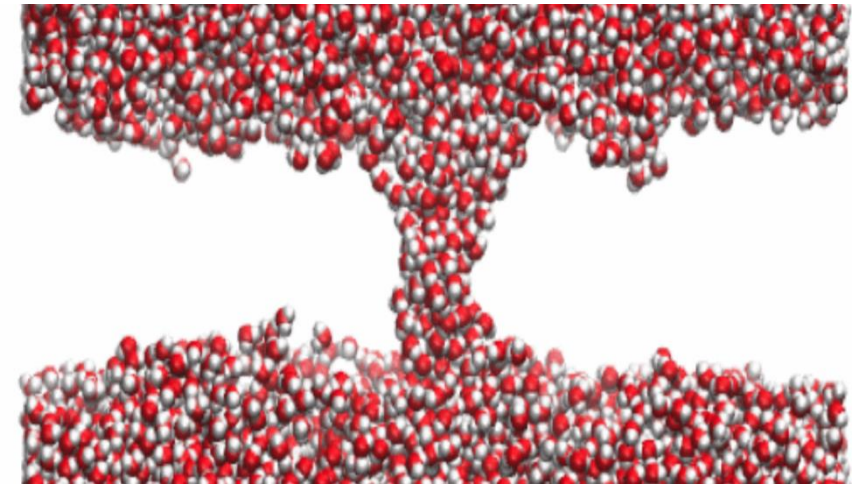

Figure 4.16 The water flow of the last frame of dexmecamylamine binding to the α7 nAChRs. Water flow during dexmecamylamine binding to α7 nAChRs is shown, with oxygen and hydrogen atoms represented by red and white, respectively.

4.3.2.4 Diameter measurement

We investigated the diameters of α7 nAChRs open state channel pores in the presence and absence of dexmecamylamine. The channel pore diameter was calculated utilizing the HOLE program. According to our findings, the narrowest diameter of α7 nAChRs open state channel pore without dexmecamylamine is 0.98 nm, while the narrowest diameter with dexmecamylamine is 0.91 nm. The binding of dexmecamylamine constricted the channel pore, functioning as a channel blocker. However, this relatively minor decrease in pore diameter may be inadequate to hinder Ca^{2+} influx. Further research, taking into account the solvation sphere radius of Ca^{2+}, is necessary to address this issue.

4.4 Conclusion of molecular modeling

In conclusion, the results of our molecular modeling study demonstrate the interactions between ligands and protein targets. The molecular docking studies enabled us to predict the binding orientation and affinity of both PNU-120596 and dexmecamylamine to the α7 nAChRs. Meanwhile, the molecular dynamic simulations provided us with insight into the dynamic behavior of the protein-ligand complex over time.

Our analysis revealed several key binding residues that contribute to the stability of the PNU-120596-α7 nAChRs (V274 and V279) and dexmecamylamine-α7 nAChRs complex (V274). These findings could potentially be utilized for the development of novel drug candidates. However, during the MD simulations, dexmecamylamine moved upward and was observed near PNU-120596 in the representative stable structure. As per our findings, dexmecamylamine failed to narrow the channel pore, thus preventing the blockade of calcium ion influx. In the next chapter, we will discuss our results, the limitations of the study, and potential directions for further research.

Chapter 5

Conclusion and discussion

5.1 General discussion

This project is divided into two sections. The first section is a meta-analysis investigating the antidepressant effect of dexmecamylamine, while the second section employs computational methods to explore the binding pose of dexmecamylamine to α7 nAChRs.

In our prior research, the antidepressant properties of mecamylamine and dexmecamylamine had not been examined using meta-analysis. It is essential to explore antidepressant drugs with novel targets since many individuals exhibit no or limited responses to first-line treatments. Discovering new therapeutic approaches for patients resistant to initial treatments is of utmost importance.

To our knowledge, this was the first meta-analysis investigating the antidepressant effect of dexmecamylamine in patients with MDD. We included a total of nine studies, conducting a risk of bias analysis for each. All nine studies were double-blind, randomized, placebo-controlled, and demonstrated an acceptable risk of bias. However, there were unclear risks in several domains, particularly the selective reporting risk. Our meta-analysis encompassed 2480 patients (1442 undergoing treatment and 1038 receiving a placebo). The total pooled effect size of the two primary endpoints, MADRS score change and HAMD-17 score change, revealed that the antidepressant effect of dexmecamylamine did not surpass that of the placebo. The pooled effect sizes of other secondary endpoints also suggested a limited antidepressant effect for dexmecamylamine. Most of the included studies employed the Hamilton Depression Rating Scale for Depression (HAMD-17) and the Montgomery Asberg Depression Rating Scale (MADRS) as primary outcomes, both of which are fully validated for assessing depression severity.

Our meta-analysis indicated that dexmecamylamine failed to reduce HAMD-17 ($p = 0.212$) or MADRS scores ($p = 0.782$), suggesting no antidepressant effect. Additionally, dexmecamylamine did not meet any other secondary endpoints. To ensure minimal heterogeneity among the included studies, we extracted data from patients with the same diagnosis, intervention duration (8 weeks), and administration (placebo vs. dexmecamylamine). The nine studies exhibited little variation.

In addition to heterogeneity, we conducted a publication bias analysis using both Egger's test and funnel plots for each group. The publication bias results indicated eight groups (score change of HAMD-17, remission rate, early and sustained response rate, sustained response rate, sustained remission rate, and score change of CGI-S, CGI-I response rate).

The heteromeric $(\alpha4)_2(\beta2)_3$ nicotinic acetylcholine receptors (nAChRs) and the homomeric α7 nAChRs represent two critical nAChR subtypes in the human brain, exhibiting significant contributions to the overall neurological landscape and playing a pivotal role in depression. Dexmecamylamine is considered a channel blocker with the potential to ameliorate depressive symptoms. This study aims to pinpoint the putative binding pocket of dexmecamylamine on α7 nAChRs and expound upon the functionality of dexmecamylamine as an α7 nAChR channel blocker. The open state of α7 nAChRs was elucidated via cryo-electron microscopy in prior research. PNU-120596 was docked to the open state α7 nAChR, followed by molecular dynamics (MD) simulation

to examine channel pore behavior. The MD simulation did not result in channel pore collapse of the PNU-120596-α7 nAChR complex. The dexmecamylamine binding site on the resolved structure of $(\alpha4)_2(\beta2)_3$ nAChRs was mapped based on previous studies. Sequence alignment facilitated the identification of essential binding residues of dexmecamylamine to α7 nAChRs. Subsequently, molecular docking was employed to investigate the dexmecamylamine binding site on the open state α7 nAChR with PNU-120596, and MD simulations were conducted to examine the motion of dexmecamylamine. Measurements of the channel pore hydrophilicity and diameter with and without dexmecamylamine were taken to depict the influx pathway of Ca^{2+}. Results suggest a minor reduction in pore diameter following dexmecamylamine binding, necessitating further investigation to determine whether this change is sufficient to impede the influx of Ca^{2+} ions.

5.2 Findings

In accordance with the meta-analysis outcomes, dexmecamylamine does not exhibit antidepressant efficacy. Subsequent molecular modeling was undertaken to scrutinize the dexmecamylamine binding site on the α7 nAChRs. It has been established that protein dynamics are strongly correlated with ligand binding affinity, suggesting that dexmecamylamine binding may be influenced by protein motion. We employed CHARMM-GUI to construct a protein-membrane complex and utilized established equilibration techniques to examine ligand behavior. Binding sites for drug molecules, including PNU-120596 and dexmecamylamine on the α7 nAChRs, were delineated. As per prior research, dexmecamylamine functions as a channel blocker for open-state nAChRs. We initially probed the binding conformation of PNU-120596 through molecular docking and MD simulations. Channel pore dynamics were assessed during MD simulations. Three iterations of MD simulations were executed. The RMSD values indicated no substantial disparities among the MD simulation replicates. All RMSD outcomes converged to analogous values; hence, we selected the MD iteration with the lowest RMSD for additional investigation. Based on RMSD, the PNU-120596-α7 nAChRs system reached stability after 150 ns. Subsequently, we employed PCA to evaluate the principal components of the system. PC1 and PC2 accounted for over 95% of the variance; thus, we used PC1 and PC2 to generate the FEL. In accordance with the FEL, we extracted the most stable conformation at the lowest energy snapshot. The MD simulation outcomes indicate that PNU-120596 can maintain the α7 nAChRs in an open state. Previous studies did not depict the binding location of PNU-120596. In our research, we investigated the binding site of PNU-120596 on the α7 nAChRs. A total of five PNU-120596 moieties bound to the α7 nAChRs. PNU-120596 inserts into the interface of two α7 nAChR subunits, with the interaction between PNU-120596 and the P274 of the α7 nAChR subunit occurring at a distance of 0.28 nm. Conversely, one PNU-120596 binding site deviates from the other four. This PNU-120596 was inserted horizontally into the two M2 helices of the α7 nAChRs subunit, interacting between he PNU-120596 and the A279 of α7 nAChR subunit at a distance of 0.25nm.

In the prior study, the dexmecamylamine binding site on $(\alpha4)_2(\beta2)_3$ nAChRs was elucidated using NMR spectroscopy, with several residues deemed crucial for binding. The sequences of $(\alpha4)_2(\beta2)_3$ nAChRs and α7 nAChRs were aligned, and based on this alignment, residue G236 on the α7 nAChRs subunit was identified as an essential binding residue. Utilizing molecular docking techniques, dexmecamylamine was docked to α7 nAChRs, functioning as a channel blocker within the channel

pore. Dexmecamylamine was found proximal to one α7 nAChR subunit rather than centrally located within the channel pore. Following initial docking, molecular dynamics (MD) simulations were conducted using GROMACS software. Three rounds of MD simulations were performed, with RMSD values exhibiting similar trends and convergence. Consequently, the MD simulation round with the lowest RMSD value was selected for further analysis. Based on the RMSD results, the dexmecamylamine-α7 nAChR system stabilized after 100 ns. Within the principal component analysis (PCA), PC1 and PC2 were identified as the system's primary components, which were subsequently utilized to construct the free energy landscape (FEL). In the FEL, energy points were dispersed, and the plot with minimized energy was extracted to represent the stable conformation, at which the dexmecamylamine binding site was analyzed. Compared to the initial binding site determined by molecular docking, dexmecamylamine shifted upward during MD simulation from near the extracellular mouth to the channel pore's midpoint. This phenomenon was observed in all three replicates. This may be attributed to dexmecamylamine's weak interactions with surrounding residues at initial binding position. Consequently, dexmecamylamine traversed the channel pore during MD simulation and bound to a site exhibiting stronger interactions. Furthermore, PNU-120596's binding may also influence dexmecamylamine's binding. The dexmecamylamine binding site was observed near PNU-120596, with non-hydrogen interactions detected between dexmecamylamine and PNU-120596. Therefore, alternative positive allosteric modulators (PAMs) should be employed to maintain α7 nAChR in an open state during MD simulations to prevent channel pore collapse. We measured the channel diameter of α7 nAChRs in the presence and absence of dexmecamylamine. The channel diameter constricted when dexmecamylamine was present, compared to its absence. Nevertheless, the diameter of Ca2+ ions remained smaller than that of the channel pore in the presence of dexmecamylamine. In our simulations, dexmecamylamine did not remain in the narrow lower region of the channel pore but migrated upwards, thereby not restricting the channel as anticipated. In future experiments, we will conduct a thorough analysis of the structure to elucidate this unforeseen behavior and contemplate conducting simulations with two to five molecules of dexmecamylamine bound within the channel pore.

5.3 Limitations and future perspectives

Our meta-analysis faces several limitations. First, only nine studies met the eligibility criteria, resulting in a limited number of studies per group (maximum 6, minimum 4). Consequently, due to the small sample size and variations among studies, it was challenging to derive a conclusive determination of dexmecamylamine's antidepressant efficacy. Second, the subjects in each study varied significantly, with studies 1 and 9 having only 21 subjects and study 3 having 813 subjects. Thus, when pooling effect results, the effect size was predominantly influenced by studies with larger sample sizes. Thirdly, we also compared our meta-analysis results with other contemporary meta-analyses, that investigated the efficacy of antidepressants for patients with depression. Ziqi and colleagues (2020) conducted a meta-analysis that included 48 studies to examine the antidepressant efficacy of antidepressants and anti-inflammatory drugs. This research considered seven first-line antidepressants (fluoxetine, paroxetine, escitalopram, sertraline, fluvoxamine, venlafaxine, and duloxetine), three types of anti-inflammatory drugs (NASIDs, cytokine-inhibitors, and pioglitazone), and ketamine (Yuan, 2020). The paper assessed the antidepressants' efficacy

through the odds ratio (OR) value of the response, defined as a 50% improvement from baseline to endpoint on depression rating scales. Publication bias was also addressed in Ziqi's study. Similar to our meta-analysis, the researchers used visual inspection of the funnel plot and the egger's test to evaluate publication bias. The results showed no publication bias, with a strictly symmetric funnel plot. In comparison, our study identified publication bias in one group. We applied the trim and fill method to explain the bias, but no articles were trimmed or filled, possibly due to the small number of included studies. Regarding heterogeneity, Ziqi's study found a high level of heterogeneity among the seven antidepressants. It may be because the study did not differentiate between various rating scales. It used a total of seven scales as indicators for response evaluation. However, there was no consistency across these scales. In contrast, our study specifically identified the scale used for each endpoint measurement.

Recent research reveals that depression treatment is primarily confined to second-generation antidepressant drugs, and some patients exhibit resistance to these medications. Therefore, it is crucial to explore novel antidepressant targets, such as channel blockers, which are vital antagonists of nicotinic acetylcholine receptors. However, current research on the 3D properties of α7 nAChRs binding sites is limited, and no studies have illustrated the binding site of α7 nAChRs. Since α7 nAChRs play a critical role in numerous mental disorders, especially depression, there is a need to elucidate the potential binding pocket of dexmecamylamine as a channel blocker.

Notably, numerous subtypes of nicotinic acetylcholine receptors exist, but our research is limited to the investigation of dexmecamylamine binding to α7 nAChRs. Future research should encompass other subtypes when additional structural information becomes available. Additionally, the accuracy of binding pose prediction may improve as higher-resolution structures of α7 nAChR and $(\alpha4)_2(\beta2)_3$ nAChRs become available.

Despite the promising antidepressant efficacy of dexmecamylamine evidenced in numerous clinical studies, our meta-analytical findings indicate that dexmecamylamine does not demonstrate antidepressant properties in humans. Nevertheless, as an ion channel receptor, nAChRs are deemed pivotal in the pathophysiology of MDD. As a result, we further investigated the binding domain of dexmecamylamine on nAChR, with the objective of comprehending why dexmecamylamine could not impede ion flux through ion channels and elucidating a binding site of the channel antagonist to nAChRs.

In accordance with our findings, dexmecamylamine is situated proximal to the M2 helix of the α7 subunit. We also discover that a singular dexmecamylamine binding is insufficient to occlude the channel pore and prevent the influx of calcium ions. The α7 nAChR is a homologous pentameric protein, and there may exist multiple α7 nAChR binding sites within the channel pore for dexmecamylamine. Consequently, in subsequent investigations, we considered the possibility of binding more than one dexmecamylamine molecule to the α7 nAChR and performed molecular dynamics (MD) simulations to assess whether it could obstruct the channel pore. Moreover, our research contributes to an enhanced understanding of the interaction between dexmecamylamine and α7 nAChRs. We can evaluate dexmecamylamine derivatives through molecular docking and select the compound with the appropriate functional group and dimensions to obstruct the

channel pore. Further MD simulations can be executed to examine the binding location and binding dynamics of this derivative.

Chapter 6

References

Ahn, E., & Kang, H. (2018). Introduction to systematic review and meta-analysis. *Korean J Anesthesiol, 71*(2), 103-112. doi:10.4097/kjae.2018.71.2.103

Albert, P. R. (2015). Why is depression more prevalent in women? *J Psychiatry Neurosci, 40*(4), 219-221. doi:10.1503/jpn.150205

Allen, M. P., & Tildesley, D. J. (1987). Computer simulation of liquids. Oxford University Press.

Alqazzaz, M., Thompson, A. J., Price, K. L., Breitinger, H. G., & Lummis, S. C. (2011). Cys-loop receptor channel blockers also block GLIC. Biophys J, 101(12), 2912-2918. doi:10.1016/j.bpj.2011.10.055

Al-Harbi K. S. (2012). Treatment-resistant depression: therapeutic trends, challenges, and future directions. Patient preference and adherence, 6, 369–388. https://doi.org/10.2147/PPA.S29716

American Psychiatric Association. (2013). Diagnostic and Statistical Manual of Mental Disorders (5th ed.). https://doi.org/10.1176/appi.books.9780890425596

Andersen, H. C. (1980). Molecular dynamics simulations at constant pressure and/or temperature. The Journal of Chemical Physics, 72(4), 2384–2393. https://doi.org/10.1063/1.439486

Arias, H. R., Rosenberg, A., Targowska-Duda, K. M., Feuerbach, D., Jozwiak, K., Moaddel, R., & Wainer, I. W. (2010). Tricyclic antidepressants and mecamylamine bind to different sites in the human alpha4beta2 nicotinic receptor ion channel. *Int J Biochem Cell Biol, 42*(6), 1007-1018. doi:10.1016/j.biocel.2010.03.002

Asharani, P. V., Ling Seet, V. A., Abdin, E., Siva Kumar, F. D., Wang, P., Roystonn, K., . . . Subramaniam, M. (2020). Smoking and Mental Illness: Prevalence, Patterns and Correlates of Smoking and Smoking Cessation among Psychiatric Patients. *Int J Environ Res Public Health, 17*(15). doi:10.3390/ijerph17155571

Bacher, I., Wu, B., Shytle, D. R., & George, T. P. (2009). Mecamylamine - a nicotinic acetylcholine receptor antagonist with potential for the treatment of neuropsychiatric disorders. *Expert Opin Pharmacother, 10*(16), 2709-2721. doi:10.1517/14656560903329102

Baddick, C. G., & Marks, M. J. (2011). An autoradiographic survey of mouse brain nicotinic acetylcholine receptors defined by null mutants. *Biochem Pharmacol, 82*(8), 828-841. doi:10.1016/j.bcp.2011.04.019

Bagby, R. M., Ryder, A. G., Schuller, D. R., & Marshall, M. B. (2004). The Hamilton Depression Rating Scale: has the gold standard become a lead weight?. The American journal of psychiatry, 161(12), 2163–2177. https://doi.org/10.1176/appi.ajp.161.12.2163

Bailar, J. C., 3rd. (1997). The promise and problems of meta-analysis. *N Engl J Med, 337*(8), 559-561. doi:10.1056/nejm199708213370810

Balhara, Y. P., & Verma, R. (2012). Schizophrenia and suicide. *East Asian Arch Psychiatry, 22*(3), 126-133.

Berger, S. I., & Iyengar, R. (2011). Role of systems pharmacology in understanding drug adverse events. *Wiley Interdiscip Rev Syst Biol Med, 3*(2), 129-135. doi:10.1002/wsbm.114

Berman, R. M., Fava, M., Thase, M. E., Trivedi, M. H., Swanink, R., McQuade, R. D., . . . Marcus, R. N. (2009)Bouzat. Aripiprazole augmentation in major depressive disorder: a double-blind, placebo-controlled study in patients with inadequate response to antidepressants. *CNS Spectr, 14*(4), 197-206. doi:10.1017/s1092852900020216

Bondarenko, V., Targowska-Duda, K. M., Jozwiak, K., Tang, P., & Arias, H. R. (2014). Molecular

interactions between mecamylamine enantiomers and the transmembrane domain of the human α4β2 nicotinic receptor. *Biochemistry, 53*(5), 908-918. doi:10.1021/bi400969x

Bondarenko, V., Wells, M. M., Chen, Q., Tillman, T. S., Singewald, K., Lawless, M. J., . . . Tang, P. (2022). Structures of highly flexible intracellular domain of human α7 nicotinic acetylcholine receptor. *Nat Commun, 13*(1), 793. doi:10.1038/s41467-022-28400-x

Bosko, J. T., Todd, B. D., & Sadus, R. J. (2005). Molecular simulation of dendrimers and their mixtures under shear: comparison of isothermal-isobaric (NpT) and isothermal-isochoric (NVT) ensemble systems. The Journal of chemical physics, 123(3), 34905. https://doi.org/10.1063/1.1946749

Bouzat, C., Lasala, M., Nielsen, B. E., Corradi, J., & Esandi, M. D. C. (2018). Molecular function of α7 nicotinic receptors as drug targets. The Journal of physiology, 596(10), 1847–1861. https://doi.org/10.1113/JP275101

Busner, J., & Targum, S. D. (2007). The clinical global impressions scale: applying a research tool in clinical practice. *Psychiatry (Edgmont), 4*(7), 28-37.

Cahill, A. L., Hurley, J. H., & Fox, A. P. (2000). Coexpression of cloned alpha(1B), beta(2a), and alpha(2)/delta subunits produces non-inactivating calcium currents similar to those found in bovine chromaffin cells. *J Neurosci, 20*(5), 1685-1693. doi:10.1523/jneurosci.20-05-01685.2000

Carrozzino, D., PaCederholmtierno, C., Fava, G. A., & Guidi, J. (2020). The Hamilton Rating Scales for Depression: A Critical Review of Clinimetric Properties of Different Versions. *Psychother Psychosom, 89*(3), 133-150. doi:10.1159/000506879

Cassano, P., & Fava, M. (2004). Tolerability issues during long-term treatment with antidepressants. *Ann Clin Psychiatry, 16*(1), 15-25. doi:10.1080/10401230490281618

Cederholm, J. M., Schofield, P. R., & Lewis, T. M. (2009). Gating mechanisms in Cys-loop receptors. *Eur Biophys J, 39*(1), 37-49. doi:10.1007/s00249-009-0452-y

Celie, P. H., van Rossum-Fikkert, S. E., van Dijk, W. J., Brejc, K., Smit, A. B., & Sixma, T. K. (2004). Nicotine and carbamylcholine binding to nicotinic acetylcholine receptors as studied in AChBP crystal structures. Neuron, 41(6), 907–914. https://doi.org/10.1016/s0896-6273(04)00115-1

Champtiaux, N., Han, Z. Y., Bessis, A., Rossi, F. M., Zoli, M., Marubio, L., . . . Changeux, J. P. (2002). Distribution and pharmacology of alpha 6-containing nicotinic acetylcholine receptors analyzed with mutant mice. *J Neurosci, 22*(4), 1208-1217. doi:10.1523/jneurosci.22-04-01208.2002

Chang, Y. C., Wu, W., Zhang, J. L., & Huang, Y. (2009). Allosteric activation mechanism of the cys-loop receptors. Acta pharmacologica Sinica, 30(6), 663–672. https://doi.org/10.1038/aps.2009.51

Changeux, J. P., & Christopoulos, A. (2016). Allosteric Modulation as a Unifying Mechanism for Receptor Function and Regulation. *Cell, 166*(5), 1084-1102. doi:10.1016/j.cell.2016.08.015

Changeux, J. P., & Edelstein, S. J. (1998). Allosteric receptors after 30 years. *Neuron, 21*(5), 959-980. doi:10.1016/s0896-6273(00)80616-9

Charlier, C., Bouvignies, G., Pelupessy, P., Walrant, A., Marquant, R., Kozlov, M., . . . Ferrage, F. (2017). Structure and Dynamics of an Intrinsically Disordered Protein Region That Partially Folds upon Binding by Chemical-Exchange NMR. *J Am Chem Soc, 139*(35), 12219-12227.

doi:10.1021/jacs.7b05823

Chen, G., Seukep, A. J., & Guo, M. (2020). Recent Advances in Molecular Docking for the Research and Discovery of Potential Marine Drugs. *Mar Drugs, 18*(11). doi:10.3390/md18110545

Chiriţă, A. L., Gheorman, V., Bondari, D., & Rogoveanu, I. (2015). Current understanding of the neurobiology of major depressive disorder. *Rom J Morphol Embryol, 56*(2 Suppl), 651-658.

Chockalingam, R., Gott, B. M., & Conway, C. R. (2019). Tricyclic Antidepressants and Monoamine Oxidase Inhibitors: Are They Too Old for a New Look?. Handbook of experimental pharmacology, 250, 37–48. https://doi.org/10.1007/164_2018_133

Collins, T., Young, G. T., & Millar, N. S. (2011). Competitive binding at a nicotinic receptor transmembrane site of two α7-selective positive allosteric modulators with differing effects on agonist-evoked desensitization. *Neuropharmacology, 61*(8), 1306-1313. doi:10.1016/j.neuropharm.2011.07.035

Corya, S. A., Williamson, D., Sanger, T. M., Briggs, S. D., Case, M., & Tollefson, G. (2006). A randomized, double-blind comparison of olanzapine/fluoxetine combination, olanzapine, fluoxetine, and venlafaxine in treatment-resistant depression. *Depress Anxiety, 23*(6), 364-372. doi:10.1002/da.20130

Couturier, S., Bertrand, D., Matter, J. M., Hernandez, M. C., Bertrand, S., Millar, N., . . . Ballivet, M. (1990). A neuronal nicotinic acetylcholine receptor subunit (alpha 7) is developmentally regulated and forms a homo-oligomeric channel blocked by alpha-BTX. *Neuron, 5*(6), 847-856. doi:10.1016/0896-6273(90)90344-f

Dajas-Bailador, F., & Wonnacott, S. (2004). Nicotinic acetylcholine receptors and the regulation of neuronal signalling. *Trends Pharmacol Sci, 25*(6), 317-324. doi:10.1016/j.tips.2004.04.006

Dani, J. A. (2015). Neuronal Nicotinic Acetylcholine Receptor Structure and Function and Response to Nicotine. *Int Rev Neurobiol, 124*, 3-19. doi:10.1016/bs.irn.2015.07.001

Davis, A. K., Barrett, F. S., May, D. G., Cosimano, M. P., Sepeda, N. D., Johnson, M. W., . . . Griffiths, R. R. (2021). Effects of Psilocybin-Assisted Therapy on Major Depressive Disorder: A Randomized Clinical Trial. *JAMA Psychiatry, 78*(5), 481-489. doi:10.1001/jamapsychiatry.2020.3285

Dineley, K. T., Pandya, A. A., & Yakel, J. L. (2015). Nicotinic ACh receptors as therapeutic targets in CNS disorders. *Trends Pharmacol Sci, 36*(2), 96-108. doi:10.1016/j.tips.2014.12.002

Duval, S., & Tweedie, R. (2000). Trim and fill: A simple funnel-plot-based method of testing and adjusting for publication bias in meta-analysis. Biometrics, 56(2), 455–463. https://doi.org/10.1111/j.0006-341x.2000.00455.x

Egger, M., Smith, G. D., & Phillips, A. N. (1997). Meta-analysis: principles and procedures. *Bmj, 315*(7121), 1533-1537. doi:10.1136/bmj.315.7121.1533

Elkins, M. R., Moseley, A. M., Sherrington, C., Herbert, R. D., & Maher, C. G. (2013). Growth in the Physiotherapy Evidence Database (PEDro) and use of the PEDro scale. *Br J Sports Med, 47*(4), 188-189. doi:10.1136/bjsports-2012-091804

Fasoli, F., & Gotti, C. (2015). Structure of neuronal nicotinic receptors. *Curr Top Behav Neurosci, 23*, 1-17. doi:10.1007/978-3-319-13665-3_1

Fedorov, N. B., Benson, L. C., Graef, J., Lippiello, P. M., & Bencherif, M. (2009). Differential pharmacologies of mecamylamine enantiomers: positive allosteric modulation and noncompetitive inhibition. *J Pharmacol Exp Ther, 328*(2), 525-532. doi:10.1124/jpet.108.146910

Ferguson, J. M. (2001). SSRI Antidepressant Medications: Adverse Effects and Tolerability. *Prim Care Companion J Clin Psychiatry, 3*(1), 22-27. doi:10.4088/pcc.v03n0105

Filatova, E. V., Shadrina, M. I., & Slominsky, P. A. (2021). Major Depression: One Brain, One Disease, One Set of Intertwined Processes. *Cells, 10*(6). doi:10.3390/cells10061283

First, M. B. (2013). Diagnostic and statistical manual of mental disorders, 5th edition, and clinical utility. *J Nerv Ment Dis, 201*(9), 727-729. doi:10.1097/NMD.0b013e3182a2168a

Fowler, C. D., Arends, M. A., & Kenny, P. J. (2008). Subtypes of nicotinic acetylcholine receptors in nicotine reward, dependence, and withdrawal: evidence from genetically modified mice. Behavioural pharmacology, 19(5-6), 461–484. https://doi.org/10.1097/FBP.0b013e32830c360e

Fu, Y. L., Wang, Y. J., & Mu, T. W. (2016). Proteostasis Maintenance of Cys-Loop Receptors. *Adv Protein Chem Struct Biol, 103*, 1-23. doi:10.1016/bs.apcsb.2015.11.002

Gerbasi, M. E., Eldar-Lissai, A., Acaster, S., Fridman, M., Bonthapally, V., Hodgkins, P., . . . Meltzer-Brody, S. (2020). Associations between commonly used patient-reported outcome tools in postpartum depression clinical practice and the Hamilton Rating Scale for Depression. *Arch Womens Ment Health, 23*(5), 727-735. doi:10.1007/s00737-020-01042-y

Gillman P. K. (2007). Tricyclic antidepressant pharmacology and therapeutic drug interactions updated. British journal of pharmacology, 151(6), 737–748. https://doi.org/10.1038/sj.bjp.0707253

Giniatullin, R. A., Sokolova, E. M., Di Angelantonio, S., Skorinkin, A., Talantova, M. V., & Nistri, A. (2000). Rapid relief of block by mecamylamine of neuronal nicotinic acetylcholine receptors of rat chromaffin cells in vitro: an electrophysiological and modeling study. *Mol Pharmacol, 58*(4), 778-787. doi:10.1124/mol.58.4.778

Goldberger, C., Guelfi, J. D., & Sheehan, D. V. (2011). Assessment of Anxiety in Clinical Trials with Depressed Patients Using the Hamilton Depression Rating Scale. *Psychopharmacol Bull, 44*(3), 34-50.

Gopalakrishnan, S., & Ganeshkumar, P. (2013). Systematic Reviews and Meta-analysis: Understanding the Best Evidence in Primary Healthcare. *J Family Med Prim Care, 2*(1), 9-14. doi:10.4103/2249-4863.109934

Gotti, C., Moretti, M., Gaimarri, A., Zanardi, A., Clementi, F., & Zoli, M. (2007). Heterogeneity and complexity of native brain nicotinic receptors. *Biochem Pharmacol, 74*(8), 1102-1111. doi:10.1016/j.bcp.2007.05.023

Gotti, C., Zoli, M., & Clementi, F. (2006). Brain nicotinic acetylcholine receptors: native subtypes and their relevance. *Trends Pharmacol Sci, 27*(9), 482-491. doi:10.1016/j.tips.2006.07.004

Gourion, D. (2008). [Antidepressants and their onset of action: a major clinical, methodological and pronostical issue]. *Encephale, 34*(1), 73-81. doi:10.1016/j.encep.2007.12.001

Green, M. A., & Halliwell, R. F. (1997). Selective antagonism of the GABA(A) receptor by ciprofloxacin and biphenylacetic acid. *Br J Pharmacol, 122*(3), 584-590. doi:10.1038/sj.bjp.0701411

Greenberg, P. E., Kessler, R. C., Birnbaum, H. G., Leong, S. A., Lowe, S. W., Berglund, P. A., & Corey-Lisle, P. K. (2003). The economic burden of depression in the United States: how did it change between 1990 and 2000? *J Clin Psychiatry, 64*(12), 1465-1475. doi:10.4088/jcp.v64n1211

Grenard, J. L., Munjas, B. A., Adams, J. L., Suttorp, M., Maglione, M., McGlynn, E. A., & Gellad, W.

F. (2011). Depression and medication adherence in the treatment of chronic diseases in the United States: a meta-analysis. *J Gen Intern Med, 26*(10), 1175-1182. doi:10.1007/s11606-011-1704-y

Grothe, M., Zaborszky, L., Atienza, M., Gil-Neciga, E., Rodriguez-Romero, R., Teipel, S. J., . . . Cantero, J. L. (2010). Reduction of basal forebrain cholinergic system parallels cognitive impairment in patients at high risk of developing Alzheimer's disease. *Cereb Cortex, 20*(7), 1685-1695. doi:10.1093/cercor/bhp232

Guedes, I. A., de Magalhães, C. S., & Dardenne, L. E. (2014). Receptor-ligand molecular docking. *Biophys Rev, 6*(1), 75-87. doi:10.1007/s12551-013-0130-2

Gulsevin, A., Papke, R. L., & Horenstein, N. (2020). In Silico Modeling of the α7 Nicotinic Acetylcholine Receptor: New Pharmacological Challenges Associated with Multiple Modes of Signaling. *Mini Rev Med Chem, 20*(10), 841-864. doi:10.2174/1389557520666200130105256

Guyatt, G. H., Oxman, A. D., Kunz, R., Woodcock, J., Brozek, J., Helfand, M., Alonso-Coello, P., Glasziou, P., Jaeschke, R., Akl, E. A., Norris, S., Vist, G., Dahm, P., Shukla, V. K., Higgins, J., Falck-Ytter, Y., Schünemann, H. J., & GRADE Working Group (2011). GRADE guidelines: 7. Rating the quality of evidence--inconsistency. Journal of clinical epidemiology, 64(12), 1294–1302. https://doi.org/10.1016/j.jclinepi.2011.03.017

Habert, J., Katzman, M. A., Oluboka, O. J., McIntyre, R. S., McIntosh, D., MacQueen, G. M., . . . Kennedy, S. H. (2016). Functional Recovery in Major Depressive Disorder: Focus on Early Optimized Treatment. *Prim Care Companion CNS Disord, 18*(5). doi:10.4088/PCC.15r01926

Hacimusalar, Y., & Eşel, E. (2018). Suggested Biomarkers for Major Depressive Disorder. *Noro Psikiyatr Ars, 55*(3), 280-290. doi:10.5152/npa.2017.19482

Hamilton M. (1960). A rating scale for depression. Journal of neurology, neurosurgery, and psychiatry, 23(1), 56–62. https://doi.org/10.1136/jnnp.23.1.56

Hansen, R. A., Gartlehner, G., Lohr, K. N., Gaynes, B. N., & Carey, T. S. (2005). Efficacy and safety of second-generation antidepressants in the treatment of major depressive disorder. *Ann Intern Med, 143*(6), 415-426. doi:10.7326/0003-4819-143-6-200509200-00006

Health, N. C. C. f. M. (2010). Depression in Adults with a Chronic Physical Health Problem: Treatment and Management. *Leicester (UK): British Psychological Society (UK)*.

Heo, M., Murphy, C. F., & Meyers, B. S. (2007). Relationship between the Hamilton Depression Rating Scale and the Montgomery-Asberg Depression Rating Scale in depressed elderly: a meta-analysis. *Am J Geriatr Psychiatry, 15*(10), 899-905. doi:10.1097/JGP.0b013e318098614e

Higgins, J. P. T., Altman, D. G., Gøtzsche, P. C., Jüni, P., Moher, D., Oxman, A. D., . . . Sterne, J. A. C. (2011). The Cochrane Collaboration's tool for assessing risk of bias in randomised trials. *Bmj, 343*(7829), 889-893. doi:10.1136/bmj.d5928

Hillhouse, T. M., & Porter, J. H. (2015). A brief history of the development of antidepressant drugs: from monoamines to glutamate. *Exp Clin Psychopharmacol, 23*(1), 1-21. doi:10.1037/a0038550

Ho, T. N. T., Abraham, N., & Lewis, R. J. (2020). Structure-Function of Neuronal Nicotinic Acetylcholine Receptor Inhibitors Derived From Natural Toxins. *Front Neurosci, 14*, 609005. doi:10.3389/fnins.2020.609005

Hopkins, C. W., Le Grand, S., Walker, R. C., & Roitberg, A. E. (2015). Long-Time-Step Molecular Dynamics through Hydrogen Mass Repartitioning. Journal of chemical theory and computation, 11(4), 1864–1874. https://doi.org/10.1021/ct5010406

Israel, J. A. (2010). The Impact of Residual Symptoms in Major Depression. *Pharmaceuticals (Basel), 3*(8), 2426-2440. doi:10.3390/ph3082426

Janowsky, D. S., David, J. M., el-Yousef, M. K., & Serkerke, H. J. (1972). Combined anticholinergic agents and atropine-like delirium. *Am J Psychiatry, 129*(3), 360-361. doi:10.1176/ajp.129.3.360-a

Jefferies, D., & Khalid, S. (2021). Atomistic and coarse-grained simulations of membrane proteins: A practical guide. Methods (San Diego, Calif.), 185, 15–27. https://doi.org/10.1016/j.ymeth.2020.02.007

Jo, S., Kim, T., & Im, W. (2007). Automated builder and database of protein/membrane complexes for molecular dynamics simulations. PloS one, 2(9), e880. https://doi.org/10.1371/journal.pone.0000880

Jones, C. K., Byun, N., & Bubser, M. (2012). Muscarinic and nicotinic acetylcholine receptor agonists and allosteric modulators for the treatment of schizophrenia. *Neuropsychopharmacology, 37*(1), 16-42. doi:10.1038/npp.2011.199

Karplus, M., & McCammon, J. A. (2002). Molecular dynamics simulations of biomolecules. *Nat Struct Biol, 9*(9), 646-652. doi:10.1038/nsb0902-646

Kennedy, S. H., Lam, R. W., McIntyre, R. S., Tourjman, S. V., Bhat, V., Blier, P., Hasnain, M., Jollant, F., Levitt, A. J., MacQueen, G. M., McInerney, S. J., McIntosh, D., Milev, R. V., Müller, D. J., Parikh, S. V., Pearson, N. L., Ravindran, A. V., Uher, R., & CANMAT Depression Work Group (2016). Canadian Network for Mood and Anxiety Treatments (CANMAT) 2016 Clinical Guidelines for the Management of Adults with Major Depressive Disorder: Section 3. Pharmacological Treatments. Canadian journal of psychiatry. Revue canadienne de psychiatrie, 61(9), 540–560. https://doi.org/10.1177/0706743716659417

Keller M. B. (2003). Past, present, and future directions for defining optimal treatment outcome in depression: remission and beyond. JAMA, 289(23), 3152–3160. https://doi.org/10.1001/jama.289.23.3152

King, M., & Ashraf, N. (2018). Tricyclic Antidepressant-Induced Anticholinergic Delirium in a Young Healthy Male Individual. *Drug Saf Case Rep, 5*(1), 1. doi:10.1007/s40800-017-0069-5

Koshland, D. E. (1958). Application of a Theory of Enzyme Specificity to Protein Synthesis. *Proc Natl Acad Sci U S A, 44*(2), 98-104. doi:10.1073/pnas.44.2.98

Krawczyk, P., & Święcicki, Ł. (2020). ICD-11 vs. ICD-10 - a review of updates and novelties introduced in the latest version of the WHO International Classification of Diseases. *Psychiatr Pol, 54*(1), 7-20. doi:10.12740/pp/103876

Kupfer, D. J., Frank, E., & Phillips, M. L. (2012). Major depressive disorder: new clinical, neurobiological, and treatment perspectives. *Lancet, 379*(9820), 1045-1055. doi:10.1016/s0140-6736(11)60602-8

Kuryatov, A., Onksen, J., & Lindstrom, J. (2008). Roles of accessory subunits in alpha4beta2(*) nicotinic receptors. *Mol Pharmacol, 74*(1), 132-143. doi:10.1124/mol.108.046789

Lane, C. A., Hardy, J., & Schott, J. M. (2018). Alzheimer's disease. *Eur J Neurol, 25*(1), 59-70. doi:10.1111/ene.13439

Lasala, M., Fabiani, C., Corradi, J., Antollini, S., & Bouzat, C. (2019). Molecular Modulation of Human

α7 Nicotinic Receptor by Amyloid-β Peptides. *Front Cell Neurosci, 13*, 37. doi:10.3389/fncel.2019.00037

Lau, J., Ioannidis, J. P., & Schmid, C. H. (1998). Summing up evidence: one answer is not always enough. *Lancet, 351*(9096), 123-127. doi:10.1016/s0140-6736(97)08468-7

Lau, J., Schmid, C. H., & Chalmers, T. C. (1995). Cumulative meta-analysis of clinical trials builds evidence for exemplary medical care. *J Clin Epidemiol, 48*(1), 45-57; discussion 59-60. doi:10.1016/0895-4356(94)00106-z

Leach, A. R. (2001). Molecular modeling: Principles and applications (2nd ed.). Prentice Hall.

Lee, C. T., Chiang, Y. C., Huang, J. Y., Tantoh, D. M., Nfor, O. N., Lee, J. F., Chang, C. C., & Liaw, Y. P. (2016). Incidence of Major Depressive Disorder: Variation by Age and Sex in Low-Income Individuals: A Population-Based 10-Year Follow-Up Study. Medicine, 95(15), e3110. https://doi.org/10.1097/MD.0000000000003110

Lembke, A., Johnson, K., & DeBattista, C. (2007). Depression and smoking cessation: does the evidence support psychiatric practice? *Neuropsychiatr Dis Treat, 3*(4), 487-493.

Lester, H. A., Dibas, M. I., Dahan, D. S., Leite, J. F., & Dougherty, D. A. (2004). Cys-loop receptors: new twists and turns. *Trends Neurosci, 27*(6), 329-336. doi:10.1016/j.tins.2004.04.002

Lester, H. A., Xiao, C., Srinivasan, R., & Son, C. D. (2017). Nicotinic acetylcholine receptors: from structure to brain function. Reviews of physiology, biochemistry and pharmacology, 173, 1-30. doi: 10.1007/112_2017_5.

Leuchter, A. F., Cook, I. A., Marangell, L. B., Gilmer, W. S., Burgoyne, K. S., Howland, R. H., Trivedi, M. H., Zisook, S., Jain, R., McCracken, J. T., Fava, M., Iosifescu, D., & Greenwald, S. (2009). Comparative effectiveness of biomarkers and clinical indicators for predicting outcomes of SSRI treatment in Major Depressive Disorder: results of the BRITE-MD study. Psychiatry research, 169(2), 124–131. https://doi.org/10.1016/j.psychres.2009.06.004

Lin, J., Su, Y., Wang, C., Yang, F., Xu, Y., Yuan, Y., . . . Si, T. (2018). Effects of tandospirone augmentation in major depressive disorder patients with high anxiety: A multicenter, randomized, parallel-controlled, open-label study. *J Psychiatr Res, 99*, 104-110. doi:10.1016/j.jpsychires.2018.01.020

Lindsley, C. W. (2010). (S)-(+)-mecamylamine (TC-5214): a neuronal nicotinic receptor modulator enters phase III trials as an adjunct treatment for Major Depressive Disorder (MDD). *ACS Chem Neurosci, 1*(8), 530-531. doi:10.1021/cn100070s

Lippiello, P. M., Beaver, J. S., Gatto, G. J., James, J. W., Jordan, K. G., Traina, V. M., . . . Bencherif, M. (2008). TC-5214 (S-(+)-mecamylamine): a neuronal nicotinic receptor modulator with antidepressant activity. *CNS Neurosci Ther, 14*(4), 266-277. doi:10.1111/j.1755-5949.2008.00054.x

Liu, J., Fan, Y., Ling-Li Zeng, Liu, B., Ju, Y., Wang, M., Dong, Q., Lu, X., Sun, J., Zhang, L., Guo, H., Futao Zhao, Weihui Li, Zhang, L., Li, Z., Liao, M., Zhang, Y., Hu, D., & Li, L. (2021). The neuroprogressive nature of major depressive disorder: evidence from an intrinsic connectome analysis. Translational psychiatry, 11(1), 102. https://doi.org/10.1038/s41398-021-01227-8

Lombardo, S., & Maskos, U. (2015). Role of the nicotinic acetylcholine receptor in Alzheimer's disease pathology and treatment. *Neuropharmacology, 96*(Pt B), 255-262. doi:10.1016/j.neuropharm.2014.11.018

Lomize, M. A., Lomize, A. L., Pogozheva, I. D., & Mosberg, H. I. (2006). OPM: orientations of proteins

in membranes database. *Bioinformatics, 22*(5), 623-625. doi:10.1093/bioinformatics/btk023

Ma, S., Yang, J., Yang, B., Kang, L., Wang, P., Zhang, N., . . . Liu, Z. (2021). The Patient Health Questionnaire-9 vs. the Hamilton Rating Scale for Depression in Assessing Major Depressive Disorder. *Front Psychiatry, 12*, 747139. doi:10.3389/fpsyt.2021.747139

MacQueen, G. M., & Memedovich, K. A. (2017). Cognitive dysfunction in major depression and bipolar disorder: Assessment and treatment options. *Psychiatry Clin Neurosci, 71*(1), 18-27. doi:10.1111/pcn.12463

Maher, C. G., Sherrington, C., Herbert, R. D., Moseley, A. M., & Elkins, M. (2003). Reliability of the PEDro scale for rating quality of randomized controlled trials. *Phys Ther, 83*(8), 713-721.

Makarewicz, T., & Kaźmierkiewicz, R. (2016). Improvements in GROMACS plugin for PyMOL including implicit solvent simulations and displaying results of PCA analysis. Journal of molecular modeling, 22(5), 109. https://doi.org/10.1007/s00894-016-2982-4

Mallamace, F., Mensitieri, G., Salzano de Luna, M., Lanzafame, P., Papanikolaou, G., & Mallamace, D. (2022). The Interplay between the Theories of Mode Coupling and of Percolation Transition in Attractive Colloidal Systems. *Int J Mol Sci, 23*(10). doi:10.3390/ijms23105316

Marcus, R. N., McQuade, R. D., Carson, W. H., Hennicken, D., Fava, M., Simon, J. S., . . . Berman, R. M. (2008). The efficacy and safety of aripiprazole as adjunctive therapy in major depressive disorder: a second multicenter, randomized, double-blind, placebo-controlled study. *J Clin Psychopharmacol, 28*(2), 156-165. doi:10.1097/JCP.0b013e31816774f9

Martin, L. F., & Freedman, R. (2007). Schizophrenia and the alpha7 nicotinic acetylcholine receptor. *Int Rev Neurobiol, 78*, 225-246. doi:10.1016/s0074-7742(06)78008-4

Millar, N. S., & Gotti, C. (2009). Diversity of vertebrate nicotinic acetylcholine receptors. *Neuropharmacology, 56*(1), 237-246. doi:10.1016/j.neuropharm.2008.07.041

Miller, D. R., Khoshbouei, H., Garai, S., Cantwell, L. N., Stokes, C., Thakur, G., & Papke, R. L. (2020). Allosterically Potentiated α7 Nicotinic Acetylcholine Receptors: Reduced Calcium Permeability and Current-Independent Control of Intracellular Calcium. *Mol Pharmacol, 98*(6), 695-709. doi:10.1124/molpharm.120.000012

Mineur, Y. S., Mose, T. N., Blakeman, S., & Picciotto, M. R. (2018). Hippocampal α7 nicotinic ACh receptors contribute to modulation of depression-like behaviour in C57BL/6J mice. *Br J Pharmacol, 175*(11), 1903-1914. doi:10.1111/bph.13769

Mizrachi, T., Vaknin-Dembinsky, A., Brenner, T., & Treinin, M. (2021). Neuroinflammation Modulation via α7 Nicotinic Acetylcholine Receptor and Its Chaperone, RIC-3. *Molecules, 26*(20). doi:10.3390/molecules26206139

Montgomery, S. A., & Asberg, M. (1979). A new depression scale designed to be sensitive to change. *Br J Psychiatry, 134*, 382-389. doi:10.1192/bjp.134.4.382

Moroni, M., Zwart, R., Sher, E., Cassels, B. K., & Bermudez, I. (2006). alpha4beta2 nicotinic receptors with high and low acetylcholine sensitivity: pharmacology, stoichiometry, and sensitivity to long-term exposure to nicotine. *Mol Pharmacol, 70*(2), 755-768. doi:10.1124/mol.106.023044

Murphy, M. P., & LeVine, H., 3rd. (2010). Alzheimer's disease and the amyloid-beta peptide. *J Alzheimers Dis, 19*(1), 311-323. doi:10.3233/jad-2010-1221

Nair, V. V., & Gorfe, A. A. (2021). Molecular Dynamics Simulation of Lipid-Modified Signaling Proteins. Methods in molecular biology (Clifton, N.J.), 2315, 141–159.

https://doi.org/10.1007/978-1-0716-1468-6_9

Nelson, J. C., Delucchi, K., & Schneider, L. S. (2009). Anxiety does not predict response to antidepressant treatment in late life depression: results of a meta-analysis. *Int J Geriatr Psychiatry, 24*(5), 539-544. doi:10.1002/gps.2233

Newman, M. B., Manresa, J. J., Sanberg, P. R., & Shytle, R. D. (2001). Nicotine induced seizures blocked by mecamylamine and its stereoisomers. Life sciences, 69(22), 2583–2591. https://doi.org/10.1016/s0024-3205(01)01338-8

Nickell, J. R., Grinevich, V. P., Siripurapu, K. B., Smith, A. M., & Dwoskin, L. P. (2013). Potential therapeutic uses of mecamylamine and its stereoisomers. Pharmacology, biochemistry, and behavior, 108, 28–43. https://doi.org/10.1016/j.pbb.2013.04.005

Noble, R. E. (2005). Depression in women. *Metabolism, 54*(5 Suppl 1), 49-52. doi:10.1016/j.metabol.2005.01.014

Noviello, C. M., Gharpure, A., Mukhtasimova, N., Cabuco, R., Baxter, L., Borek, D., . . . Hibbs, R. E. (2021). Structure and gating mechanism of the α7 nicotinic acetylcholine receptor. *Cell, 184*(8), 2121-2134.e2113. doi:10.1016/j.cell.2021.02.049

Olfson, M., & Marcus, S. C. (2008). A case-control study of antidepressants and attempted suicide during early phase treatment of major depressive episodes. *J Clin Psychiatry, 69*(3), 425-432. doi:10.4088/jcp.v69n0313

Olfson, M., Marcus, S. C., & Shaffer, D. (2006). Antidepressant drug therapy and suicide in severely depressed children and adults: A case-control study. *Arch Gen Psychiatry, 63*(8), 865-872. doi:10.1001/archpsyc.63.8.865

Olver, J. S., Burrows, G. D., & Norman, T. R. (2001). Third-generation antidepressants: do they offer advantages over the SSRIs? *CNS Drugs, 15*(12), 941-954. doi:10.2165/00023210-200115120-00004

Otte, C., Gold, S. M., Penninx, B. W., Pariante, C. M., Etkin, A., Fava, M., . . . Schatzberg, A. F. (2016). Major depressive disorder. *Nat Rev Dis Primers, 2*, 16065. doi:10.1038/nrdp.2016.65

Papke, R. L., Sanberg, P. R., & Shytle, R. D. (2001). Analysis of mecamylamine stereoisomers on human nicotinic receptor subtypes. *J Pharmacol Exp Ther, 297*(2), 646-656.

Papke, R. L., & Lindstrom, J. M. (2020). Nicotinic acetylcholine receptors: Conventional and unconventional ligands and signaling. Neuropharmacology, 168, 108021. https://doi.org/10.1016/j.neuropharm.2020.108021

Paterson, D., & Nordberg, A. (2000). Neuronal nicotinic receptors in the human brain. *Prog Neurobiol, 61*(1), 75-111. doi:10.1016/s0301-0082(99)00045-3

Philip, N. S., Carpenter, L. L., Tyrka, A. R., & Price, L. H. (2010). Nicotinic acetylcholine receptors and depression: a review of the preclinical and clinical literature. *Psychopharmacology (Berl), 212*(1), 1-12. doi:10.1007/s00213-010-1932-6

Posadas, I., López-Hernández, B., & Ceña, V. (2013). Nicotinic receptors in neurodegeneration. *Curr Neuropharmacol, 11*(3), 298-314. doi:10.2174/1570159x11311030005

Ripoll, N., Bronnec, M., & Bourin, M. (2004). Nicotinic receptors and schizophrenia. *Curr Med Res Opin, 20*(7), 1057-1074. doi:10.1185/030079904125004060

Rollema, H., Guanowsky, V., Mineur, Y. S., Shrikhande, A., Coe, J. W., Seymour, P. A., & Picciotto, M. R. (2009). Varenicline has antidepressant-like activity in the forced swim test and augments sertraline's effect. *Eur J Pharmacol, 605*(1-3), 114-116. doi:10.1016/j.ejphar.2009.01.002

Rucktooa, P., Haseler, C. A., van Elk, R., Smit, A. B., Gallagher, T., & Sixma, T. K. (2012). Structural characterization of binding mode of smoking cessation drugs to nicotinic acetylcholine receptors through study of ligand complexes with acetylcholine-binding protein. *J Biol Chem, 287*(28), 23283-23293. doi:10.1074/jbc.M112.360347

Sabri, O., Meyer, P. M., Gräf, S., Hesse, S., Wilke, S., Becker, G. A., . . . Brust, P. (2018). Cognitive correlates of α4β2 nicotinic acetylcholine receptors in mild Alzheimer's dementia. *Brain, 141*(6), 1840-1854. doi:10.1093/brain/awy099

Salmaso, V., & Moro, S. (2018). Bridging Molecular Docking to Molecular Dynamics in Exploring Ligand-Protein Recognition Process: An Overview. *Front Pharmacol, 9*, 923. doi:10.3389/fphar.2018.00923

Saragoussi, D., Touya, M., Haro, J. M., Jönsson, B., Knapp, M., Botrel, B., . . . Rive, B. (2017). Factors associated with failure to achieve remission and with relapse after remission in patients with major depressive disorder in the PERFORM study. *Neuropsychiatr Dis Treat, 13*, 2151-2165. doi:10.2147/ndt.S136343

Sastry, G. M., Adzhigirey, M., Day, T., Annabhimoju, R., & Sherman, W. (2013). Protein and ligand preparation: parameters, protocols, and influence on virtual screening enrichments. Journal of computer-aided molecular design, 27(3), 221–234. https://doi.org/10.1007/s10822-013-9644-8

Séguéla, P., Wadiche, J., Dineley-Miller, K., Dani, J. A., & Patrick, J. W. (1993). Molecular cloning, functional properties, and distribution of rat brain alpha 7: a nicotinic cation channel highly permeable to calcium. *J Neurosci, 13*(2), 596-604. doi:10.1523/jneurosci.13-02-00596.1993

Sforzini, L. (2021). Lost in translation. The quest for definitions of treatment-resistant depression with a focus on inflammation-related gene expression. *Brain Behav Immun Health, 16*, 100331. doi:10.1016/j.bbih.2021.100331

Sharpe, D. (1997). Of apples and oranges, file drawers and garbage: why validity issues in meta-analysis will not go away. *Clin Psychol Rev, 17*(8), 881-901. doi:10.1016/s0272-7358(97)00056-1

Shelton, R. C., Osuntokun, O., Heinloth, A. N., & Corya, S. A. (2010). Therapeutic options for treatment-resistant depression. *CNS Drugs, 24*(2), 131-161. doi:10.2165/11530280-000000000-00000

Sher, E., Chen, Y., Sharples, T. J., Broad, L. M., Benedetti, G., Zwart, R., . . . De Filippi, G. (2004). Physiological roles of neuronal nicotinic receptor subtypes: new insights on the nicotinic modulation of neurotransmitter release, synaptic transmission and plasticity. *Curr Top Med Chem, 4*(3), 283-297. doi:10.2174/1568026043451393

Shytle, R. D., Penny, E., Silver, A. A., Goldman, J., & Sanberg, P. R. (2002). Mecamylamine (Inversine): an old antihypertensive with new research directions. *J Hum Hypertens, 16*(7), 453-457. doi:10.1038/sj.jhh.1001416

Shytle, R. D., Silver, A. A., Lukas, R. J., Newman, M. B., Sheehan, D. V., & Sanberg, P. R. (2002). Nicotinic acetylcholine receptors as targets for antidepressants. *Mol Psychiatry, 7*(6), 525-535. doi:10.1038/sj.mp.4001035

Smart, O. S., Goodfellow, J. M., & Wallace, B. A. (1993). The pore dimensions of gramicidin A. Biophysical journal, 65(6), 2455–2460. https://doi.org/10.1016/S0006-3495(93)81293-1

Snaith, R. P. (1996). Hamilton rating scale for depression (HAM-D). In M. E. Maruish (Ed.), The use of psychological testing for treatment planning and outcomes assessment (pp. 3-21). Lawrence Erlbaum Associates Publishers.

Sparling, B. A., & DiMauro, E. F. (2017). Progress in the discovery of small molecule modulators of the Cys-loop superfamily receptors. *Bioorg Med Chem Lett, 27*(15), 3207-3218. doi:10.1016/j.bmcl.2017.04.073

Stevens, R. D., & Wu, C. L. (2007). Strengths and limitations of meta-analysis. *J Cardiothorac Vasc Anesth, 21*(1), 1-2. doi:10.1053/j.jvca.2006.09.006

Sun, Y., Fu, Z., Bo, Q., Mao, Z., Ma, X., & Wang, C. (2020). The reliability and validity of PHQ-9 in patients with major depressive disorder in psychiatric hospital. *BMC Psychiatry, 20*(1), 474. doi:10.1186/s12888-020-02885-6

As discussed above, we used the PCA method to recognize the most prominent displacements in both PNU-120596-α 7 nAChRs and the dexmecamylamine-α 7 nAChRs complex forms during the MD simulations. The first two eigenvectors, which can explain most variances of the system, were projected to a 2D space than contains Carbon-alpha residues to analyze the conformational changes of the complexes during MD.

Taly, A., Corringer, P. J., Guedin, D., Lestage, P., & Changeux, J. P. (2009). Nicotinic receptors: allosteric transitions and therapeutic targets in the nervous system. *Nat Rev Drug Discov, 8*(9), 733-750. doi:10.1038/nrd2927

Tarawneh, R., & Holtzman, D. M. (2012). The clinical problem of symptomatic Alzheimer disease and mild cognitive impairment. Cold Spring Harbor perspectives in medicine, 2(5), a006148. https://doi.org/10.1101/cshperspect.a006148

Thompson, A. J., Lester, H. A., & Lummis, S. C. (2010). The structural basis of function in Cys-loop receptors. *Q Rev Biophys, 43*(4), 449-499. doi:10.1017/s0033583510000168

Tripathi, A., & Bankaitis, V. A. (2017). Molecular Docking: From Lock and Key to Combination Lock. Journal of molecular medicine and clinical applications, 2(1), 10.16966/2575-0305.106. https://doi.org/10.16966/2575-0305.106

Uwada, J., Nakazawa, H., Mikami, D., Islam, M. S., Muramatsu, I., Taniguchi, T., & Yazawa, T. (2020). PNU-120596, a positive allosteric modulator of α7 nicotinic acetylcholine receptor, directly inhibits p38 MAPK. Biochemical pharmacology, 182, 114297. https://doi.org/10.1016/j.bcp.2020.114297

Unwin, N. (2013). Nicotinic acetylcholine receptor and the structural basis of neuromuscular transmission: insights from Torpedo postsynaptic membranes. *Q Rev Biophys, 46*(4), 283-322. doi:10.1017/s0033583513000061

Uteshev V. V. (2012). α7 nicotinic ACh receptors as a ligand-gated source of Ca(2+) ions: the search for a Ca(2+) optimum. Advances in experimental medicine and biology, 740, 603–638. https://doi.org/10.1007/978-94-007-2888-2_27

Voineskos, D., Daskalakis, Z. J., & Blumberger, D. M. (2020). Management of Treatment-Resistant Depression: Challenges and Strategies. *Neuropsychiatr Dis Treat, 16*, 221-234. doi:10.2147/ndt.S198774

Wada, E., Wada, K., Boulter, J., Deneris, E., Heinemann, S., Patrick, J., & Swanson, L. W. (1989). Distribution of alpha 2, alpha 3, alpha 4, and beta 2 neuronal nicotinic receptor subunit mRNAs in the central nervous system: a hybridization histochemical study in the rat. *J Comp Neurol, 284*(2), 314-335. doi:10.1002/cne.902840212

Wallace, T. L., Ballard, T. M., Pouzet, B., Riedel, W. J., & Wettstein, J. G. (2011). Drug targets for cognitive enhancement in neuropsychiatric disorders. *Pharmacol Biochem Behav, 99*(2), 130-145. doi:10.1016/j.pbb.2011.03.022

Wang, H. Y., Lee, D. H., D'Andrea, M. R., Peterson, P. A., Shank, R. P., & Reitz, A. B. (2000). beta-Amyloid(1-42) binds to alpha7 nicotinic acetylcholine receptor with high affinity. Implications for Alzheimer's disease pathology. *J Biol Chem, 275*(8), 5626-5632. doi:10.1074/jbc.275.8.5626

Wan, X., Wang, W., Liu, J., & Tong, T. (2014). Estimating the sample mean and standard deviation from the sample size, median, range and/or interquartile range. BMC medical research methodology, 14, 135. https://doi.org/10.1186/1471-2288-14-135

Wang, Z., Ma, X., & Xiao, C. (2019). Standardized Treatment Strategy for Depressive Disorder. *Adv Exp Med Biol, 1180*, 193-199. doi:10.1007/978-981-32-9271-0_10

Whiteaker, P., Cooper, J. F., Salminen, O., Marks, M. J., McClure-Begley, T. D., Brown, R. W., Collins, A. C., & Lindstrom, J. M. (2006). Immunolabeling demonstrates the interdependence of mouse brain alpha4 and beta2 nicotinic acetylcholine receptor subunit expression. The Journal of comparative neurology, 499(6), 1016–1038.

Williams, D. K., Wang, J., & Papke, R. L. (2011). Investigation of the molecular mechanism of the α7 nicotinic acetylcholine receptor positive allosteric modulator PNU-120596 provides evidence for two distinct desensitized states. Molecular pharmacology, 80(6), 1013–1032. https://doi.org/10.1124/mol.111.074302

Wu, J., & Mukherji, D. (2022). Comparison of all atom and united atom models for thermal transport calculations of amorphous polyethylene. Computational Materials Science, 211, 111539. https://doi.org/10.1016/j.commatsci.2022.111539

Yakel, J. (2010). Advances and hold-ups in the study of structure, function and regulation of Cys-loop ligand-gated ion channels and receptors. *J Physiol, 588*(Pt 4), 555-556. doi:10.1113/jphysiol.2009.185488

Yamodo, I. H., Chiara, D. C., Cohen, J. B., & Miller, K. W. (2010). Conformational changes in the nicotinic acetylcholine receptor during gating and desensitization. Biochemistry, 49(1), 156–165. https://doi.org/10.1021/bi901550p

Yanagawa, B., Tam, D. Y., Mazine, A., & Tricco, A. C. (2018). Systematic review and meta-analysis in cardiac surgery: a primer. *Curr Opin Cardiol, 33*(2), 184-189. doi:10.1097/hco.0000000000000496

Young, G. T., Zwart, R., Walker, A. S., Sher, E., & Millar, N. S. (2008). Potentiation of alpha7 nicotinic acetylcholine receptors via an allosteric transmembrane site. *Proc Natl Acad Sci U S A, 105*(38), 14686-14691. doi:10.1073/pnas.0804372105

Yu, C. R., & Role, L. W. (1998). Functional contribution of the alpha7 subunit to multiple subtypes of nicotinic receptors in embryonic chick sympathetic neurones. *J Physiol, 509 (Pt 3)*(Pt 3), 651-665. doi:10.1111/j.1469-7793.1998.651bm.x

Yu, W., & MacKerell, A. D., Jr. (2017). Computer-Aided Drug Design Methods. *Methods Mol Biol, 1520*, 85-106. doi:10.1007/978-1-4939-6634-9_5

Yuan, Z., Chen, Z., Xue, M., Zhang, J., & Leng, L. (2020). Application of antidepressants in depression: A systematic review and meta-analysis. Journal of clinical neuroscience : official journal of the Neurosurgical Society of Australasia, 80, 169–181. https://doi.org/10.1016/j.jocn.2020.08.013

Zapletal, V., Mládek, A., Melková, K., Louša, P., Nomilner, E., Jaseňáková, Z., Kubáň, V., Makovická, M., Laníková, A., Žídek, L., & Hritz, J. (2020). Choice of Force Field for Proteins Containing Structured and Intrinsically Disordered Regions. Biophysical journal, 118(7), 1621–1633. https://doi.org/10.1016/j.bpj.2020.02.019

Zhang, B., Li, H., Yu, K., & Jin, Z. (2022). Molecular docking-based computational platform for high-throughput virtual screening. CCF transactions on high performance computing, 4(1), 63–74. https://doi.org/10.1007/s42514-021-00086-5

Zhang, J. C., Yao, W., Ren, Q., Yang, C., Dong, C., Ma, M., . . . Hashimoto, K. (2016). Depression-like phenotype by deletion of α7 nicotinic acetylcholine receptor: Role of BDNF-TrkB in nucleus accumbens. *Sci Rep, 6*, 36705. doi:10.1038/srep36705

Zhao, Y., Liu, S., Zhou, Y., Zhang, M., Chen, H., Eric Xu, H., . . . Tian, C. (2021). Structural basis of human α7 nicotinic acetylcholine receptor activation. *Cell Res, 31*(6), 713-716. doi:10.1038/s41422-021-00509-6

Zoli, M., Léna, C., Picciotto, M. R., & Changeux, J. P. (1998). Identification of four classes of brain nicotinic receptors using beta2 mutant mice. *J Neurosci, 18*(12), 4461-4472. doi:10.1523/jneurosci.18-12-04461.1998

Zoli, M., Pucci, S., Vilella, A., & Gotti, C. (2018). Neuronal and Extraneuronal Nicotinic Acetylcholine Receptors. *Curr Neuropharmacol, 16*(4), 338-349. doi:10.2174/1570159x15666170912110450

Zusky, P. M., Biederman, J., Rosenbaum, J. F., Manschreck, T. C., Gross, C. C., Weilberg, J. B., & Gastfriend, D. R. (1988). Adjunct low dose lithium carbonate in treatment-resistant depression: a placebo-controlled study. *J Clin Psychopharmacol, 8*(2), 120-124.

Appendix

Table A1 Essential study characteristics, including country, study period, study type, intervention duration, intervention dosage, and sample character (sample size, gender ratio, average age, and clinical diagnosis)

ID	Study	Year	country	study type	disease type	Sample(exp/con)	Age(exp/con)	Sex(exp/con)	Intervention(exp/con)	Intervention time
1	Tony P	2008	canada	random control	MDD	11/10	49.6 (8.6)/ 48.3(10.3)	4/17	Mecamylamine hydrochloride (MEC) up to 10 mg/ placebo group	8 week
2	Sajjad A.khan	2016	U.S.A	random control	MDD	586	36.4	273/313	Dexmecamylamine up to 4 mg/ placebo group	8 week
3	Raj Tummala	2015	U.S.A	random control	MDD	610/203	43.2(0.47)/42.8(0.82)	247/566	Dexmecamylamine 1-4 mg BID+SSRI/SNRI/placebo+SSRI/SNRI	52 week
4	Hans-Jürgen Möller,	2014	U.S.A	random control	MDD	160/161	42.1(11.8)/43.2(11.9)	132/189	Dexmecamylamine 4mg+SSRI/SNRI/placebo+SSRI/SNRI	8 week
5	Hans-Jürgen Möller,	2014	Europe	random control	MDD	174/174	45.6(10.8)/45.8(11.8)	102/244	Dexmecamylamine 4mg+SSRI/SNRI/placebo+SSRI/SNRI	8 week
6	Eduard vieta	2013	U.S.A+India	random control	MDD	159/160	39.7(11.37)/41.0(11.53)	119/200	Dexmecamylamine 4mg+SSRI/SNRI/placebo+SSRI/SNRI	8 week
7	Eduard vieta	2013	Europe	random control	MDD	147/148	46.1(11.25)/43.4(11.31）	106/189	Dexmecamylamine 4mg+SSRI/SNRI/placebo+SSRI/SNRI	8 week
8	Hans A Eriksson	2012	U.S.A	random control	MDD	35/37	40.3(12.5)/40.1(10.49)	26/45	Dexmecamylamine 4mg/placebo	8 week
9	Elizabeth Ralevski	2014	U.S.A	random control	MDD	11/10	48.2(9.84)/50.91(8.43)	15/6	Mecamylamine 10mg/placebo	8 week

Notes: exp=experimental group; con=control group;

Table A2 The extracted data of HAMD-17 score change group.

id	study	year	country	exp				con			
				mean1	se1	sd1	n1	mean2	se2	sd2	n2
4	Hans-Jürgen Möller	2014	U.S.A	-9.5	0.79	9.993	160	-9.1	0.79	10.02	161
5	Hans-Jürgen Möller	2014	U.S.A	-9.07	0.597	7.875	174	-11.16	0.592	7.809	174
6	Eduard vieta	2013	U.S.A+India	-9.7	0.96	11.318	139	-9.3	0.96	11.56	145
7	Eduard vieta	2013	Europe	-9.4	0.56	6.507	135	-9.8	0.55	6.484	139

Notes: exp=experimental group; con=control group; se=standard error; sd=standard deviation; n=number;

Table A3 The extracted data of MADRS score change group.

id	study	year	country	exp				con			
				mean1	se1	sd1	n1	mean2	se2	sd2	n2
3	Raj Tummala	2015	U.S.A	-11.6	0.5	8.53	291	-11.5	0.87	8.743	101
4	Hans-Jürgen Möller	2014	U.S.A	-11.3	0.84	10.356	152	-11.2	0.8	10.02	157
5	Hans-Jürgen Möller	2014	U.S.A	-12.2	0.69	8.996	170	-12.7	0.65	8.574	174
6	Eduard vieta	2013	U.S.A+India	-12.7	0.8	9.831	151	-11.7	0.8	10.02	157
7	Eduard vieta	2013	Europe	-11.7	0.71	8.55	145	-11.6	0.7	8.429	145
8	Hans A Eriksson	2012	U.S.A	-11.4	2.14	12.66	35	-7.6	2.19	12.39	32

Notes: exp=experimental group; con=control group; se=standard error; sd=standard deviation; n=number;

Table A4 The extracted data of response rate group.

id	study	year	country	exp		con	
				event1	total1	event2	total2
4	Hans-Jürgen Möller	2014	U.S.A	36	152	47	157
5	Hans-Jürgen Möller	2014	U.S.A	51	170	64	173
6	Eduard vieta	2013	U.S.A+India	30.5	151	24.2	157
7	Eduard vieta	2013	Europe	33.8	145	26.9	145

Notes: exp=experimental group; con=control group;

Table A5 The extracted data of remission rate group.

id	study	year	country	exp		con	
				event1	total1	event2	total2
4	Hans-Jürgen Möller	2014	U.S.A	39	152	43	157
5	Hans-Jürgen Möller	2014	U.S.A	41	170	54	174
6	Eduard vieta	2013	U.S.A+India	42	151	47	157
7	Eduard vieta	2013	Europe	48	145	49	145

Notes: exp=experimental group; con=control group;

Table A6 The extracted data of sustained response rate group.

id	study	year	country	exp		con	
				event1	total1	event2	total2
4	Hans-Jürgen Möller	2014	U.S.A	20	143	23	145
5	Hans-Jürgen Möller	2014	U.S.A	25	163	41	173
6	Eduard vieta	2013	U.S.A+India	14.2	151	11.8	157
7	Eduard vieta	2013	Europe	14.5	145	16.3	145
3	Raj Tummala	2015	U.S.A	18.2	391	20.6	136

Notes: exp=experimental group; con=control group;

Table A7 The extracted data of sustained remission rate group

id	study	year	country	exp		con	
				event1	total1	event2	total2
4	Hans-Jürgen Möller	2014	U.S.A	11	144	14	152
5	Hans-Jürgen Möller	2014	U.S.A	13	163	21	173
6	Eduard vieta	2013	U.S.A+India	9.5	151	6.5	157
7	Eduard vieta	2013	Europe	7.9	145	9.2	145

Notes: exp=experimental group; con=control group;

Table A8 The extracted data of CGI-I response group

id	study	year	country	exp		con	
				event1	total1	event2	total2
4	Hans-Jürgen Möller	2014	U.S.A	57	152	75	157
5	Hans-Jürgen Möller	2014	U.S.A	100	170	118	174
6	Eduard vieta	2013	U.S.A+India	56.3	151	51	157

Notes: exp=experimental group; con=control group;

Table A9 The extracted data of CGI-S score change group

id	study	year	country	exp				con			
				mean1	se1	sd1	n1	mean2	se2	sd2	n2
3	Raj Tummala	2015	U.S.A	-1.8	NR	1.17	176	-1.6	NR	1.17	68
4	Hans-Jürgen Möller	2014	U.S.A	-1.2	0.11	1.356	152	-1.2	0.1	1.253	157
5	Hans-Jürgen Möller	2014	U.S.A	-1.7	0.1	1.303	170	-1.7	0.09	1.187	174
6	Eduard vieta	2013	U.S.A+India	-1.4	0.11	1.352	151	-1.3	0.11	1.378	157
7	Eduard vieta	2013	Europe	-1.6	0.11	1.325	145	-1.6	0.11	1.325	145

Notes: exp=experimental group; con=control group; se=standard error; sd=standard deviation; n=number;